

# **Low Cycle Fatigue Estimation of Welded Butt Joints and Weld Treatments Subjected to Cyclic Bending**

*by*

**Ali Gharizadeh**

*A dissertation submitted in fulfilment of the requirements for the degree of*

***Master of Engineering***



University of Technology Sydney

**October 2014**

**Faculty of Engineering & Information Technology**

**School of Civil and Environmental Engineering**

## **CERTIFICATE OF AUTHORSHIP/ORIGINALITY**

I certify that the work in this thesis has not previously been submitted for a degree nor has it been submitted as part of requirements for a degree except as fully acknowledged within the text.

I also certify that the thesis has been written by me. Any help that I have received in my research work and the preparation of the thesis itself has been acknowledged. In addition, I certify that all information sources a literature used are indicated in the thesis.

Signature of Student

## ABSTRACT

In this report a procedure to estimate fatigue life for welded joints under bending load has been presented. The methodology of fatigue life prediction used in this investigation is based on strain-life method. The research carried out within the project develops a method for determination of plastic stress and strain distribution in welded parts by using three-dimensional solid cubic finite elements.

The first part of the research deals with fatigue analysis of a welded butt joint in a cantilever type flat plate under periodic bending load. Elasto-plastic finite element analysis has been carried out for this joint using software ANSYS. The local plastic stress and strain obtained from ANSYS were used in Morrow's modified Manson-Coffin equation and Smith-Watson-Topper damage equation to estimate the number of cycles the weld can tolerate.

One of the most important and influential phenomena in fatigue life prediction is residual stress. The presence of residual stresses in welded parts can noticeably affect fatigue behaviour. Tensile Residual stress generated during the welding process is inevitable. Therefore, applying residual stress as an initial condition in finite element analysis is an important part of the modelling. The stress and strain distributions at critical regions caused by combination of residual stress and loading were obtained for chosen specimens and subsequently used to determine the fatigue life. The effect of residual stress on fatigue life and positive improvement of weld durability against cyclic loads by eliminating of residual stress or converting tensile stress to compressive stress in high cycle fatigue cases are well known and clear but these effects in low cycle cases are less clear and known. The finite element modellings undertaken in this study show that although the presence of tensile residual stress has a significant effect on fatigue life in high cycle cases, in low cycle fatigue situations, it is almost unimportant and negligible. This finding reveals that any effort and cost to eliminate the residual stress or improve it, when the low cycle fatigue is the main problem, would be unnecessary and uneconomical.

The stress concentration is another phenomenon that effects on fatigue life. Any irregularity, discontinuity or abrupt changes in cross section such as holes, notches or angels could change stress distribution so that the common stress equations no longer work to describe the stress field at these locations. Real stress due to stress concentration is higher than nominal stress calculated by regular methods. Stress concentration factor is directly related to the geometry. The materials protruded outside the base plate at the weld zone produce sharp angles between weld material and base plate material which is the main reason of the stress concentration. By removing the material protruding outside the base plate to eliminate the discontinuity angels, it could be assumed that the stress concentration factor has been eliminated and the stress has been reduced, subsequently, the fatigue life has been improved. Grinding is a very common weld finishing and treating method that removes the stress concentration sources.

Comparison between regular weld and grinding finite element models reveals that the stress concentration factor has important effects on both high-cycle and low-cycle fatigue situations so that improving the stress concentration condition by using a grinding process can significantly increase the fatigue life.

In order to compare and validate the predicted fatigue lives by numerical modellings with the experimental data, a series of laboratory tests were performed. Therefore, a fatigue testing set-up was prepared. This set-up consists of a cantilever type flat plate set on a frame and the whole assembly is then installed on a shake table. A loading arm installed to a fixed frame next to the shake table, generated constant amplitudes of bending deflection on the specimens. The experimental testing included two parts. Firstly, fatigue tests were performed for five different loading situations applied on the regular weld specimens. Secondly, the same loading situations were used for welded specimens ground by hand disk grinder. To achieve an acceptable statistical accuracy three samples for each loading were tested. The experimental tests show a good agreement with computational models for regular weld specimens but contrarily, in ground specimen cases the opposite results were observed which would be discussed in the body of the thesis.

## **PUBLICATION BASED ON THIS RESEARCH PROGRAM**

- **“Investigation of Residual Stress Effect on Fatigue Life of Butt Weld Joints Subjected to Cyclic Bending”**, A. Gharizadeh, B. Samali, A. Saleh, 5th Asia Pacific Congress on Computational Mechanics (APCOM2013) 11th-14th Dec. 2013, Singapore. (accepted and presented)
- **“Effect of weld treatments to improve residual stress and stress concentration on fatigue strength”**, A. Gharizadeh, B. Samali, International Journal of Fatigue. (under review)
- **“Experimental and Numerical Study of low cycle Fatigue Life for Welded Butt Joints and Weld Treatments Subjected to Cyclic Bending”**”, A. Gharizadeh, B. Samali, International Journal of Fatigue. (under review)

## **ACKNOWLEDGMENT**

I would like to mention my deepest and most sincere gratitude to my supervisor Professor Bijan Samali for his continuous guidance, encouragement and sharing valuable times throughout the work.

I also wish to thank the staff of the School of Civil and Environmental Engineering especially the staff of Structures Laboratory for their sincere co-operation during this research work.

I am deeply indebted to my parents for their love, encouragements and supports.

# TABLE OF CONTENT

Abstract .....	ii
Publication based on this research program .....	iv
Acknowledgment .....	v
Table of content .....	vi
List of tables .....	viii
List of figures .....	ix
Notation .....	xiii
CHAPTER 1 INTRODUCTION .....	1
1.1 Preamble .....	1
1.2 Background .....	3
1.3 Objectives of this research .....	4
1.4 Project plan and time table .....	5
1.5 Thesis Overview .....	6
CHAPTER 2 LITERATURE REVIEW .....	7
2.1 Introduction .....	7
2.2 Fatigue analysis methodology .....	7
2.2.1 Stress-life method .....	8
2.2.2 Strain-life method .....	9
2.2.3 Linear-Elastic Fracture Mechanics (LEFM) method .....	12
2.3 Residual stress in welded joints .....	15
2.3.1 Neuber Rule for contribution of residual stress in actual total stress .....	19
2.3.2 Residual stress relief .....	21
2.4 Stress Concentration and Stress Distribution near the Weld Area .....	22
2.4.1 Stress concentration improvement .....	31
2.5 Finite Element Modelling .....	32
2.6 Material properties .....	34
CHAPTER 3 NUMERICAL SOLUTION FOR A BUTT WELD JOINT .....	37
3.1 Introduction .....	37
3.2 Modelling Approach .....	37
3.3 Finite Element Analysis using ANSYS .....	39

3.3.1	Element type.....	39
3.3.2	Material properties.....	39
3.3.3	Model geometry.....	44
3.3.4	Residual stress modelling.....	54
3.4	Loading in presence of residual stress for regular weld shape model.....	59
3.5	Loading in absence of residual stress for regular weld shape.....	65
3.6	Loading in presence of residual stress for ground weld model.....	68
3.7	Results and Discussion.....	70
3.7.1	The Effect of Residual Stress on Fatigue life.....	70
3.7.2	The Effect of Stress Concentration on Fatigue life.....	76
<b>CHAPTER 4 EXPERIMENTAL FATIGUE TESTS.....</b>		<b>82</b>
4.1	Introduction.....	82
4.2	Testing conditions and specimens preparation.....	82
4.3	Equipment and Test Set-up.....	84
4.4	Regular Weld Fatigue Tests.....	87
4.5	Ground flush specimens fatigue Tests.....	90
4.6	Test Results and Discussion.....	92
<b>CHAPTER 5 COMPARISON OF NUMERICAL AND EXPERIMENTAL RESULTS.....</b>		<b>94</b>
5.1	Introduction.....	94
5.2	Comparison between numerical modelling and experimental data for regular weld.....	94
5.3	Comparison between numerical modelling and experimental data for ground flush specimens ...	97
<b>CHAPTER 6 CONCLUSIONS AND RECOMMENDATIONS FOR FURTHER RESEARCH.....</b>		<b>99</b>
6.1	Conclusion.....	99
6.2	Recommendation for future work.....	100
<b>REFERENCES.....</b>		<b>101</b>



## LIST OF TABLES

Table 3-1: Chemical Properties of steel AS/NZS 3679.1-300 grade.....	39
Table 3-2: Mechanical properties of steel AS/NZS 3679.1-300 grade.....	40
Table 3-3: Mechanical properties for material produced by E6013 electrode.....	41
Table 3-4: Fatigue parameters for steel AS/NZS 3679.1-300 grade.....	41
Table 3-5: Simulation data for five meshed models with different element edge length subjected to 1 N bending load.....	53
Table 3-6: Comparison of data generated from the simulation of regular weld.....	63
Table 3-7: Fatigue life for the regular weld in presence of residual stress estimated from ANSYS simulation data by the Morrow equation and Smith–Watson–Topper Equation.....	64
Table 3-8: Comparison of data generated by simulations of regular weld shape model when the residual stresses are relieved.....	66
Table 3-9: Fatigue lives for regular weld in absence of residual stress estimated from ANSYS simulations data and by Morrow equation and Smith–Watson–Topper Equation.....	67
Table 3-10: Comparison of data generated by simulations of ground weld shape.....	69
Table 3-11: Fatigue lives for a ground weld shape specimen estimated from ANSYS simulations data and by Morrow equation and Smith–Watson–Topper equation.....	69
Table 3-12: Comparison between stress data of regular weld model and stress relief model generated by ANSYS.....	74
Table 3-13: Comparison between strain data of regular weld model and stress relief model generated using ANSYS.....	75
Table 3-14: Comparison between stress data of regular weld models and ground models generated by ANSYS.....	79
Table 3-15: Comparison between strain data of regular weld model and ground model generated using ANSYS.....	80
Table 3-16: Comparison between fatigue life estimations for regular weld models and ground models generated by Eqs. (2-5) and (2-6).....	81
Table 5-1: Experimental and numerical load-deflections.....	95

## LIST OF FIGURES

Figure 2-1: An S-N diagram plot of the results of fatigue test for a ferrous metal (Shigley et al., 2004) .....	8
Figure 2-2: True stress–true strain hysteresis loops (Shigley et al., 2004) .....	9
Figure 2-3: log-log graph of true-strain amplitude related to the fatigue life for hot-rolled SAE 1020 steel. (Shigley et al., 2004) .....	10
Figure 2-4: a) Different mean stress with the same cycle amplitude b) effect of various mean stress level on strain amplitude (Malik, 2006) .....	11
Figure 2-5: Fatigue crack growth curve ( $da/dN$ vs. $\Delta K$ ) (Shigley et al., 2004) .....	13
Figure 2-6: Geometry of single-pass butt-welds. (Teng et al., 2003) .....	16
Figure 2-7: Longitudinal residual stress distribution along the X-direction.(Teng et al., 2003) .....	17
Figure 2-8: Longitudinal residual stress distribution along the Y-direction. (Teng et al., 2003) .....	17
Figure 2-9: Transverse residual stress distribution along the Y-direction. (Teng et al., 2003) .....	18
Figure 2-10: Transverse residual stress distribution through the thickness.(Teng et al., 2003) .....	18
Figure 2-11: The relationship between the notch tip elastic and corresponding elastic-plastic stress and strain response according to Neuber’s (1946) rule .....	20
Figure 2-12: Neuber rule in the presence of the residual stress (Kahvaie-Zad, 2005)....	21
Figure 2-13: Stress state at the weld toe region .....	23
Figure 2-14: Stress distribution through thickness and longitudinal direction near the weld toe for welded specimen subjected to axial and bending load. ....	25
Figure 2-15: Weld geometry parameters.....	27
Figure 2-16: Hou (2007) specimen geometry and stress contour plot of cruciform welded joint subjected to axial tensile load .....	29
Figure 2-17: Stress concentration factor along the weld toes for four sides of a cruciform welded joints subjected to axial loading (Hou, 2007).....	30
Figure 2-18: Probability density histogram of stress concentration factor appearing in weld lines (Hou, 2007).....	31
Figure 2-19: Crack initiation zone (Hobbacher, 2008) .....	35
Figure 3-1: The weld zone and AS/NZS 3679.1-300 grade material properties .....	42
Figure 3-2: Stress-Strain behaviour after unloading .....	42
Figure 3-3: Typical hysteresis loop in the stress-strain curve for fully reversible loading .....	43

Figure 3-4: Total stress -total strain for multi-linear kinematic hardening (ANSYS 14.5 Document).....	43
Figure 3-5: Test set up used by Baik et al. (2011) to study of fatigue life for a welded specimen subjected to bending .....	45
Figure 3-6: 3D finite element solid model of a butt weld joint.....	45
Figure 3-7: Initial meshing.....	46
Figure 3-8: X direction Stress distribution around the weld toe .....	46
Figure 3-9: Changing the mesh size along the plate width (Z direction).....	47
Figure 3-10: Stress and strain distribution along the attachment line of the weld toe for two types of meshing .....	48
Figure 3-11: Typical stress distribution near the weld zone of a welded joint subjected to bending.....	49
Figure 3-12: A schematic of mesh size effect on the stress concentration factor.....	49
Figure 3-13: Stress distribution around the weld toe for the two geometries .....	50
Figure 3-14: Five types of meshing to investigate the effect of cross section meshing size. The elements edge length at the weld toe is (a) 0.50 mm, (b) 0.40 mm, (c) 0.31 mm, (d) 0.25 mm and (e) 0.20 mm. ....	52
Figure 3-15: Stress concentration factor vs element edge length at the weld toe .....	54
Figure 3-16: Residual stress contour for regular weld produced by applying the initial strain ( $\epsilon_z$ ) of 0.004 at the base plate surface's elements near the weld toe (1 mm depth and 7 mm length) .....	55
Figure 3-17: Residual stress contour for ground weld produced by applying the initial strain ( $\epsilon_z$ ) of 0.004 at the base plate surface's elements near the weld toe (1 mm depth and 7 mm length) .....	56
Figure 3-18: Transverse residual stress distribution along the X-direction generated in ANSYS.....	57
Figure 3-19: Longitudinal residual stress distribution along the X-direction generated in ANSYS.....	58
Figure 3-20: Transverse residual stress distribution along the Z-direction generated in ANSYS.....	58
Figure 3-21: Longitudinal residual stress distribution along the Z-direction generated in ANSYS.....	59
Figure 3-22: Bending moment per unit width versus deflection .....	60
Figure 3-23: Stress-Strain ( $\sigma_x$ - $\epsilon_x$ ) hysteresis loop for a 70 mm cyclic deflection.....	61
Figure 3-24: An enlarged portion of hysteresis loop around the maximum stresses and strains .....	62

Figure 3-25: Hysteresis loops in the critical element at the base plate surface and plane of symmetry generated by bending load for regular weld shape in presence of residual stress.....	63
Figure 3-26: Stress distribution along the weld toe for deflection amplitude of 50 mm	65
Figure 3-27: Strain distribution along the weld toe for deflection amplitude of 50 mm	65
Figure 3-28: Hysteresis loops in the element at the base plate surface and plane of symmetry generated by bending load for regular weld shape in the absence of residual stress.....	66
Figure 3-29: Hysteresis loops in the element at the base plate surface and plane of symmetry generated by bending load for ground weld shape in the presence of residual stress.....	68
Figure 3-30: Longitudinal stress distributions of residual stress, external loading stress and a combination of external loading stress and residual stress.....	71
Figure 3-31: Hysteresis loops for cyclic bending with deflection of 40 mm.....	72
Figure 3-32: Hysteresis loops for cyclic bending with deflection of 90 mm.....	72
Figure 3-33: Comparison between maximum stresses of regular weld model and residual stress relief model for different loadings.....	73
Figure 3-34: Comparison between maximum strains of regular weld model and residual stress relief model for different loadings .....	73
Figure 3-35: Low cycle fatigue life estimation by two equations for two conditions of regular weld model and residual stress relief model.....	76
Figure 3-36: Hysteresis loops for cyclic bending with deflection of 40 mm.....	77
Figure 3-37: Hysteresis loops for cyclic bending with deflection of 90 mm.....	77
Figure 3-38: Comparison between maximum stresses of regular weld model and ground model for different loadings.....	78
Figure 3-39: Comparison between maximum strains of regular weld model and ground model for different loadings.....	78
Figure 3-40: Low cycle fatigue life estimation by two equations for two conditions of regular weld model and ground model.....	81
Figure 4-1: Welding preparation and fit-out.....	83
Figure 4-2: Welded joints specimen .....	83
Figure 4-3: Common test set-up for bending fatigue test .....	84
Figure 4-4: Test set up prepared for the current study.....	85
Figure 4-5: Shake table limitation chart.....	86
Figure 4-6: Load cell.....	87
Figure 4-7: Reversible displacement input .....	88

Figure 4-8: Displacement and loading amplitudes, (a1) displacement amplitude at the test start, (a2) loading amplitude at the test start, (b1) displacement amplitude at the middle of the test, (b2) loading amplitude at the middle of the test, (c1) displacement amplitude at the end of the test, (c2) loading amplitude at the end of the test and (d) peak loads vs number of cycles.....	88
Figure 4-9: Fully developed fatigue crack along the weld toe.....	89
Figure 4-10: Weld quality in the middle and at the end of specimens.....	90
Figure 4-11: Fully developed fatigue crack along the weld toe in a ground flush specimen.....	91
Figure 4-12: Major defects and porosities in welds material that led to ignoring some specimen test results.....	91
Figure 4-13: Maximum bending loads in each cycle applied on regular weld specimens .....	92
Figure 4-14: Maximum bending loads in each cycle applied on ground flush specimens .....	93
Figure 4-15: Failure cross section.....	93
Figure 5-1: Load-deflection graph .....	95
Figure 5-2: Numerical and experimental data comparison for regular weld specimens	96
Figure 5-3: Semi-analytical and experimental data comparison for ground flush specimens .....	97
Figure 5-4: Comparison of experimental result for regular weld and ground flush .....	98

## NOTATION

The symbols used in this report, including their definitions, are listed below.

$\epsilon_e$	Amplitude of the elastic component
$\epsilon_p$	Amplitude of the plastic component
$\sigma'_f$	Fatigue strength coefficient
$\epsilon'_f$	Fatigue ductility coefficient
$E$	Modulus of elasticity
$N$	Number of cycles to failure
$b$	Fatigue strength exponent
$c$	Fatigue ductility exponent
$\Delta\epsilon$	Total strain range
$\Delta\sigma$	Total stress range
$\sigma_m$	Mean stress
$S$ or $\sigma_n$	Nominal stress
$\sigma_{max}$ or $\sigma_{peak}$	Maximum stress
$\sigma_{min}$	Minimum stress
$\sigma_r$	Residual stress
$\epsilon_r$	Residual strain
$e$	Nominal strain
$K_I$	Stress intensity factor
$\Delta K_I$	Stress intensity range per cycle
$\beta$	Stress intensity modification factor
$a$	Crack length
$C$	Strain-strengthening coefficient (empirical material constants)

$m$	Strain-strengthening exponent (empirical material constants)
$a_i$	Initial crack size
$a_c$	Final (critical) crack size
$K_t$	Theoretical stress concentration factor
$K_\sigma$	Local stress concentration factor
$K_\varepsilon$	Local strain concentration factor
$K_w$	Notch stress concentration factor
$K_{t,hs}$	Hot spot stress concentration factor
$\sigma_{hs}$	Hot spot stress
$\sigma_{hs}^m$	Pure axial hot spot stress
$\sigma_{hs}^b$	Pure bending is hot spot stress
$K_{t,hs}^m$	Axial stress concentration factor
$K_{t,hs}^b$	Bending stress concentration factor
$K_w$	Notch SCF due to the weld profile
$\theta$	Local weld angle
$\rho$	Weld toe radius
$t$	Plate thickness
BM	Bending moment per unit width
F	Bending load
l	Length
w	Width

# CHAPTER 1 INTRODUCTION

## 1.1 Preamble

The advantages of welding as a joining process include high joint efficiency, simple set up and low fabrication costs. These advantages are the reasons that most steel structures in engineering practice today are fabricated by welding. Welded zones are usually the weakest section of a structure. One of the most serious challenges in construction industry is welded steel structures' failure and the majority of these mechanical failures in welded structures are due to fatigue. Cyclic loading is a major concern that produces fatigue damage in welded components of a steel structure. It is very common that a welded joint withstands frequent load cycles. Progressive damage due to repeated loading is failure cause. The damage starts with a small crack which gradually propagates through the substance. To design components safe, engineers are keen to deal with welds with consistently higher fatigue strength and reasonable cost. Thus, a better understanding of the fatigue behaviour, as one of the most important damage criteria, is necessary. Fatigue cracks in fabricated steel structures often occur due to stress concentrations caused by geometry and welding process. The rate of fatigue crack propagation varies and depends on stress intensity, the number of loading cycles and many other shape and material factors.

Heating locally, highly non-uniform temperature distribution and sudden cooling cause severe thermal stresses. This thermal stress, in the form of residual stress, remains in the welding zone. The presence of residual stresses in welded structures increase the probability of brittle failure and during external cyclic loading and this has significant effect on the fatigue behaviour (Taljat et al., 1998).

To generate the elementary stress equations for axial loading, bending or torsion, it is assumed that there are no irregularities in the part under consideration while avoiding cross section changes in design is quite difficult most of the time. Any holes, grooves, shoulders, notches or other cross section discontinuities in a specimen can alter the stress field near the discontinuity and, therefore, that basic stress equations can no longer determine the stress state at these locations. These irregularities are named stress



raiser and the areas in which they appear are called stress concentration regions. For the welded joints fatigue failure originates at the stress concentration zone while occurs at the weld toe. The stress peak at the critical points, which are called hot spot regions, is used to determine estimation for fatigue life.

The following issues must be considered in safe fatigue design of a welded joint:

- Estimation of material and weld mechanical properties
- Stress analysis
- Fatigue life prediction
- Fatigue testing

The basis of fatigue life prediction for welded structures is stress analysis carried out using Finite Element Method (FEM). Finite Element software like ANSYS could help analyse the nonlinear model of weld geometry and provide the required stresses and strains. The ability to model arbitrary complex geometry is the greatest practical advantage of FEM and has made it a powerful accepted tool in recent years. ANSYS allows different material properties to be applied to different zones and it can also handle imposed residual stress. The fatigue life prediction of welded joints based on stress analysis using FEM can be carried out in many different ways with varying degrees of time investment and accuracy. A large FEM model increases the model preparation time, also the computation time and requires substantial computing resources which may make solving such problems impossible. Choosing critical locations and model simplifications would help make the process shorter, while the accuracy of the analysis could remain the same as the one achieved from complex finite element models (Kahvaie-Zad, 2005).

The focus of this research is on low cycle fatigue caused by extreme but short cyclic loads such as cyclonic wind loads. A feature of a low cycle fatigue problem is high stresses and low load cycles versus traditional fatigue problems involving low stress levels and very large number of load cycles.

## 1.2 Background

Northern Australia faces cyclonic wind events every year from October to May. Cyclonic winds can produce strong fluctuating and sustained forces on structures exposed to wind. Highway traffic signs, light poles, mobile antenna towers, metal roof claddings, guyed masts, chimneys and long span bridges are the type of structures which can suffer severe damage by large amplitude self-excited vibrations at strong wind velocities and subsequently, fail due to low cycle fatigue (Repetto and Solari, 2010, Henderson and Ginger, 2011). Cyclone Yasi with peak gust wind speed of 285 km/h crossed the Queensland coast in February 2011, causing a total loss of approximately A\$3.5 billion. Engineers are keen to maximise their design effectiveness by conceptual understanding of inelastic material behaviour especially under cyclic loads. To ensure reliability and efficiency of design, having knowledge about low cycle fatigue life in locations with more chance of failure is critical.

Welds are susceptible to fail by fatigue due to high tensile residual stresses, stress concentration, and material discontinuities introduced by the welding process. Residual stresses add to loading stresses and cause reduction of both high- and low-cycle fatigue strengths at the weld toe, especially for high cycle fatigue. A considerable amount of research has been performed to date on the concept of fatigue life prediction of welded joints and different aspects of this phenomenon like effects of welding process, geometry, loading type, effects of residual stress and weld treatment effects on life, have been considered, but limited studies have been performed on structural analysis of a welded joint by means of FEM and applying residual stress and loading at the same time.

It has been proven that weld treatment techniques have positive effects on extending life of welded joints subjected to high cycle fatigue (Roy and Fisher, 2008). However, this effect for low cycle fatigue has not yet been studied as widely as high cycle fatigue. Weigand and Berman (2012) worked on weld treatment on low-carbon steel butt weld joint under cyclic axial load to improve low cycle fatigue life. They used several different weld treatments like ground flush, burr ground and TIG dressed (remelting of the burrs by TIG electrode at the weld toe).

Ground flush treatment removes the slag inclusions and surface defects left after the welding process and also changes the weld geometry discontinuities and consequently changes the stress concentration. Stress concentration factor reduction can help decrease the peak stress at the hot spot and increase the weld fatigue life. This positive effect is clear for high cycle fatigue situations but in low cycle fatigue cases has to be investigated more thoroughly.

To achieve more accurate estimation of the welded joints fatigue life, the initial residual stress should be considered because it can shift the loading stress and strain range as the mean stresses do (Weigand and Berman, 2012). Therefore, the relaxation of residual stresses can reduce the risk of failure. Heat treatment is the most common method to enhance the fatigue life. Heat treatment can cause the residual stress to be mitigated or eliminated and can help increase the life especially in high cycle fatigue cases (Nunes and Committee, 1991) but as the stress concentration effect, the residual effect on life in low-cycle fatigue loading cases is less clear.

### **1.3 Objectives of this research**

The main objective of this study is to investigate the low cycle fatigue behaviour of low carbon steel butt-welded joints subjected to bending cyclic loads for two different weld treatment situations. They include weld heat treatment which eliminates residual stress, and flush grinding which improves stress concentration condition, compared to ordinary weld shape in the presence of residual stress in order to determine the significance of residual stresses and stress concentration in estimating the fatigue life of welded joints in low cycle fatigue situations. Although flush grinding may somehow cause the release of residual stress, the pessimistic assumption is that it does not have any effect on the residual stress distribution.

Accordingly, this research work shall aim to extend the knowledge and develop a procedure to obtain stress and strain data from 3 dimensional finite element models and use the data for weld life estimation. Thus, after a wide literature review on previous research about welded joints fatigue life estimation, welded butt joints under bending load were selected to be investigated.

The main goal of this research project is to develop a method to generate the stress and strain distributions around the weld zone produced by a combination of actual loading and residual stress by means of ANSYS software. This would allow the analyst to benefit from the analytical data and calibrate the FE model by the use of experimental results.

The work to be carried out by the candidate address the following:

- Creating a stress field which represents the residual stress as the initial state;
- Determining stress and strain through weld toe line by applying the peak load of the cyclic loading;
- Predicting the total fatigue life as a function of the stress and strain distribution;
- Experimental testing and comparison of results with the finite element modelling data.

To verify the accuracy and reliability of the analytical study of welded joints fatigue life, using experimental testing is inevitable. Therefore, a fatigue test set-up is needed for testing specimens subjected to cyclic loadings.

#### **1.4 Project plan and time table**

Regarding the project plan with due regard to time available, the entire project is divided into three main phases. Phase 1 was the literature search. In this phase, previous investigations on fatigue analysis methodology, effects of residual stress, effects of stress concentration, finite element modelling and weld material properties were studied. Phase 2 consisted of modelling, analytical study and project experimental works. In the third phase, the final laboratory testing and computational modellings were performed and the data obtained from finite element modelling and experimental testing were analysed.

Phase 1 - Literature studies (3 months)

Phase 2 - Experimental works and data analysis (10 months)

Phase 3 – Final testing and data analysis (4 months)

## 1.5 Thesis Overview

Chapter 1 provides a brief introduction to welded joints fatigue life and a background providing motivation to initiate this research study. In this chapter the objectives relevant to this research are stated and the whole project plan is explained.

Chapter 2 gives a review of the literature on subjects related to the fatigue analysis methodology of the steel structures. It also introduces the factors that influence the fatigue failure of a welded joints including presence of residual stress and stress concentration. They are the factors that intensify the risk of failure. Finally, in this chapter, brief reviews of the literature on finite element modelling and former works on material properties of the weld zone are described.

Chapter 3 presents an analytical solution to estimate the fatigue life for butt weld joints under three conditions. The first condition is regular weld which contains residual stress as well as stress concentration factor. In the second condition, the residual stress distributions in the welded specimen models are eliminated. The geometry that produces the stress concentration in weld toe is changed in the third condition. The stress and strain distributions generated by the finite element software (ANSYS) are used to analyse the effect of these changes on fatigue life.

Chapter 4 contains a comprehensive description about destructive fatigue tests performed in laboratory to verify the findings in the previous chapter. All details, limitations and test procedure are explained in this chapter. The experimental tests are divided into two parts. In part I, 5 different loads are applied on regular welds and in part II; the same loads are applied on ground flush specimens. 3 specimens for each load and 30 specimens in total are used to study the trends of number of cycles to failure for each load case.

Chapter 5 presents the comparison between the analytical predictions and experimental results of the low cycle fatigue life for butt welded joints.

Finally, significant conclusions draw from this research are presented together with some recommendations for future works in Chapter 6.

## CHAPTER 2 LITERATURE REVIEW

### 2.1 Introduction

Study on fatigue behaviour of steel structures started in the middle of the 19th century when rail infrastructures such as locomotive axles starting to fail under cyclic loading (Bhat and Patibandla, 2011). Engineers began to study the effects of cyclic loads on iron and steel specimens. The first study of metal fatigue is believed to have been conducted by a German mining engineer, Albert, (1838). He worked on mine-hoist chains made from iron. The first systematic investigation of the fatigue phenomenon was performed by Wohler (1867). He introduced the concept of the S-N diagram and showed that the fatigue life decreases as the stress amplitude increases and under certain stress amplitudes test samples do not fail. Basquin (1910) proposed an empirical law to mathematically describe the fatigue S-N curves. He showed that in the finite life region the S-N curve could be represented as a linear log-log relationship. Langer (1937) studied fatigue under variable amplitude loading and separated the fatigue life into the crack initiation and crack propagation phases. Moreover, Neuber (1946) investigated the notch effect, Tavernelli and Coffin (1962) and Manson et al. (1963) presented the plastic strains idea and also, the stress intensity factor,  $K$ , was introduced by Irwin (1957). Until 1990 many researchers studied the complicated problems like fatigue growth rate, threshold stress intensity factor, in-phase and out-of-phase multi-axial fatigue. The fatigue design philosophy for welded components was first introduced in design guidelines for tubular joints in offshore structures, based on the hot spot stress concept (ANSI/AWS-D1, 1990).

### 2.2 Fatigue analysis methodology

Three major fatigue life estimation methods are used to predict the number of cycles which an object withstands till final failure. These methods are listed below (Shigley et al., 2004):

- Stress-life method
- Strain-life method

- Linear-elastic fracture mechanics method

### 2.2.1 Stress-life method

The most traditional and least accurate approach, especially for low cycle fatigue applications, is *the stress-life* method which is based on stress level only. In this method, a large number of similar specimens are subjected to different range of cyclic loads while the cycles to failure are counted. These results will form S-N diagram for that geometry. For ferrous metals this log-log chart would be divided into three distinguished regions, from  $N = 1$  to  $N = 1000$  is classified as low cycle fatigue, from lifetime  $N = 1000$  to  $10^7$  or  $10^6$  as high cycle fatigue and more than this range will be infinite life region (Figure 2-1).

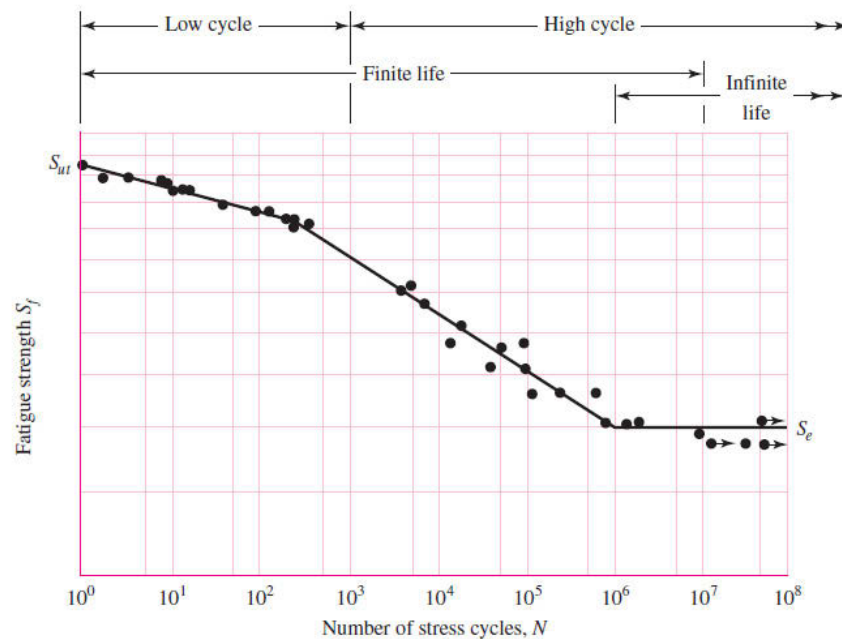


Figure 2-1: An S-N diagram plot of the results of fatigue test for a ferrous metal (Shigley et al., 2004)

In the case of steel, the strength corresponding to the infinite-life region is called the endurance limit  $S_e$ , or the fatigue limit.

This method is the easiest to apply for a wide range of fatigue design applications, especially in high cycle cases, but care should be exercised when it is used for low-cycle

cases because it cannot account for the true stress-strain behaviour when localised yielding occurs.

### 2.2.2 Strain-life method

The best approach to study the fatigue failure, especially in low cycle case, is the *strain-life* method which is based on occurring plastic strain at a local discontinuity that caused stress concentration. At the discontinuity, plastic strains will appear when the stress level exceeds the elastic limit (Figure 2-2).

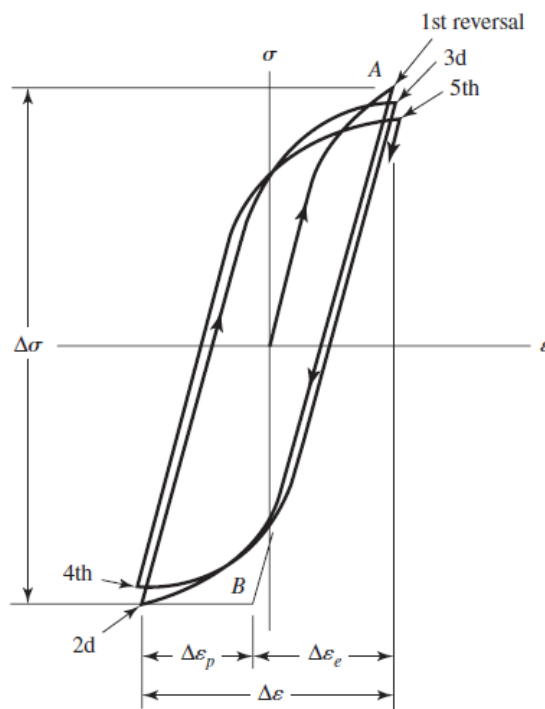


Figure 2-2: True stress–true strain hysteresis loops (Shigley et al., 2004)

Basquin (1910) worked on the relationship between the elastic strain amplitude and number of cycles to failure and also Manson et al. (1963) and Tavernelli and Coffin (1962) found the equation relating the plastic strain to the cycles. The mathematical equations are as follows:

$$\varepsilon_e = \frac{\sigma'_f}{E} (2N)^b \quad (2-1)$$



$$\varepsilon_p = \varepsilon'_f (2N)^c \quad (2-2)$$

Where  $\varepsilon_e$  and  $\varepsilon_p$  are amplitudes of the elastic and plastic strain components, respectively,  $\sigma'_f$  and  $\varepsilon'_f$  are fatigue strength and fatigue ductility coefficients, respectively, E is modulus of elasticity, N is the number of cycles to failure, b and c are fatigue strength and fatigue ductility exponents.

Figure 2-3 shows the results from Basquin, Manson and Coffin (Shigley et al., 2004) as a log-log diagram which relates fatigue life to the true strain amplitude for hot-rolled SAE 1020 steel.

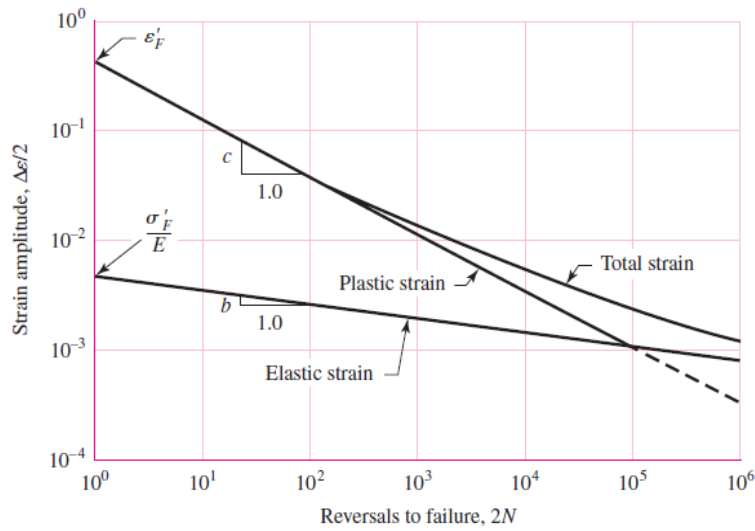


Figure 2-3: log-log graph of true-strain amplitude related to the fatigue life for hot-rolled SAE 1020 steel. (Shigley et al., 2004)

According to this approach the total-strain range is:

$$\varepsilon = \varepsilon_e + \varepsilon_p \quad (2-3)$$

This can be clearly seen in Eq. (2-3), by summing the plastic and elastic strains, the total strain-life equation known as the Manson-Coffin equation can be derived as follows:

$$\frac{\Delta\varepsilon}{2} = \frac{\sigma'_f}{E} (2N)^b + \varepsilon'_f (2N)^c \quad (2-4)$$

This equation is generated for fully reversed cyclic stress with zero mean stress but so often the loading fluctuates around non-zero values. Therefore, in practice, applying some modifications is necessary. The effect of mean stress on strain-life curve is shown in Figure 2-4.

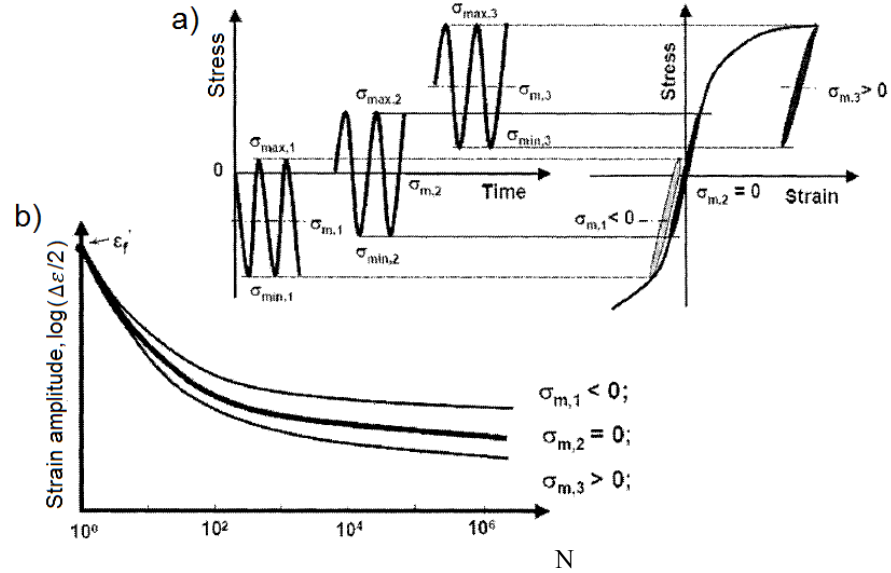


Figure 2-4: a) Different mean stress with the same cycle amplitude b) effect of various mean stress level on strain amplitude (Malik, 2006)

It is clear that various mean stresses, but with similar cyclic stress amplitudes, will significantly change fatigue lives so that the tensile mean stress decreases the life while the compressive mean stress has life increasing effects.

There are different models to modify the strain-life of Eq. (2-4). Morrow (1968) and Smith et al. (1969) modified the Manson–Coffin equation and suggested the following equations, respectively:

$$\frac{\Delta\varepsilon}{2} = \frac{\sigma'_f - \sigma_m}{E} (2N)^b + \varepsilon'_f (2N)^c \quad \text{Morrow Eq.} \quad (2-5)$$

$$\sigma_{\max} \frac{\Delta\varepsilon}{2} = \frac{\sigma'_f{}^2}{E} (2N)^{2b} + \sigma'_f \varepsilon'_f (2N)^{b+c} \quad \text{Smith–Watson–Topper Eq.} \quad (2-6)$$

Where  $\sigma_m$  is the mean stress and  $\sigma_{\max}$  is the maximum stress.

The SWT parameter ( $\sigma_{\max} \frac{\Delta \varepsilon}{2}$ ) shows that when the maximum stress is zero or the stress is compressive, no fatigue occurs. This situation should be considered when the Morrow equation is used for a case with the maximum stress of zero or less.

### 2.2.3 Linear-Elastic Fracture Mechanics (LEFM) method

According to this method, a fatigue process has three stages. At stage I, crystal slip happens through contiguous grains, inclusions and surface imperfections. This is invisible and just involves several grains. The second stage is crack extension. In this phase new areas are created and the crack propagates so that it can be observed with available instruments like electron microscope. The crack grows until stage III. At stage III the crack is long enough so that the material cannot resist the stress amplitude and rapid acceleration of crack growth occurs (Anderson, 2005).

LEFM method is based on the analysis of fatigue crack propagation. The stress intensity factor,  $K_I$ , is used in fracture mechanics to define the stress state near the tip of a crack and it represents the combination of stress and crack geometry in the case of monotonic load and  $\Delta K_I$  is used for cyclic loading. The stress intensity range per cycle is:

$$\Delta K_I = \beta(\sigma_{\max} - \sigma_{\min})\sqrt{\pi a} = \beta \Delta \sigma \sqrt{\pi a} \quad (2-7)$$

Where  $\beta$  is the stress intensity modification factor and  $a$  is the crack length.

The fatigue crack propagation data are usually plotted on log-log coordinates in the form of the fatigue crack growth rate,  $da/dN$ , versus stress intensity range factor,  $\Delta K_I$ . a schematic of this log-log curve is shown in Figure 2-5. The curve is limited by the threshold stress intensity range where a crack does not grow below this amount and the critical stress intensity factor. The critical stress intensity factor is also called the fracture toughness of the material.

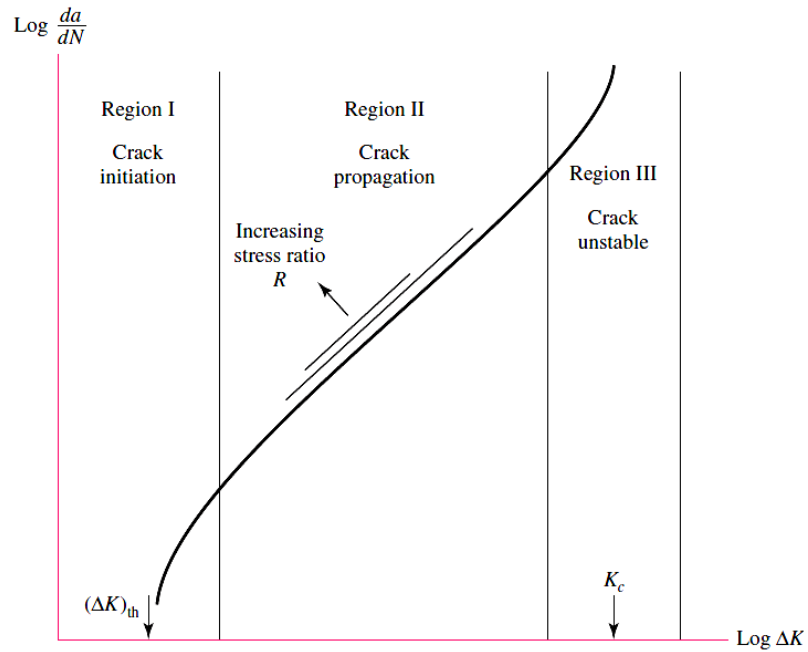


Figure 2-5: Fatigue crack growth curve ( $da/dN$  vs.  $\Delta K$ ) (Shigley et al., 2004)

The three stages of crack growth are clear in Figure 2-5 and stage II data show a linear behaviour on log-log scale.

The fatigue crack growth is described by an expression which is a function of stress intensity range:

$$\frac{da}{dN} = f(\Delta K) \quad (2-8)$$

As described above, the fatigue crack growth curve in log-log scale in the mid region is essentially linear. Paris and Erdogan (1960) proposed the most accepted fatigue crack propagation relationship as below:

$$\frac{da}{dN} = C(\Delta K)^m \quad (2-9)$$

Where  $C$  and  $m$  are empirical material constants.

By integrating Eq. (2-9), the crack growth life can be calculated. The number of cycles to failure will then be:

$$N_f = \int_0^{N_f} dN = \int_{a_i}^{a_c} \frac{da}{C(\Delta K)^m} = \frac{1}{C} \int_{a_i}^{a_c} \frac{da}{(\beta \Delta \sigma \sqrt{\pi a})^m} \quad (2-10)$$

Where  $a_i$  is the initial crack size and  $a_c$  is the final (critical) crack size.

It should be noted that just tensile stress has an effect on crack propagation and compressive stress cannot cause fatigue failure. For this reason, in the presence of compressive stress it is necessary to employ some correction in the integration above as below:

$$\begin{aligned} \Delta K &= K_{\max} - K_{\min} & \text{if} & & K_{\min} > 0 \\ \Delta K &= K_{\max} & \text{if} & & K_{\min} < 0 \\ \Delta K &= 0 & \text{if} & & K_{\max} < 0 \end{aligned} \quad (2-11)$$

A crack starts growing when the stress intensity range exceeds threshold stress intensity range and the crack growth increases cycle by cycle. If the stress intensity modification factor ( $\beta$ ) or stress range ( $\Delta\sigma$ ) varies in the integration above, it would be impossible to calculate the life directly. In this situation, by means of the Paris equation, the crack length increment in each cycle can be calculated. The whole crack length is determined by summation of individual crack increments in each cycle,

$$a_N = a_0 + \sum_{i=1}^N \Delta a_i = a_0 + \sum_{i=1}^N C(\Delta K)^m \quad (2-12)$$

$$N = \sum_{i=1}^n \Delta N_i = \sum_{i=1}^n \frac{\Delta a_i}{C(\Delta K_i)^m} \quad (2-13)$$

The numerical integration of crack increments terminates when the maximum stress intensity factor exceeds the fracture toughness or in other words, when the crack size exceeds the critical crack.

Very accurate measurement of crack length and monitoring of crack propagation during fatigue process, are the prerequisites of using this method which are very hard and complicated in practice compared with other approaches.

### 2.3 Residual stress in welded joints

Incompatible internal permanent strain is the main reason of residual stress. In engineering structures or components, the presence of residual stresses may have significantly useful or harmful effects on the fatigue behaviour during external cyclic loading depending on its type, magnitude and distribution.

Only tensile stresses can cause fatigue failures by helping increase the growth of the fatigue crack, and so, anything that decreases or eliminates tensile stress can also decrease or eliminate the probability of a fatigue failure. In some situations, residual stresses may enhance the endurance limit and increase the fatigue life. In general, compressive residual stress is beneficial and on the contrary, tensile residual stress will be detrimental. Shot peening, hammering, and cold rolling are some means that generate compressive stresses into the surface and improvement of the endurance limit will follow.

In weld fabricated structures, due to local plastic deformation from thermal and mechanical operations and also large volume changes because of the phase transformation during the manufacturing, residual stresses are present. These stresses near welds will always be tensile with maximum values of tensile residual stresses equal to or more than the yield strength of the base plate.

Jonassen et al. (1946) studied the effect of welding procedures on residual welding stresses for butt-welded steel plates. Watanabe et al. (1955) described the effect of welding sequences on the residual stress distribution of welded joints. Kihara (1957) investigated similar effects on a shrinkage in slit-type welds and circular-path welds.

Finch and Burdekin (1992) worked on effects of applied and typical welding residual stress distributions and the significance of defects in various geometries of welded joint like butt-welded plate, weld-root defects in a thick butt-welded plate, and a pipe-on-plate butt weld. Barsoum and Barsoum (2009) developed a welding simulation procedure of the welding manufacturing process in order to predict temperature, Heat Affected Zone (HAZ) weld penetration and residual stresses by means of the FE software ANSYS. In their welding simulation, at first the temperature distributions were

predicted, then, the results from the thermal analysis were used as loads in the elastic–plastic mechanical analysis, while the mechanical material properties were considered as a function of temperature.

Teng et al. (2003) studied thermo-mechanical behaviour of welding process and evaluated the residual stress magnitude and distribution along weld line with various types of welding sequence in single-pass, multi pass butt welded plates and circular patch welds. For the analysis of the single pass butt weld, they used specimens with material SAE 1020 and geometry as in Figure 2-6.

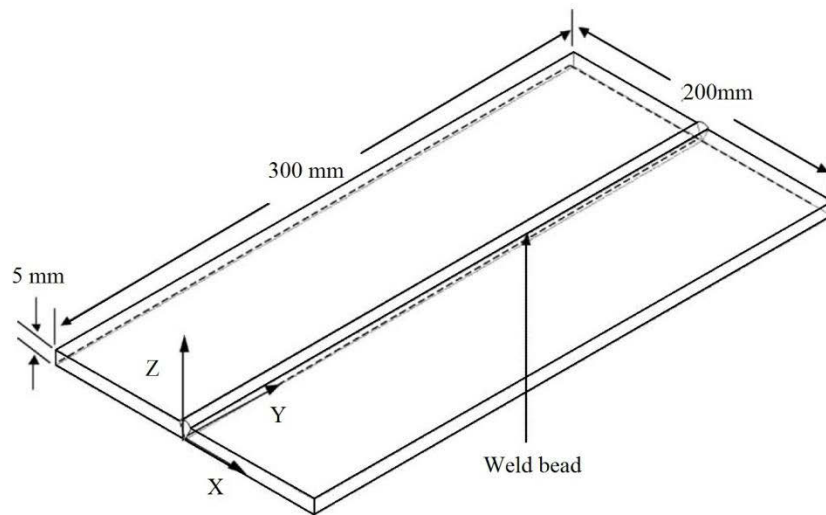


Figure 2-6: Geometry of single-pass butt-welds. (Teng et al., 2003)

They showed residual stress magnitude and distribution along weld lines as shown in Figures 2-7 to 2-10. According to their findings, for longitudinal residual stresses ( $\sigma_y$ ) along the X direction, an intensely tensile stress appears close to the weld toe and it gradually decrease until a slight compressive stress occurs far from the weld line (Figure 2-7). The longitudinal residual stress ( $\sigma_y$ ) behaviour along the Y direction is almost uniformly distributed and at the two ends it tends to zero (Figure 2-8). Transverse residual stresses ( $\sigma_x$ ) along the Y direction will be tensile with uniform distribution all across the weld line except near the two ends where they become compressive (Figure 2-10). The residual stress at the surface is tensile and gradually decreases toward the depth (Figure 2-10).

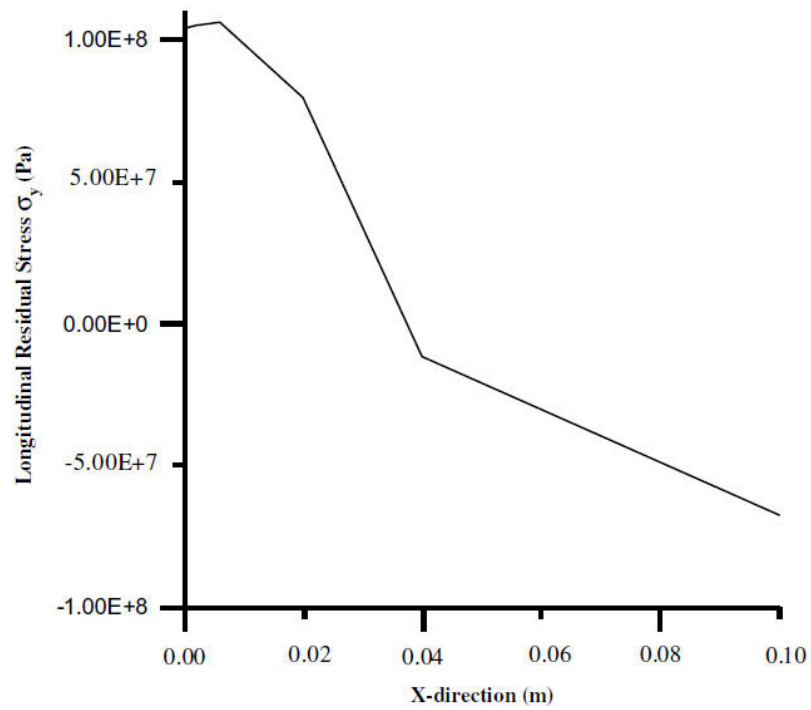


Figure 2-7: Longitudinal residual stress distribution along the X-direction.(Teng et al., 2003)

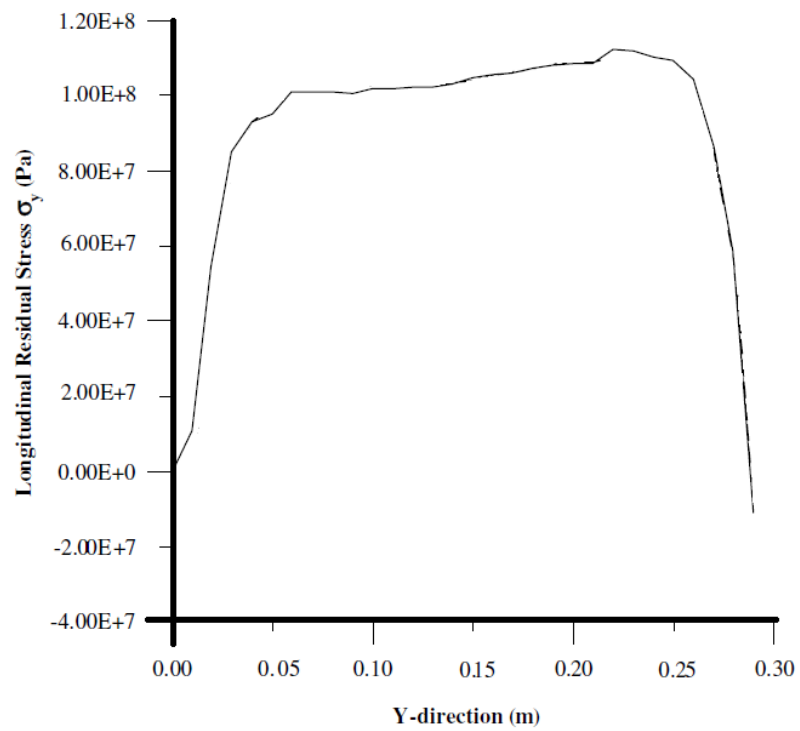


Figure 2-8: Longitudinal residual stress distribution along the Y-direction. (Teng et al., 2003)



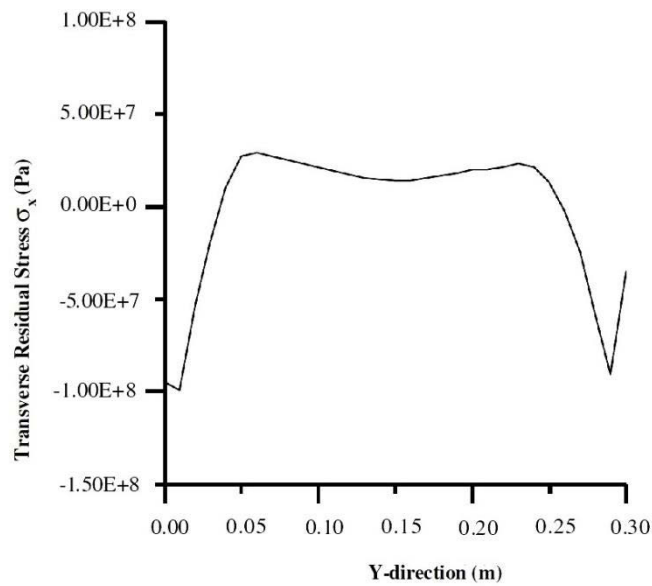


Figure 2-9: Transverse residual stress distribution along the Y-direction. (Teng et al., 2003)

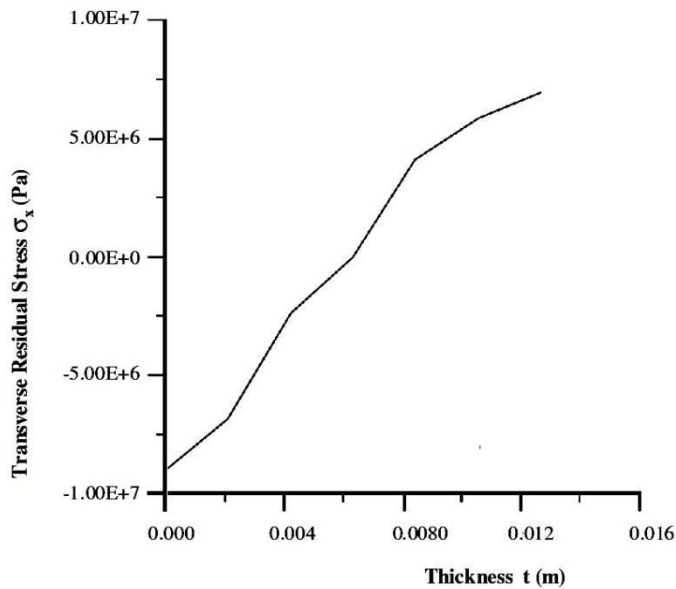


Figure 2-10: Transverse residual stress distribution through the thickness.(Teng et al., 2003)

After the conceptual understanding of the symptoms, distribution and magnitude of the residual stresses around the weld, and also determining the loading type and stress and strain distribution during the loading time, one will be able to judge the fatigue behaviour and life. Then, the question will be raised on how we could treat this

phenomenon to increase the quality of the joint service life. Some techniques are used to improve the weld profile by reducing the weld stress concentration such as pre-heating, heating after the welding process and grinding while some other techniques such as Peening methods, Overloading and stress relief treatments, all aim to relieve tensile residual stress and/or introduce compressive residual stress (Kirkhope et al., 1999). For instance, Rybicki and McGuire (1982) developed a method to reduce tensile stress of the girth welded pipes based on induction heating with flowing water. Chou and Lin (1992) presented a method to reduce residual stress for stainless steel specimens by parallel heat welding.

There are various methods for determining and characterising residual stresses in engineering components at the scale of industry or laboratory. These measurement methods are classified into three categories, Non-destructive procedures (such as X-Ray, Neutron Diffraction, Electron Diffraction, Ultra-Sonic, Electro-Magnetic, Thermo-elastic, and photo-elastic Techniques), Destructive procedures (for example, Slitting, Contour Method and Ring Core Method) and Semi-destructive procedures (such as Hole drilling and Deep Hole Drilling). Selecting the appropriate method depends on size and shape of the components, desired depth, accuracy, stress type (micro or macro), required resolution, price and many other factors (Pardowska et al., 2008).

It is impossible to linearly add the residual stress to the actual stress. When the local stress and stress at the crack tip exceed the yield limit, they do not show a linear behaviour. Neuber (1946) suggested a method to determine the actual elasto plastic stress and strain at the notch tip which is well-known as the Neuber rule.

### **2.3.1 Neuber Rule for contribution of residual stress in actual total stress**

The Neuber rule is very common to estimate plastic stress and strain at notch tip based on elastic stress and strain. According to Neuber rule, the geometric mean of the stress and strain concentration factors remain equal even when plastic yielding takes place. This constant value is called the theoretical stress concentration factor,

$$K_t = \sqrt{K_\sigma K_\epsilon} \quad (2-14)$$

where:  $K_t$  is the theoretical stress concentration factor,

$K_\sigma = \sigma/S$  is the local stress concentration factor ( $\sigma$  is the local stress,  $S$  is the nominal stress)

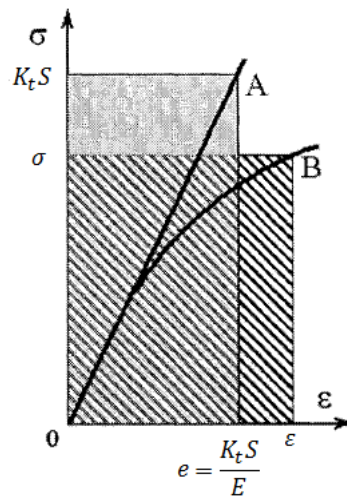
$K_\epsilon = \epsilon/e$  is the local strain concentration factor ( $\epsilon$  is the local strain,  $e$  is the nominal strain)

With the assumption that nominal stress and strain remain elastic ( $e = S/E$ ), Neuber rule derives a very important relationship between applied load and actual elasto-plastic stress and strain at the notch tip as follows:

$$\frac{(K_t S)^2}{E} = \sigma \cdot \epsilon \quad (2-15)$$

Applied load                  Notch tip Response

The Neuber rule which defines the relationship between nominal stress and strain and actual notch tip stress and strain response is shown in Figure 2-11.



$$K_t S \cdot e = \sigma \epsilon \rightarrow K_t S \cdot \frac{K_t S}{E} = \sigma \epsilon \rightarrow \frac{(K_t S)^2}{E} = \sigma \epsilon$$

Figure 2-11: The relationship between the notch tip elastic and corresponding elastic-plastic stress and strain response according to Neuber's (1946) rule

Based on the Neuber rule, the strain energy density remains the same for two cases. By means of the Neuber rule, it is possible to determine the plastic stress and strain in the presence of residual stress. At first, the equivalent elastic stress and strain of the loading should be calculated and then the residual stress could be added linearly to the equivalent elastic stress and after that, the Neuber rule should be used again to find the real stress and strain (Figure 2-12). The formulation of the Neuber rule in the presence of residual stress is as below:

$$\frac{(K_r S + \sigma_r)^2}{E} = \sigma_2 \varepsilon_2 \quad (2-16)$$

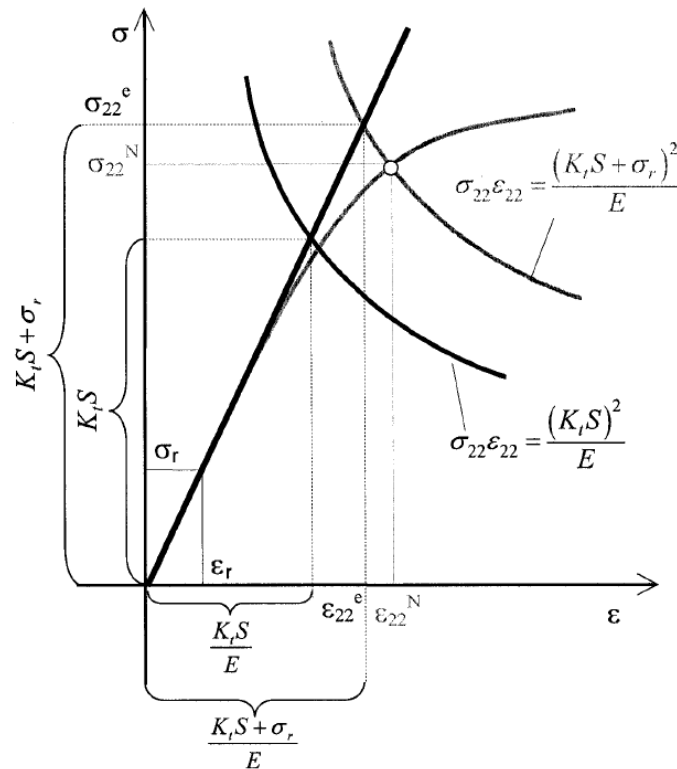


Figure 2-12: Neuber rule in the presence of the residual stress (Kahvaie-Zad, 2005).

### 2.3.2 Residual stress relief

Stress relief by post heat treatment processes are used nowadays to relieve residual stresses remaining in structures due to different manufacturing and metal forming processes like plastic bending, drawing, machining and welding.

During the heat treating, the atoms are rearranged from a momentary equilibrium situation with high potential energy level to a stable situation with lower potential energy range. The amount of stress relieved by post heat treatment relates to heating temperature and heating duration time. More residual stress relief can be achieved by longer heating period and higher temperatures (Nunes and Committee, 1991).

Olabi and Hashmi (1993) showed that by post weld heat treatment of low carbon steel AISI 1020 welded components, with soaking temperature of 650 °C, heating rate of 400 °C/hr, duration time at the maximum temperature of 2 hours and cooling rate of 40 °C/hr, the residual stresses due to welding can be almost eliminated.

Heat treatment is the most common method to enhance the fatigue life. Heat treatment can cause the RS to be mitigated or eliminated and can help increase the fatigue life, especially in high cycle fatigue cases (Nunes and Committee, 1991) but in low cycle fatigue cases, it has been studied less.

#### **2.4 Stress Concentration and Stress Distribution near the Weld Area**

Fatigue failure tends to originate at the regions with higher stress concentration like at the weld toe. The stress distribution and magnitude control the fatigue crack initiation and propagation. The stress concentration factor can be used to determine the maximum of the stress at the weld toe. Stress concentration factors are related to the geometry and loading type and all geometries have their own unique amount. The classical formulation to determine stress concentration factors only apply to simple models while the welded joints are more complicated with multiple loading types so that it is difficult to prepare a unique pattern for stress. The hot spot concept is used to overcome the problem which was first introduced in design guidelines for tubular joints in offshore structures industry (Marshall, 1991).

The 3D finite element can be applied to find out the maximum stress at the weld toe but at first the stress concentration factor should be determined. Stress concentration factors are different for different types of loading even for the same geometry. This increases the complexity of the analysis when various loads are applied at the same time. Weld

toe generally shows multi-axial stress state but usually there is no external load or stress normal to base plate surface, therefore, the stress state tensor can be simplified by plane stress state with two normal and one shear stresses (Figure 2-13).

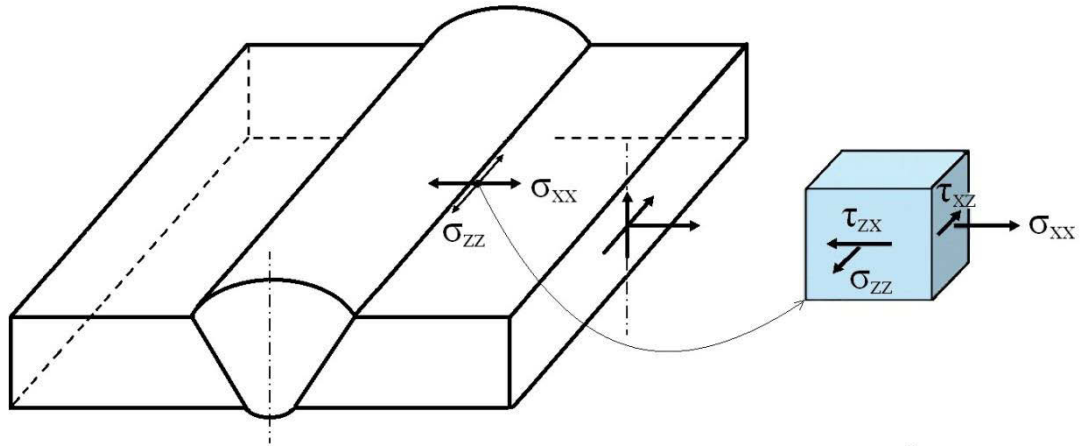


Figure 2-13: Stress state at the weld toe region

When there are no cross section discontinuities or angles, the nominal stresses are calculated by common axial or bending stress equations, but the presence of cross section discontinuities change the stress distribution along the thickness and longitudinal direction and convert them from linear and simple patterns into nonlinear and complex distributions. The real peak stresses are always higher than nominal stresses and they are related together through the following equation.

$$\sigma_{peak} = K_t \sigma_n \quad (2-17)$$

Where  $\sigma_{peak}$  is the maximum stress,  $K_t$  is stress concentration factor and  $\sigma_n$  is the nominal stress. If the stress concentration factor and nominal stress are known, the peak stress can be determined. Based on the hot spot method, it is necessary to specify the stress concentration factor and nominal stress at the location where the peak stress is important. Sometimes due to the geometry complexity in welded joints the determination of nominal stress is complicated. Therefore, the hot spot stress concept is used instead of nominal stress. The benefit of hot spot concept, compared with applying nominal stress, is that the stresses at any arbitrary cross section of the component are

determined independently. This is very practical when the geometries and loading types are complex. The peak stress based on hot spot concept is formulated as follows:

$$\sigma_{peak} = K_{t,hs}\sigma_{hs} \quad (2-18)$$

Where  $K_{t,hs}$  is the hot spot stress concentration factor and  $\sigma_{hs}$  is the hot spot stress.

The loading amplitude and gradient impact the peak stress and stress concentration factor. It means for various loading combinations applied on a specific geometry with the same  $\sigma_{hs}$ , the  $\sigma_{peak}$  and  $K_{t,hs}$  might be produced. Thus, the definition of only hot spot is not enough to arrive at an accurate stress concentration factor. To arrive at an independent stress concentration factor just related to the geometry, the magnitude part and gradient part of the hot spot load must be separated. Niemi (1995) suggested that the linearised hot spot distribution be separated into the axial and bending loads and appropriate peak stress  $\sigma_{peak}$  would be a combination of axial and bending hot spot stresses and axial and bending stress concentration factors as follows:

$$\sigma_{peak} = \sigma_{hs}^m K_{t,hs}^m + \sigma_{hs}^b K_{t,hs}^b \quad (2-19)$$

Where  $\sigma_{hs}^m$  is the pure axial hot spot stress,  $\sigma_{hs}^b$  is the pure bending hot spot stress, and  $K_{t,hs}^m$  and  $K_{t,hs}^b$  are corresponding axial and bending stress concentration factors, respectively.

The peak stress derived from stress concentration factor and hot spot stress concept is used to evaluate the fatigue strength so that several welded joints fatigue design codes and guidelines are based on this concept (Marshall, 1991). Figure 2-14 clearly shows the stress distribution along thickness and longitudinal direction for two types of loading.

As in Figure 2-14, the angle at the weld toe alters and increases the stresses in the concentration area and also, each loading produces a different stress concentration factor, therefore, the axial and bending loads with the same hot spot stress magnitudes at the surface generate different actual stresses. The actual stress field depends on the

geometric parameters such as thickness, weld toe angle and weld toe radius, while linearised hot spot stresses are independent of the geometric parameters.

In this research the hot spot approach is used to derive an appropriate three dimensional finite element model. In the hot spot concept it is assumed that for a specific welded joint geometry and for each loading type, just one stress concentration factor can be defined to describe the stress distribution through an arbitrary cross section.

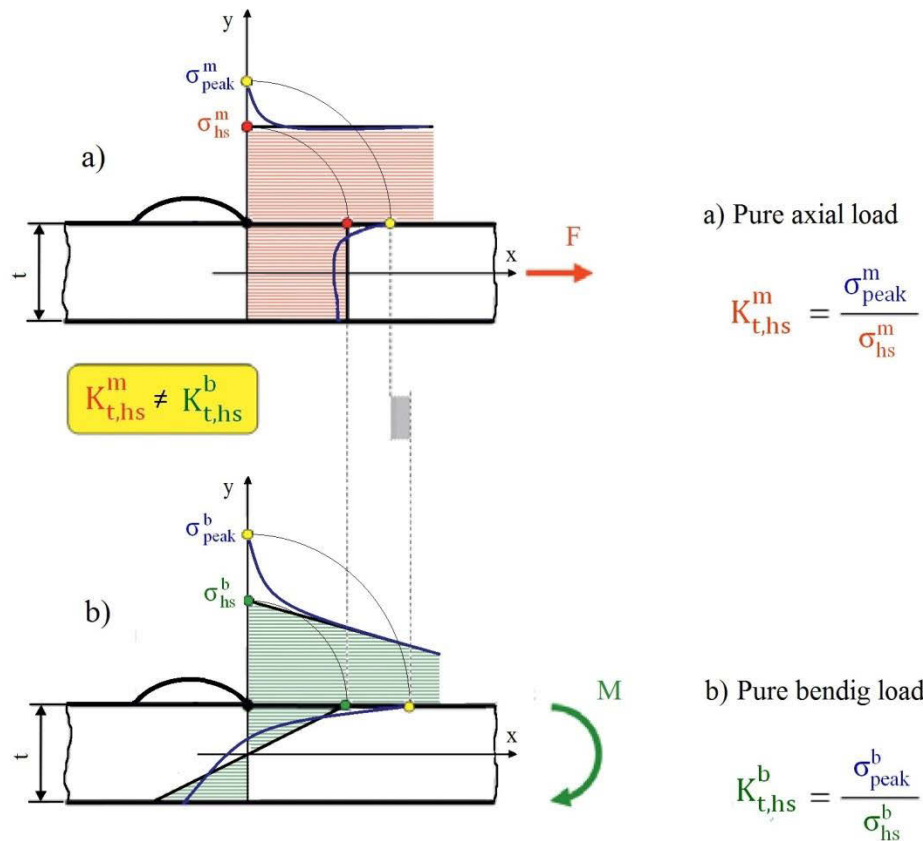


Figure 2-14: Stress distribution through thickness and longitudinal direction near the weld toe for welded specimen subjected to axial and bending load.

It is worth illustrating the distinction between the traditional nominal stress and the linearised hot spot stress. Classical nominal stress definition cannot distinguish between various loadings while the axial hot spot stress,  $\sigma_{hs}^m$ , and bending hot spot stress,  $\sigma_{hs}^b$ , can be used uniquely at any region of the weld toe.



In order to establish a reference for stress concentration factor, the hot spot stresses are generated by linearisation of the bending and axial stress fields through the cross section as follows:

$$\sigma_{hs}^m = \frac{\int_{-t/2}^{t/2} \sigma(x=0, y) dy}{t} \quad (2-20)$$

$$\sigma_{hs}^b = \frac{6 \int_{-t/2}^{t/2} \sigma(x=0, y) y dy}{t^2} \quad (2-21)$$

For external axial loading situation, the axial hot spot stress will be equal to nominal stress ( $\sigma_{hs}^m = \sigma_n$ ) and similarly, for external bending loads the bending hot spot stress will be the same as nominal stress as well ( $\sigma_{hs}^b = \sigma_n$ )

The stress concentration factors for each loading mode and specific geometry are usually defined by numerical analysis or experimental techniques. In this case, the hot spot stress being similar nominal stress, could help use the classical solution to find the appropriate stress concentration factor based on nominal stress. In the case of butt welded joints subjected to a bending load which is the focus of this thesis issue, the hot spot stress is only the bending hot spot stress and itself is equal to nominal stress,

$$\sigma_{hs} = \sigma_{hs}^b = \sigma_n \quad (2-22)$$

The following equations are used for axial and bending stress concentration factors which are derived from weld parameters (Monahan, 1995),

$$K_{t,hs}^m = 1 + 0.388 \times (\theta)^{0.37} \times \left( \frac{t}{\rho} \right)^{0.454} \quad (2-23)$$

$$K_{t,hs}^b = 1 + 0.512 \times (\theta)^{0.572} \times \left( \frac{t}{\rho} \right)^{0.469} \quad (2-24)$$

Where  $K_w$  is the notch SCF due to the weld profile,  $\theta$  is the local weld angle in radians,  $\rho$  is the weld toe radius and  $t$  is the thickness (Figure 2-15).

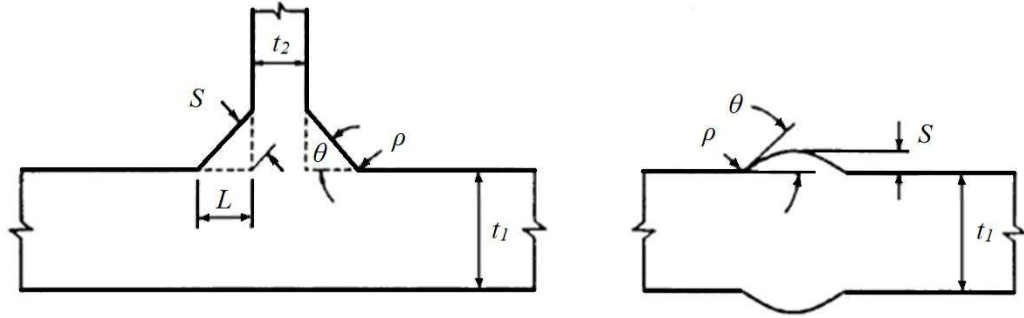


Figure 2-15: Weld geometry parameters

Monahan (1995) obtained, numerically, equations for actual stress distributions along thickness for axial and bending loads separately. For external axial loading the stress distribution through thickness is approximated by the following equation:

$$\sigma^m(0 \leq y \leq t) = \frac{K_{t,hs}^m \cdot \sigma_{hs}^m}{2\sqrt{2}} \left[ \left( \frac{y}{\rho} + \frac{1}{2} \right)^{-\frac{1}{2}} + \frac{1}{2} \left( \frac{y}{\rho} + \frac{1}{2} \right)^{-\frac{3}{2}} \right] \frac{1}{G_m} \quad (2-25)$$

where:

$$K_{t,hs}^m = 1 + 0.388 \times (\theta)^{0.37} \times \left( \frac{t}{\rho} \right)^{0.454}$$

$$G_m = 1 \quad \text{for} \quad \frac{y}{\rho} \leq 0.3$$

$$G_m = 0.06 + \frac{0.94 \times \exp(-E_m \cdot T_m)}{1 + E_m^3 \cdot T_m^{0.8} \times \exp(-E_m \cdot T_m^{1.1})} \quad \text{for} \quad \frac{y}{\rho} > 0.3$$

$$E_m = 1.05 \times \theta^{0.18} \times \left( \frac{\rho}{t} \right)^q$$

$$q = -0.12 \times \theta^{-0.62}$$

$$T_m = \frac{y}{t} - 0.3 \frac{\rho}{t}$$

From this equation, the actual stress at the surface ( $y=0$ ) will be equal to  $\sigma_{peak}^m = K_{t,hs}^m \cdot \sigma_{hs}^m$ . And also for external bending load, the stress distribution through thickness is estimated by the following equation:

$$\sigma^b(0 \leq y \leq t) = \frac{K_{t,hs}^b \cdot \sigma_{hs}^b}{2\sqrt{2}} \left[ \left( \frac{y}{\rho} + \frac{1}{2} \right)^{-\frac{1}{2}} + \frac{1}{2} \left( \frac{y}{\rho} + \frac{1}{2} \right)^{-\frac{3}{2}} \right] \frac{1 - 2 \left( \frac{y}{t} \right)}{G_m} \quad (2-26)$$

where:

$$K_{t,hs}^b = 1 + 0.512 \times (\theta)^{0.572} \times \left( \frac{t}{\rho} \right)^{0.469}$$

$$G_b = 1 \quad \text{for} \quad \frac{y}{\rho} \leq 0.4$$

$$G_b = 0.07 + \frac{0.93 \times \exp(-E_b \cdot T_b)}{1 + E_m^3 \cdot T_m^{0.6} \times \exp(-E_m \cdot T_m^{1.2})} \quad \text{for} \quad \frac{y}{\rho} > 0.4$$

$$E_b = 0.9 \times \left( \frac{\rho}{t} \right)^{-\left( 0.0026 + \frac{0.0825}{\theta} \right)}$$

$$T_b = \frac{y}{t} - 0.4 \frac{\rho}{t}$$

For external bending load situation, as well as external axial loading, actual stress at the surface ( $y = 0$ ) will be equal to  $\sigma_{peak}^b = K_{t,hs}^b \cdot \sigma_{hs}^b$ .

If the loading is a combination of axial and bending loads, superposition of through-thickness bending and axial stress distributions can give the actual stress distribution along the thickness at the weld toe.

Here in this study, to predict the welded joint fatigue life, the determination of stress distributions through the weld thickness is not necessary and only determination of the stress magnitude at the surface is sufficient. The preparation of appropriate stress

concentration factor will be enough to have a good estimation of the hot spot stress at the weld toe and, consequently, the specimen fatigue strength can be determined.

According to Monahan equations, the stress concentration factor is a function of weld geometry factors such as weld toe angle,  $\theta$ , weld toe radius,  $\rho$  and plate thickness,  $t$ . Also, there are lots of irregularities along the weld line that can influence these parameters. Since the verification of weld parameters is a very complicated task, some researchers like, Dijkstra et al. (1989), Lu (1996), Bowness and Lee (2000), prefer to ignore these irregularities and use theoretically perfect and regular weld shapes. On the other hand, some other researchers have paid more attention to statistical definition of the weld toe geometry factors over the entire weld toe line (Hou, 2007).

There is only one weld toe radius if it is assumed that the weld is perfect with quite regular and smooth shape. Hou (2007) used three dimensional laser scanning technology to obtain a high resolution 3D model for stress analysis. He used scanned results to obtain stress concentration factor through the weld line by finite element stress analysis when axial loading is applied on the specimen and then performed fatigue tests on the scanned specimens to verify the analytical results. His specimen was a cruciform welded joint that contained two attachment plates with 6 mm thickness welded to the base plate with dimensions of  $200 \times 40 \times 6$  by the shield metal arc weld as shown in Figure 2-16.

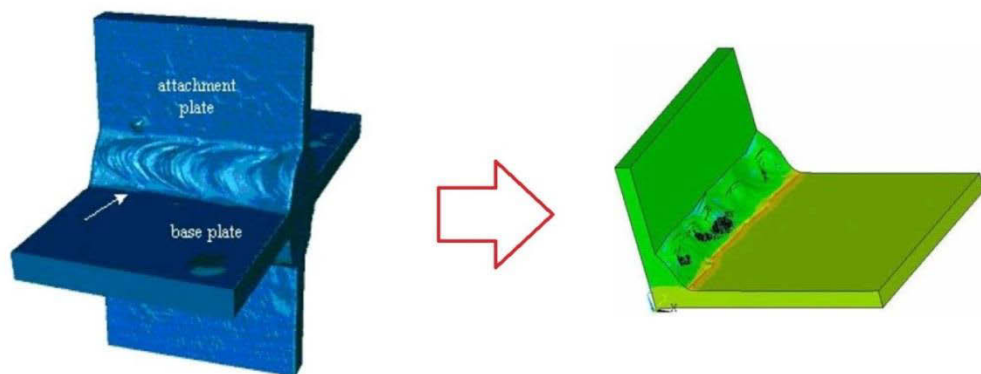


Figure 2-16: Hou (2007) specimen geometry and stress contour plot of cruciform welded joint subjected to axial tensile load

The minimum weld toe radius that could be captured by his method was about 0.4 mm while Engesvik and Moan (1983) showed that the range of weld toe radii is from 0.1 to 12 mm. However, Hou (2007) prepared several stress concentration factor graphs for each weld sides of a cruciform welded joint as shown in Figure 2-17.

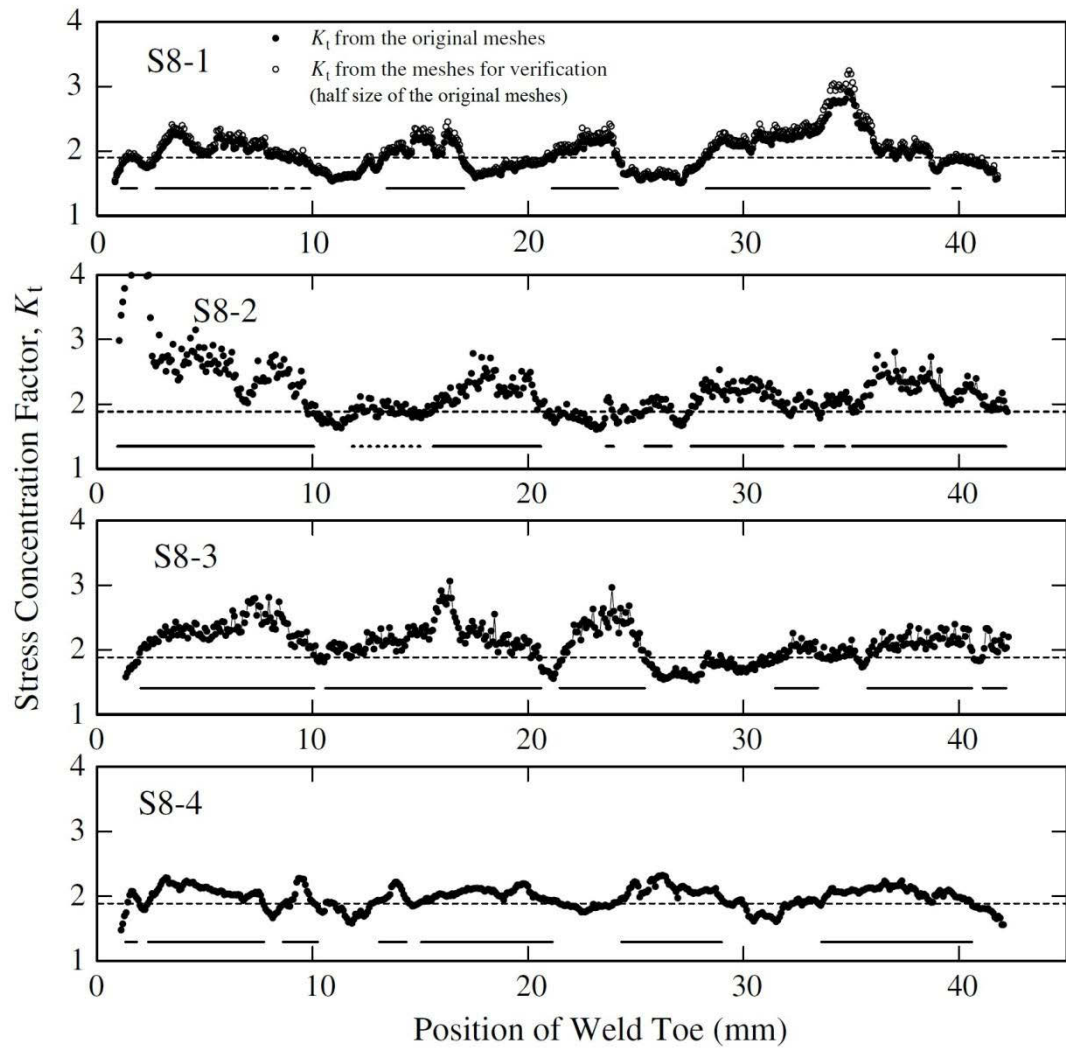


Figure 2-17: Stress concentration factor along the weld toes for four sides of a cruciform welded joints subjected to axial loading (Hou, 2007).

According to these data, the mean value of the stress concentration factor for axial loading was 2.08 with a standard deviation of 0.34 and approximately 2% of stress concentration factors were higher than 3 (Figure 2-18).

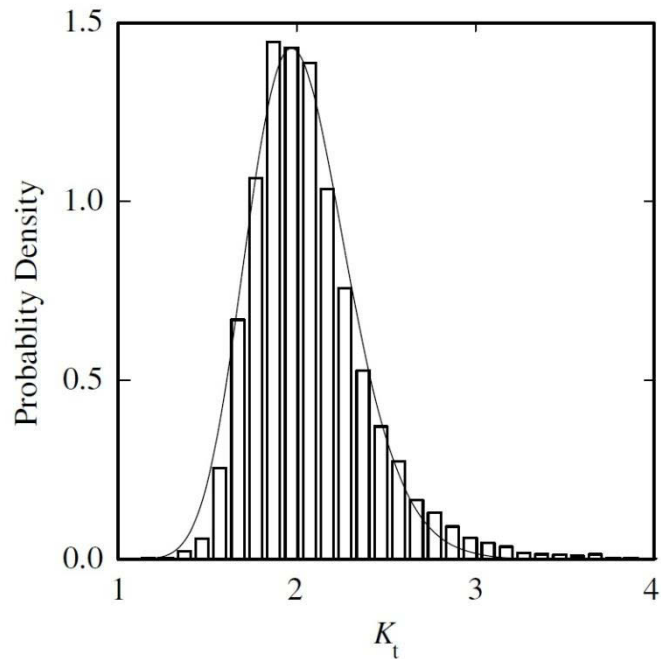


Figure 2-18: Probability density histogram of stress concentration factor appearing in weld lines (Hou, 2007).

Although it supposes that the fatigue cracks should be initiated from the location with maximum stress concentration at the weld toe, his experimental tests showed that fatigue cracks do not necessarily follow this hypothesis.

#### 2.4.1 Stress concentration improvement

Flush grinding is a very common weld treatment method which eliminates geometrical stress concentration by changing weld shape and removing weld flaws from the locations where fatigue failure typically occurs. Consequently, fatigue life for weld ground flush goes beyond what is assigned to ordinary weld. Zhao et al. (2012) studied the effect of flush grinding on super-long fatigue regime ( $10^8$ - $10^{10}$  cycles) behaviour of a butt weld specimen. Weigand and Berman (2012) worked experimentally on weld treatment of low-carbon steel butt weld joint samples under cyclic axial load to improve low cycle fatigue life. They used several different weld treatment methods like ground flush, burr ground and TIG (tungsten inert gas) dressed to re-melt the burrs by TIG electrode at the weld toe and compared these methods together. His experimental tests

showed that by flush grinding, which eliminates the stress concentration source; one could improve low cycle fatigue life of a butt weld joint subjected to axial cyclic loading.

## **2.5 Finite Element Modelling**

FEM (Finite Element Method) is used today in many engineering applications and every year extensive research are undertaken to optimise and increase the efficiency of designs by means of this method. It is hard to find a project that needs modern engineering analysis and some type of FEM are not used. Finite element codes (for instance ANSYS) are utilised by thousands of researchers to solve a wide range of complicated problems in thermodynamics, fluid mechanics, vibration, dynamics, solid mechanics, electromagnetics or combination of those.

Stress analysis of mechanical devices is one of the most important and widely used applications of FEM. The determination of stress data for fatigue analyses involves solving complex boundary conditions using the FEM. The Finite Element Analysis (FEA) was developed in the 1950's. In the early 70's, the FEA was restricted to expensive mainframe computers possessed by the automotive, aeronautics, nuclear and defence industries. With the advent of low cost powerful computers, the FEA has been improved to a very popular and high precision daily engineering tool. It helps designers predict the stress and fatigue life of a component or structure by modelling the effects of cyclic loading on the behaviour of materials and structures. Such analysis can reveal the areas where the crack initiation and propagation is most likely to occur.

Unfortunately, the FEA results can be affected by the finite element meshing and the element properties. Many researchers have worked to recommend suitable models for different problems, for instance, Niemi (1995) presented several simple models for welded joints. The fatigue analysis requires evaluation of the peak stress at the weld toe and the stress distribution through thickness in the plate. Experimentally, strains and stresses can be measured only away from the weld toe. Therefore, procedures need to be developed, addressing the problem, to directly determine the peak stresses and stress distribution in welds near the toe. The 3D finite element modelling is the most

commonly-used numerical solution but it is too time consuming and expensive. The shell finite element model is an example of 3D models to analyse the welded joints fatigue problems (Kahvaie-Zad, 2005).

Ślęczka (2004) worked on low cycle fatigue strength assessment of butt and fillet weld connections. In this case welded connections between I- or H-profile and gusset plates were under axially tensile force. His approach was based on the local strain state and he used 2D and 3D models to analyse additional stresses caused by geometry of the weld. Also, Wang and Shang (2009) have analytically studied low cycle fatigue phenomenon. They also used the local strain life approach, to predict low-cycle fatigue life of resistance spot welds. They carried out elasto-plastic 3D finite element analysis with ANSYS for single spot tensile shear spot welds to achieve local stresses and strains. The local stress and strain are used in Morrow's modified Manson–Coffin equation and Smith–Watson–Topper damage equation to predict fatigue life. They also used hardness distribution to determine the weld zone material properties as proportional to base metal properties.

Baik et al. (2011) investigated fatigue crack initiation and propagation for flat plate with a notch, stud-welded plate, T-shaped fillet welded joint and cruciform fillet welded joint under bending load. Their approach was based on fracture mechanics method and they used 3D finite element models to compare with experimental test results. Their minimum mesh size was in weld toe region with 0.05 mm element edge length and the models were generated by using 8-noded three dimensional elements.

Finch and Burdekin (1992) used ABAQUS finite element software to evaluate effects of applied and typical welding residual stress distributions and significance of defects in various geometries of welded joints like butt-welded plate, weld-root defects in a thick butt-welded plate, and a pipe-on-plate butt weld.

Barsoum and Barsoum (2009) used FE software ANSYS and 2D models to develop a welding simulation procedure of the welding manufacturing process in order to predict temperature, Heat Affected Zone (HAZ) weld penetration and residual stresses. They



developed a procedure for linear elastic fracture mechanics analysis in 2D in order to determine the crack path of propagating fatigue cracks.

## **2.6 Material properties**

As mentioned above, welding is one of the best ways to connect steel components permanently. Although this fabrication method has many advantages which made it popular and wide spread all over the world, some unpleasant characteristics have limited welding applications. The mechanical properties differ significantly all through the welding region because of the severe chemical and metallurgical interactions. The heat input creates a heat affected zone (HAZ) with noticeable variation in hardness. Furthermore, residual stress concentration in welded zones will be higher in comparison with other regions (Moraes, 2001).

Failures under repeated loading result from progressive damage, starting with a small crack which gradually propagates through the material. The rate of crack propagation varies depending on the intensity of stress, loading type, crack geometry and a number of other related factors (Hobbacher, 2008). Understanding the relationship between the weld qualities and welding process would enable engineers to find suitable solutions to solve challenges in steel structure construction and welding industry. This can be more important when a structure is subjected to cyclic loading.

The fatigue cracks initiate from weld toe because of the severe tensile residual stress and local stress concentrations due to irregularities and weld geometry. This can be clearly seen in Figure 2-19. According to the strain-life method, it is necessary to determine the stress and strain on the weld toe when the cyclic load is at its maximum level. Finite Element software like ANSYS could help analyse the nonlinear model of weld geometry and assess the required stress and strain. In low cycle fatigue, dislocations and micro-voids are rearranged and their association and linkage form a single small crack. Low cycle fatigue life for welded joints will be lower than base metal life (Besansky, 1987).

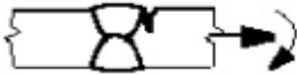
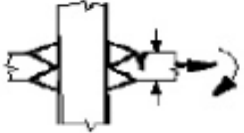
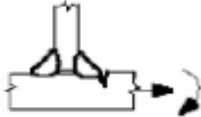
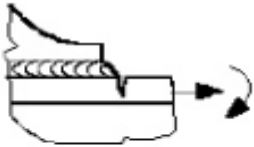

No	Structural detail	Description
1		Butt joint
2		Cruciform or T-joint with full penetration K-butt welds
3		Non load-carrying fillet welds
4		Bracket ends, ends of longitudinal stiffeners
5		Cover plate ends and similar joints

Figure 2-19: Crack initiation zone (Hobbacher, 2008)

Although experimental tests are used to obtain material mechanical properties, it is difficult to clarify these parameters for weld zone due to size limitation. Since hardness is easier than other mechanical properties to determine and also it does not require much space or material, using the hardness distribution to determine mechanical properties in a tight space by establishing a relationship between them is a very common method among researchers (Chang et al., 2001; Lee et al., 2005).

On the other hand, Kisioglu (2005) conducted some tests to identify the weld zone material properties for SAE-1008 steel to investigate of weld zone material properties. He carried out tensile tests and used quite uniform weld zone geometries to avoid the

effects of stress concentration. After converting the engineering stress strain data to true stress strain curve, he obtained weld mechanical properties as: Ultimate Tensile Strength (UTS): 84,900 psi (585.4 MPa), Tensile Yield Strength (TYS): 70,900 psi (488.8 MPa), and Elongation: 26.25%.

Since the yield strength and ultimate strength for SAE-1008 steel are 198 MPa and 351 MPa, respectively, Kisioglu's findings show that the weld zone yield strength is much higher than base plate ultimate strength for this steel grade.

In summary, this chapter contained a review of the literature and former research on subjects related to the fatigue analysis methodology of the steel structures and their advantages and disadvantages. It presented the different aspects that influence the fatigue failure of a welded joints including presence of residual stress and stress concentration. They are the factors that intensify the threat of failure. Finally, a brief review of the literature on finite element modelling and former works on material properties of the weld zone has been conducted.

# CHAPTER 3 NUMERICAL SOLUTION FOR A BUTT WELD JOINT

## 3.1 Introduction

As mentioned in literature, heat treating and flush grinding are two weld treatment ways which can improve fatigue strength and increase the components durability when they are subjected to cyclic loadings. Heat treatment relieves the residual stress by rearranging the atoms in the crystal structure of the material and flush grinding eliminates the geometrical sources of stress concentration. To characterise the impact of weld treatments to improve the residual stress and stress concentration on fatigue strength, three dimensional models for regular weld and ground weld geometries are used to obtain the elasto-plastic stress and strain distribution caused by the combination of residual stress and loading.

Butt weld connections using mild steel subjected to cyclic bending load in low-cycle fatigue situations are the cases that have to be analysed. Finite element analysis is carried out using commercial software ANSYS14 to estimate the fatigue life based on the strain-Life method.

The simulations are performed in three separate stages. The first stage of simulation is modelling the regular weld with residual stress subjected to bending loads. The second stage is modelling the same geometry of the weld, the same material properties and the same loading types and amplitudes but without residual stress. In this step the presence of residual stress compares with the situation that the residual stress has been relieved. At the final stage, the weld with the same material properties, the same loading types and amplitudes and also the same residual stress condition, when the weld material protruding outside the plates are removed, will be simulated.

## 3.2 Modelling Approach

According to the Morrow and Smith–Watson–Topper equations, determination of some parameters like maximum stress and strain on critical points will be necessary. This

means static loading on a 3D model should be used to obtain the necessary data for each case. Each model contains three volumes which two volumes representing the base plates and the third one the weld volume. The modelling exercise consists of three steps.

The first step is to prepare a 3D model in ANSYS R14.5 with nonlinear material properties and perform some initial analyses to achieve the best mesh sizes and shapes. This step will somehow be based on trial and error method, therefore, a wide range of modellings will be carried out to study the mesh size sensitivity.

The second step is to add residual stress to the model. Therefore, after preparing the model with suitable meshing, a matrix of stresses or strains to produce desired residual stress will be applied to the elements. It would be possible to apply a stress field as an initial stress state to the elements via the INISTATE command in ANSYS R14.5.

At the third step, the simulations of welded butt joint with an appropriate residual stress under different bending loads will be performed. The stresses and strains from these simulations will be used to obtain the relationship between loading and fatigue life.

It might seem that it is better and simpler to perform fatigue evaluation directly by ANSYS, but after completing a stress solution, an appropriate S-N curve has to be assigned to the model to activate the fatigue calculations. This solution approach is based on the stress-life method mentioned before. This method is not accurate enough, especially in low cycle fatigue cases, and fatigue life is only related to stress amplitude while in the strain-life method, which is more accurate especially in low cycle fatigue condition, fatigue life is related to mean stress and strain amplitude according to Morrow Equation (2-5) and maximum stress and strain amplitude according to S-W-T Equation (2-6). Based on the chosen approach (the strain-life method) for this study, ANSYS is used here for applying the residual stress and determining loading stress and strain fields and not used for fatigue evaluation.

### 3.3 Finite Element Analysis using ANSYS

#### 3.3.1 Element type

“SOLID186” has been chosen for this study. It is a 20-node 3D solid element with quadratic displacement behaviour. Each element has 20 nodes with three degrees of freedom at each node. The element supports plasticity, hyper-elasticity, creep, stress stiffening, large deflection, and large strain capabilities. It has also a capability for simulating deformations of elasto-plastic materials. Another advantage of this element type is a capability for applying an initial stress state via the INISTATE command.

#### 3.3.2 Material properties

Chemical composition and mechanical properties of the steel (AS/NZS 3679.1-300 grade) are given in Tables 3-1 and 3-2, respectively.

Table 3-1: Chemical Properties of steel AS/NZS 3679.1-300 grade

CHEMICAL COMPOSITION		
ELEMENT	GURUNTEEED MAXIMUM (%)	TYPICAL (%)
Carbon	0.25	0.19
Silicon	0.50	0.18
Manganese	1.60	0.80
Phosphorus	0.04	0.007
Sulphur	0.04	0.018
Copper	0.50	0.26
Nickel	0.50	0.08
Chromium	0.30	0.10
Molybdenum	0.10	0.02
Titanium	0.04	0.001
Niobium	0.02	0.001
Vanadium	0.03	0.002
Aluminium	0.15	0.002
CEQ <sup>(*)</sup>	0.44	0.38

$$(*) CEQ = C + \frac{Mn}{6} + \frac{(Cr+Mo+V)}{5} + \frac{(Cu+Ni)}{15}$$

Table 3-2: Mechanical properties of steel AS/NZS 3679.1-300 grade

<b>BASE PLATE MECHANICAL PROPERTIES</b>		
<b>Tensile properties (longitudinal)</b>	<b>GURUNTEED MINIMUM</b>	<b>TYPICAL</b>
<b>Yield strength <math>S_y</math> (MPa)</b>	300	374
<b>Ultimate Strength <math>S_u</math> (MPa)</b>	440	545
<b>Elongation (%)</b>	22	28
<b>Elastic modulus <math>E</math> (GPa)</b>	-	205
<b>Poisson's Ratio</b>		0.3

This grade of hot rolled structural and plate steels with minimum yield strength of 300 MPa, good ductility and good weld-ability are very applicable in industry and used across a wide range of industrial and structural applications. Various shapes of AS/NZS 3679.1-300 grade like universal beams and columns, Parallel flange channels, equal angles, unequal angles, merchant bar and plate, are produced for consumption in building structures, major mining and industry infrastructures and even for aesthetic structural use such as shipping terminals and airports (HOGAN and KEY, 2012).

Welding electrodes used for this project were E6013 according to AS/NZS 4855 standard (Table 3-3). This type of electrode is a high titanium coating electrode used for low and mild carbon steels. In this welding electrode the amount of spatter is negligible and in addition to splashing they produce less smoke, dust and toxicity. The slag is fluid and when hardened it can be easily removed. The weld appearance is well shaped, smooth and shiny. Welding electrode E6013 can be applied in all welding positions and can use both A.C. and D.C electricity flows and can produce excellent welding performance and a satisfactory weld. These advantages make this electrode suitable for welding sheet metal structures made of ordinary tensile strength low or mild steel structures, such as buildings, bridges, ships, vehicles, and industrial machinery.

Table 3-3: Mechanical properties for material produced by E6013 electrode

<b>WELD ZONE MECHANICAL PROPERTIES</b>	
<b>Tensile properties (longitudinal)</b>	<b>GURUNTEEED MINIMUM</b>
<b>Yield strength <math>S_y</math></b>	63,000 psi (434 MPa)
<b>Ultimate Strength <math>S_u</math></b>	71,000 psi (490 MPa)
<b>Elongation</b>	24 %
<b>Elastic modulus <math>E</math></b>	205 GPa
<b>Poisson's Ratio</b>	0.3

Since the yield strength of weld material is close to the ultimate strength of base plate, there is no need to apply nonlinear material properties for weld zone because before the plastic deformation occur in the weld zone, final fracture will happen in the base plate.

The nonlinear relationship between true stress and true strain for materials in their plastic deformation position are defined according to the Ramberg and Osgood (1943) equation:

$$\varepsilon = \frac{\sigma}{E} + \left( \frac{\sigma}{K'} \right)^{\frac{1}{n'}} \quad (3-1)$$

Where  $\varepsilon$  and  $\sigma$  are true strain and true stress,  $E$  is elastic modulus,  $K'$  is cyclic strength coefficient and  $n'$  is cyclic strain hardening exponent.

The fatigue parameters for this steel grade are given in Table 3-4.

Table 3-4: Fatigue parameters for steel AS/NZS 3679.1-300 grade

Fatigue strength coefficient ( $\sigma'_f$ )	895 (MPa)
Fatigue strength exponent ( $b$ )	-0.12
Fatigue ductility coefficient ( $\varepsilon'_f$ )	0.41
Fatigue ductility exponent ( $c$ )	-0.51
Cyclic strength coefficient ( $K'$ )	1962 (MPa)
Cyclic strain hardening exponent ( $n'$ )	0.321



Figure 3-1 shows evaluation of the weld zone material properties and a comparison with the steel AS/NZS 3679.1-300 grade mechanical properties. These two strain stress graphs are used in this study as the base plate and weld zone material properties.

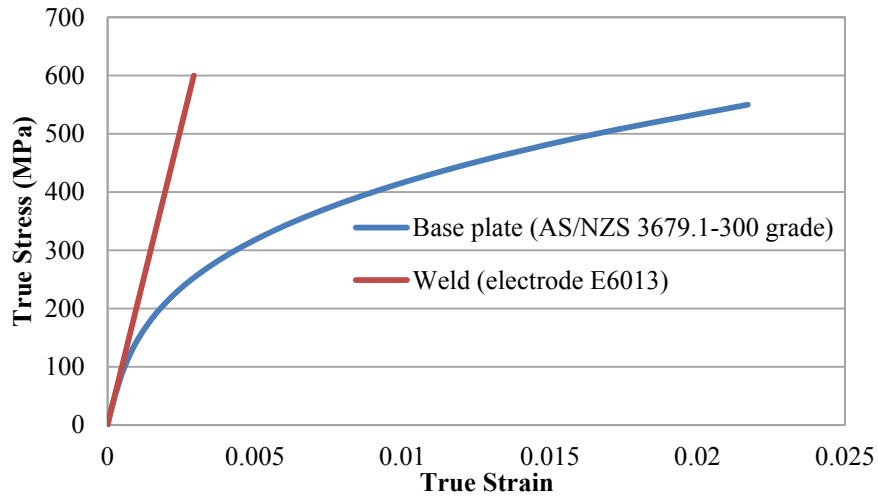


Figure 3-1: The weld zone and AS/NZS 3679.1-300 grade material properties

During the loading process, when the specimen is unloaded or the applied load is reversed, the stress-strain curve follows a path with the slope of elastic modulus  $E$  (Figure 3-2). It should be noted that when the specimen is subjected to a compressive load, the material starts yielding at a stress level different from the actual yield stress. The unloading curve from A to C can be modelled by expanding the original stress-strain curve O-A by a factor of two (Dowling, 2012).

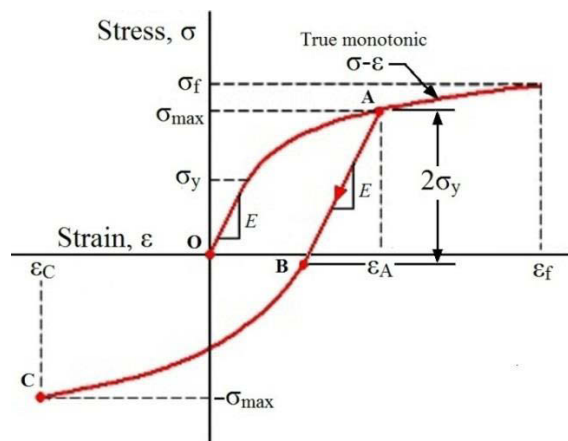


Figure 3-2: Stress-Strain behaviour after unloading

When the loading process continues from  $-\sigma_{\max}$  to  $\sigma_{\max}$  a stress-strain hysteresis loop is generated as shown in Figure 3-3. This hysteresis loop represents the first cycle of fatigue stress and strain.

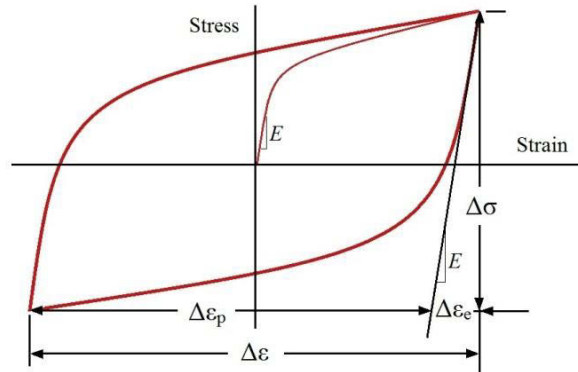


Figure 3-3: Typical hysteresis loop in the stress-strain curve for fully reversible loading

According to mechanical behaviour of material during unloading, the mechanical properties definition in ANSYS for this study will be based on *Multi-linear kinematic Hardening*. The behaviour of multi-linear kinematic hardening is similar to bilinear kinematic hardening except that a multi-linear stress versus total or plastic strain curve is used instead of a bilinear curve. The multi-linear hardening behaviour is described by a piece-wise linear total stress-total strain curve, starting at the origin and defined by sets of positive stress and strain values, as shown in Figure 3-4.

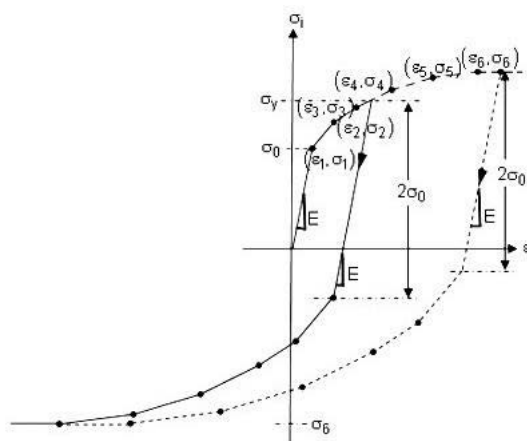


Figure 3-4: Total stress -total strain for multi-linear kinematic hardening (ANSYS 14.5 Document)

The experimental tests verify the material properties applied in these simulations. The details of finite element analysis and experimental tests will be more explained in the following paragraphs of this chapter and the next chapter. However, for more clarification, in the simulation section, different appropriate bending loadings are applied on the model when the stresses around the weld zone are in the plastic range of material properties. The deflections at the force application point are the output of these bending loads and prepare a load-deflection graph which could be compared with those from the experiments. This process for experimental tests is done in reverse side. It means the inputs are deflections and the loadings detected by load cells in the loading arm will be the outputs.

Experimental tests verify the material properties used in these modellings. The load-deflection graphs generated by finite element modelling and experimental tests have been compared in chapter 5 which they have a good agreement. It shows that the stress-strain diagrams used for finite element modelling as material properties for base plate and weld zone are acceptable.

### **3.3.3 Model geometry**

Baik et al. (2011) used the following experimental model for analysis of fatigue crack propagation for T-shaped fillet welded joint and cruciform fillet welded joint subjected to bending (Figure 3-5).

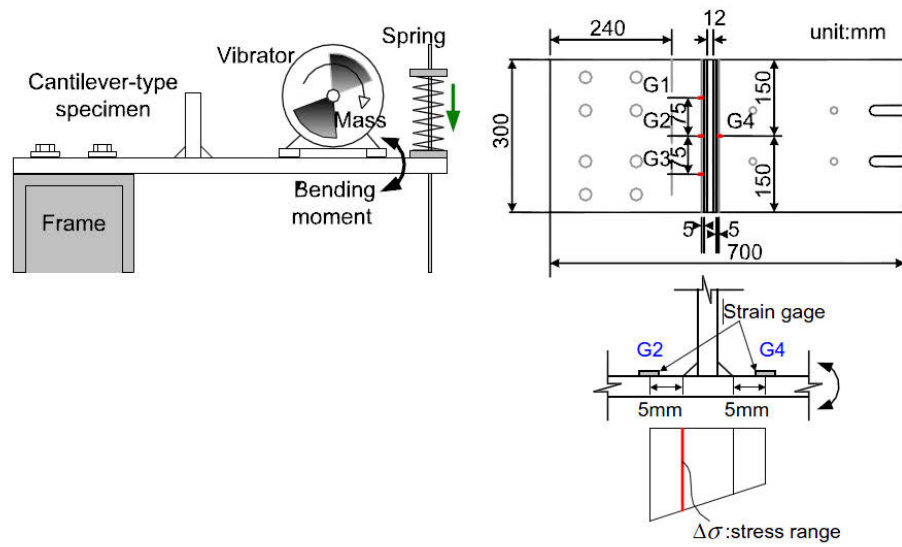


Figure 3-5: Test set up used by Baik et al. (2011) to study of fatigue life for a welded specimen subjected to bending

To model a welded joint, a 3D finite element solid model of the specimen was devised and shown in Figure 3-6.

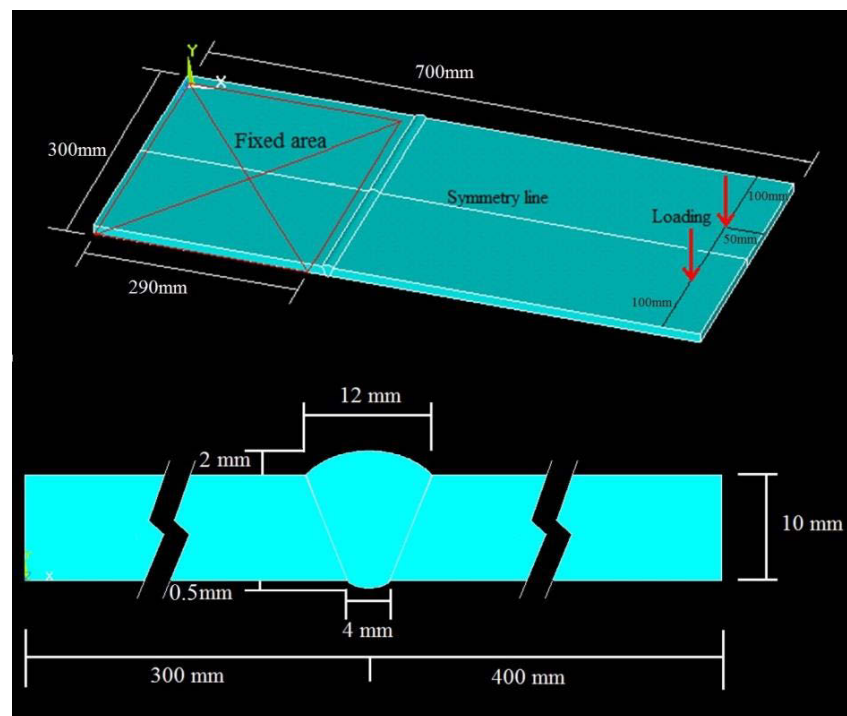


Figure 3-6: 3D finite element solid model of a butt weld joint

In the simulation of the butt weld joint, only half of the section is modelled due to the symmetry of the model. An initial mesh distribution with the element length edge of 10 mm along the plate width and also 1 N of loading are used. (Figure 3-7)

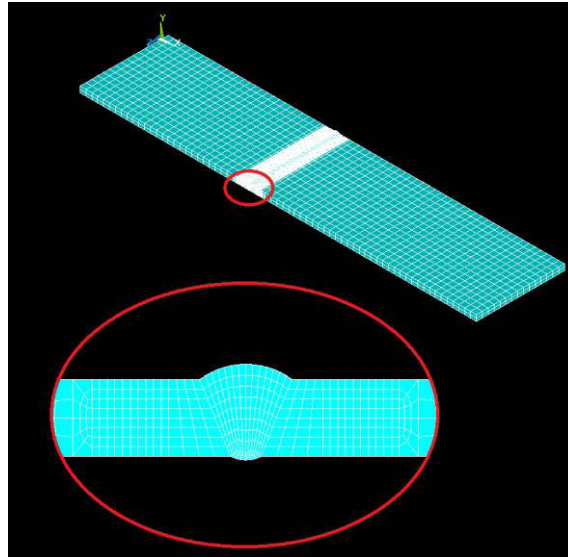


Figure 3-7: Initial meshing

From the stress distribution, it can be clearly seen that the most significant location for fatigue crack initiation and propagation will be on the weld toe where the weld material is attached to the base plate (Figure 3-8).

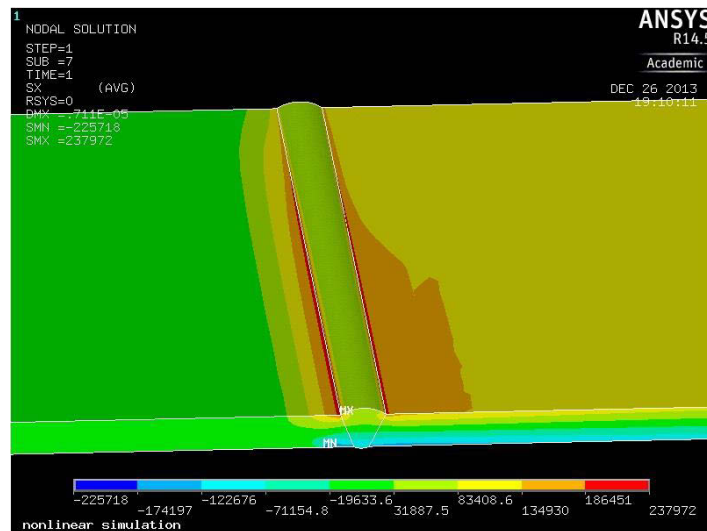


Figure 3-8: X direction Stress distribution around the weld toe

To investigate the mesh size effects on the modelling and stress and strain distribution, some mesh sensitivity studies should be performed. For this reason, similar models with different meshing sizes in each direction are simulated. Figure 3-9 shows two meshing distributions differing only along the Z direction. The element edge length along the Z direction for the first model is 10 mm while for the second one it is 5 mm.

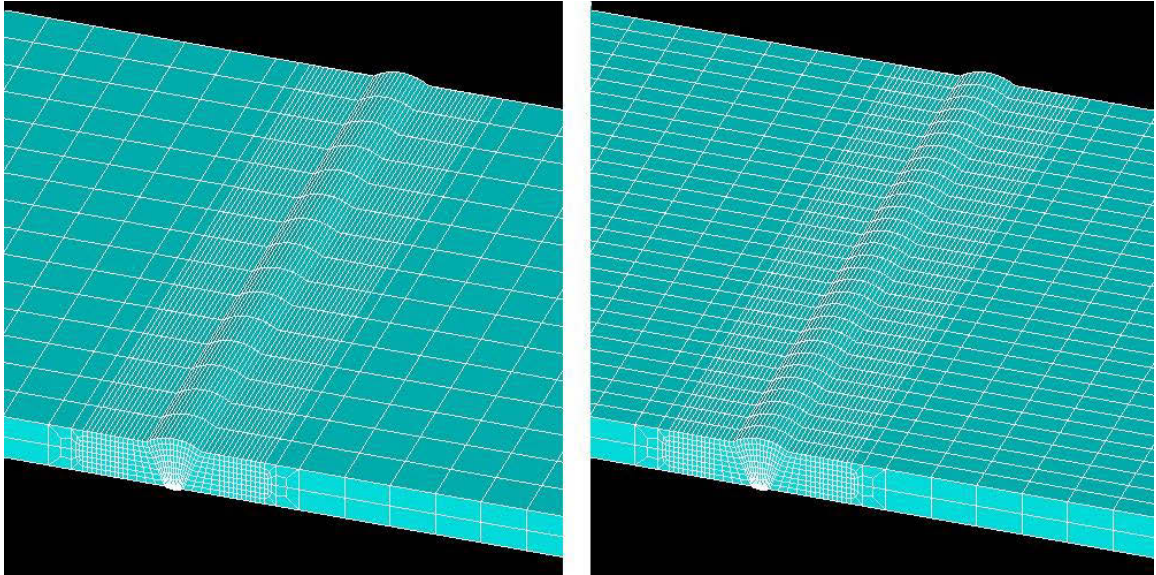


Figure 3-9: Changing the mesh size along the plate width (Z direction)

Stress and strain distributions along the attachment line of the weld toe are shown in Figure 3-10. It is clear that the stress and strain distribution graphs for these two different meshing are almost the same, therefore, the larger element length size, which produces a model with fewer elements, can be used unless the element length sizes in other directions do not allow this, forcing the use of smaller size mesh to achieve better elements' aspect ratio.

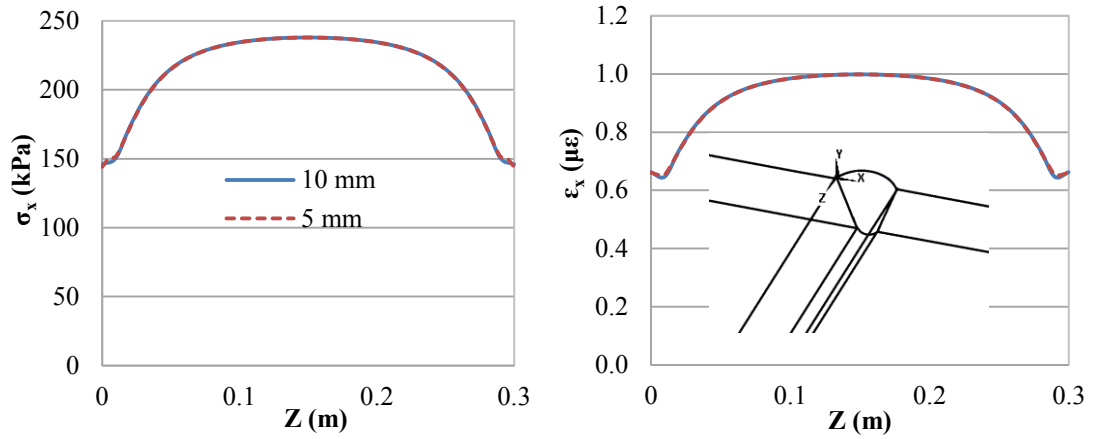


Figure 3-10: Stress and strain distribution along the attachment line of the weld toe for two types of meshing

The next step is evaluation of the mesh size in the perpendicular direction of the weld line. The stress concentration factor dictates the appropriate element length size. The value of stress concentration factor at the weld toe is determined by the Monahan equation (2-24) and the element edge lengths that produce this stress concentration factor would be ideal meshing. Figure 3-11 shows the typical stress distribution near the weld zone at the surface of a weld joint subjected to bending. Proportion of  $\sigma_{peak}^b$  to  $\sigma_{hs}^b$  determines the stress concentration factor  $K_{t,hs}^b$ . Similar to the weld toe radius, by decreasing the element edge length the stress concentration factor will be increased. Figure 3-12 shows a schematic of mesh size effect on stress concentration calculated by simulation.

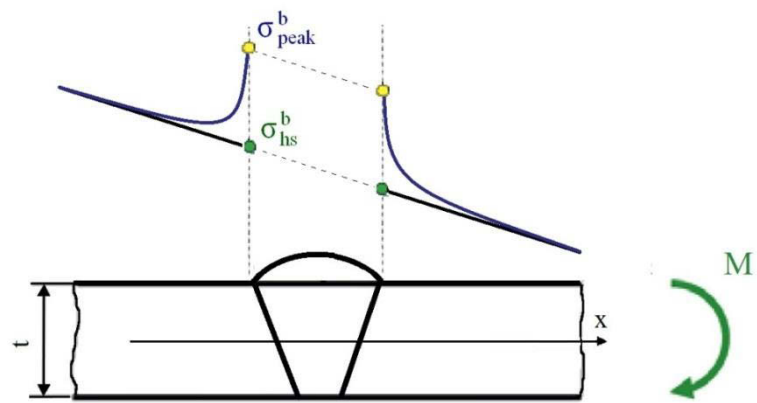


Figure 3-11: Typical stress distribution near the weld zone of a welded joint subjected to bending

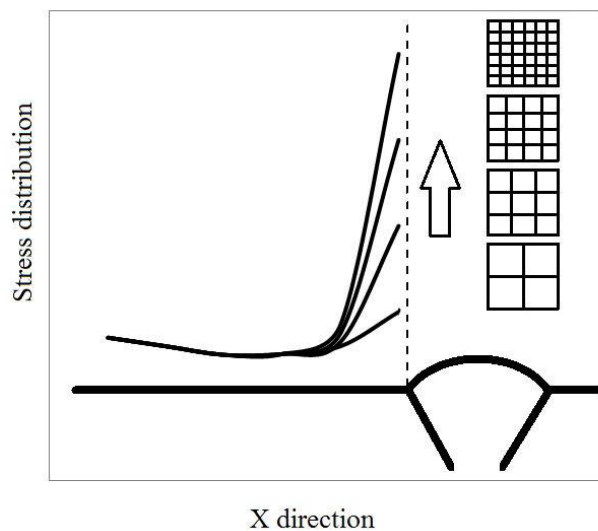


Figure 3-12: A schematic of mesh size effect on the stress concentration factor.

Figure 3-13 shows the stress distribution near the weld zone at the surface of the specimen subjected to bending load for two geometries that are simulated using ANSYS. The first geometry is the regular weld shape and for second geometry, the weld material protruding outside the plane thickness is removed. The effect of stress concentration is clear when two graphs are compared.



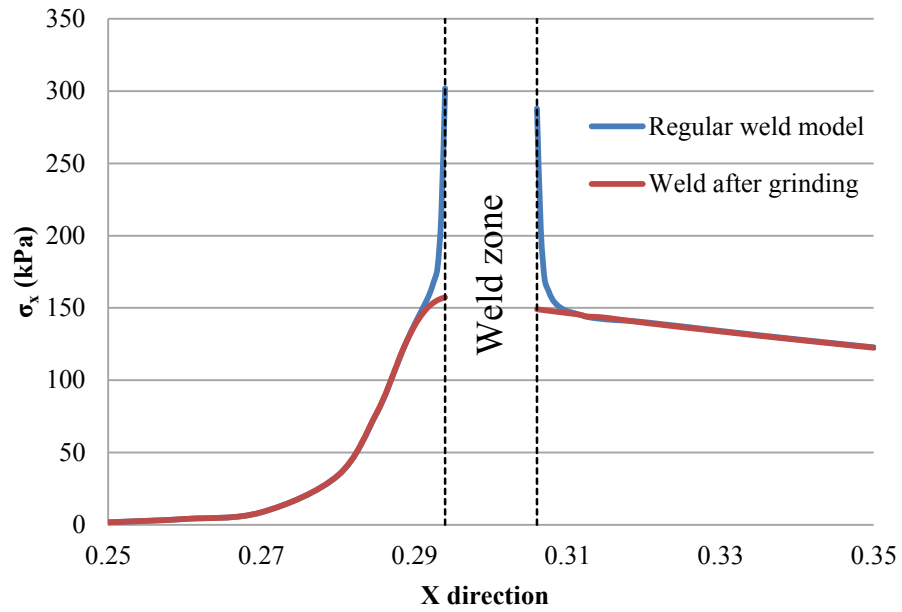


Figure 3-13: Stress distribution around the weld toe for the two geometries

To achieve the suitable mesh size, at first, stress concentration at the weld toe must be determined. According to Hou's (2007) study, for a welded joint subjected to axial load with the weld toe angle of  $60^\circ$  and thickness of 6 mm, the mean value of the stress concentration factor for axial loading was 2.08. With this axial stress concentration factor and Monahan equation (2-23), predominant weld toe radius could be determined. This weld toe radius is used in the bending stress concentration equation to generate bending stress concentration which is necessary for determination of the appropriate mesh size.

For Hou's model:  $\theta = 60^\circ$ ,  $K = 2.08$ ,  $t = 6$  mm

Axial load stress concentration factor equation:

$$K_{t,hs}^m = 1 + 0.388 \times \theta^{0.37} \times \left( \frac{t}{\rho} \right)^{0.454} \quad (2-23)$$

$$\Rightarrow \rho = 0.65 \text{ mm}$$

For this study:  $\theta = 37^\circ$ ,  $t = 10$  mm,  $\rho = 0.65$  mm

Bending load stress concentration factor equation:

$$K_{t,hs}^b = 1 + 0.512 \times \theta^{0.572} \times \left( \frac{t}{\rho} \right)^{0.469} \quad (2-24)$$

$$\Rightarrow K_{t,hs}^b = 2.43$$

Desired stress concentration factor at the weld toe for this model is equal to 2.43 and the meshing with element edge length that could generate this stress concentration will be adequate. In this step, several types of meshing with alternate element edge lengths are prepared. Figure 3-14 shows five types of meshing with various sizes. Element sizes in Z direction have been previously set and here in this step, the element sizes in X and Y directions will be set together with the same size. The elements at the weld toe angles and the base plate surface are the basis of the meshing and the stress concentration factor at these elements should reach a magnitude equal to 2.43.

The element edge length sizes in X and Y directions for these five meshing models are equal to 0.50 mm, 0.40mm, 0.31mm, 0.25 mm and 0.20 mm, respectively.

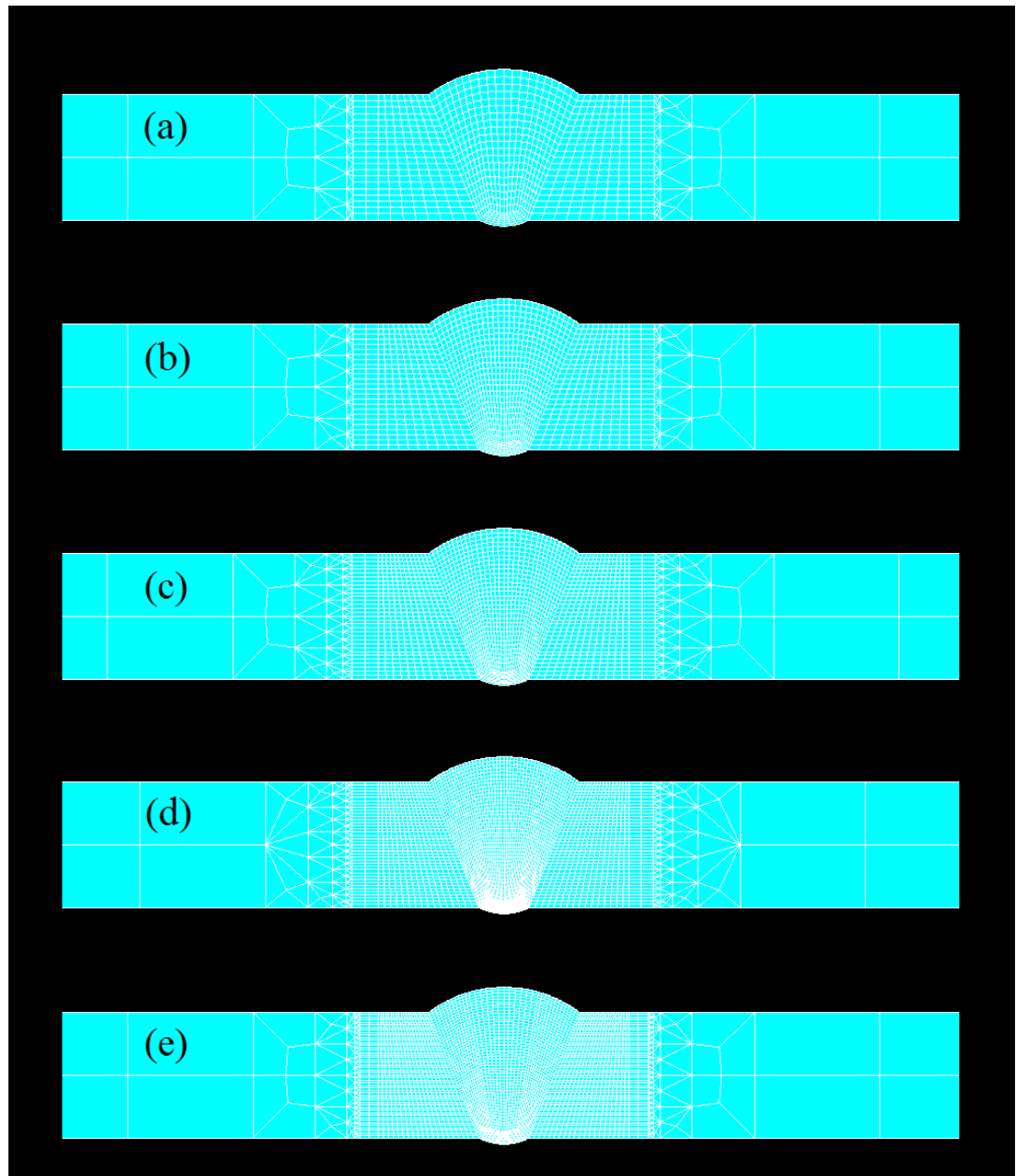


Figure 3-14: Five types of meshing to investigate the effect of cross section meshing size. The elements edge length at the weld toe is (a) 0.50 mm, (b) 0.40 mm, (c) 0.31 mm, (d) 0.25 mm and (e) 0.20 mm.

Table 3-5 shows some information on these meshed models when 1 N bending load is applied. The third column shows the total number of elements for each meshing. The number of elements can directly affect the solution time. For example, the solution time duration for the first model with 0.50 mm element edge length at the weld toe and the total number of elements equals to 19,377 will be about 15 minutes while it takes more

than 5 hours to solve the last model with an element edge length of 0.20 mm and the total number of elements being 141,784. Nominal stresses X at the weld toe for all cases are similar and equal to 157.2 kPa. The maximum stress X at weld toe for these five meshing are given in column 5. The magnitude of maximum stress at the weld toe for the model with mesh size of 0.50 mm is 302.2 kPa and it gradually grows to 389.3 kPa for the model with mesh size of 0.20 mm. The stress concentration factors which are given in the last column are produced by dividing the maximum stresses by nominal stress values.

Table 3-5: Simulation data for five meshed models with different element edge length subjected to 1 N bending load

No.	Element edge length (mm)	Total Number of elements	Nominal Stress X, (kPa)	Maximum Stress X, (kPa)	Stress concentration factor
1	0.50	19,377	157.2	302.2	1.92
2	0.40	27,730	157.2	320.4	2.04
3	0.31	44,054	157.2	343.1	2.18
4	0.25	89,122	157.2	363.2	2.31
5	0.2	141,784	157.2	389.3	2.48

As mentioned before, the suitable magnitude for stress concentration factor is 2.43 and a mesh size necessarily should be chosen that creates this stress concentration factor. The stress concentration factors vs element edge lengths for above modellings and also their power trend line are drawn in Figure 3-15. The graph shows that the appropriate mesh size to reach the stress concentration factor 2.43 will be equivalent to 0.21 mm. Therefore, in all following simulations for regular weld models and ground models, the final cross sectional mesh size around the weld toe will be equal to 0.21 mm.

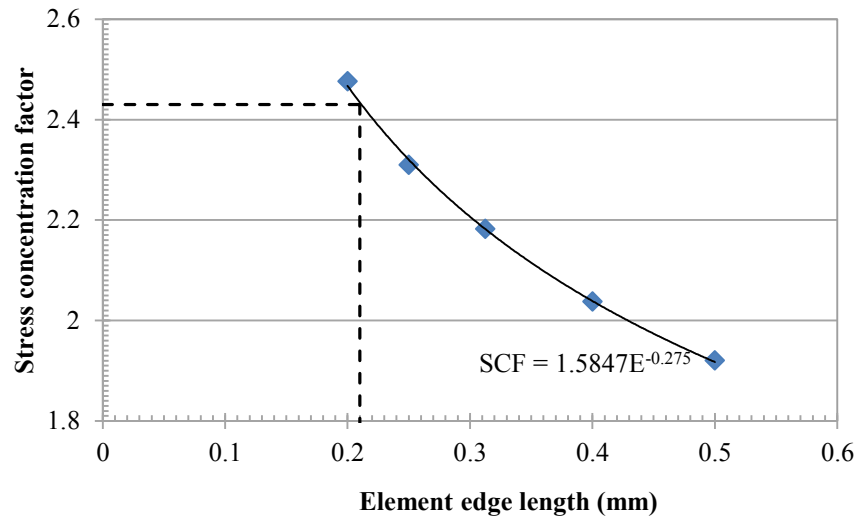


Figure 3-15: Stress concentration factor vs element edge length at the weld toe

In summary, the effect of element size change on modelling accuracy in each direction has been investigated. The final model has 128,404 elements with cross sectional element edge lengths of 0.21 mm in the vicinity of weld and 5 mm elements edge lengths in Z direction.

### 3.3.4 Residual stress modelling

Although a considerable amount of advanced finite element modellings have so far been performed by different researchers in order to predict the generation of residual stresses during welding by simulation of the manufacturing process, which in turn is related to the non-linear temperature dependent behaviour and material phase transformation, limited analyses have been performed on the loading situations in the presence of residual stress field as an initial condition. The question is that, what is the best way to apply residual stresses as an initial condition for a complex problem when their value and distribution are known? The initial states are related to the condition of a model at the beginning of the analysis. Usually, it is assumed that the initial states of a structure are undeformed and unstressed, but such ideal assumptions are not always correct and realistic.

ANSYS Rev 14 has capability to define initial strain and initial stress. This feature can be used to apply a stress-strain field as residual stress-strain state from previous

loadings. Since the residual stress has a self-equilibrium characteristic, the initial state applied to the model would not be the desired residual stress because each element shares the stress with its neighbours until the whole specimen is balanced. Therefore, after analysing the model with initial state, the results, as the balanced stress-strain field, would be the demanded residual stress. Applying Z direction initial strain ( $\epsilon_{i,z}$ ) equal to 0.004 with 1 mm depth and over 7 mm around the weld toe produces a residual stress field as seen in Figure 3-16 that shows the Z direction stress field as the desired residual stress field generated by INISTATE command.

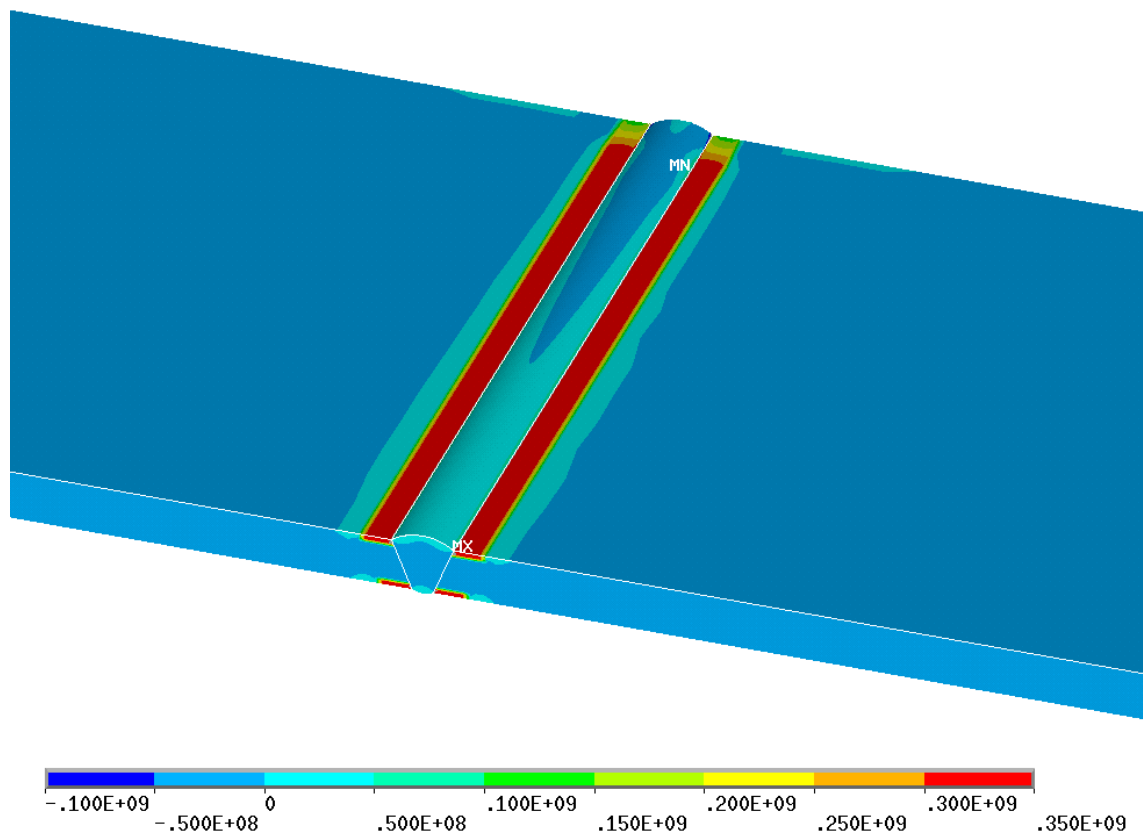


Figure 3-16: Residual stress contour for regular weld produced by applying the initial strain ( $\epsilon_z$ ) of 0.004 at the base plate surface's elements near the weld toe (1 mm depth and 7 mm length)

It is clear that the residual stresses in the weld toe and plate thickness have been ignored and only the surfaces around the weld toe have been considered for application of residual stress because these areas are the locations for initiation and propagation of

fatigue induced cracks and the stress due to bending would be more severe there. In addition, welding zone material has higher yield strength than base plate so that in high quality welding and external bending situation, failure always occurs in base plate and not in weld toe.

This process can be used to generate residual stress in a ground weld model. The residual stress distribution in ground weld model is very similar to the stress field in the regular weld (Figure 3-17).

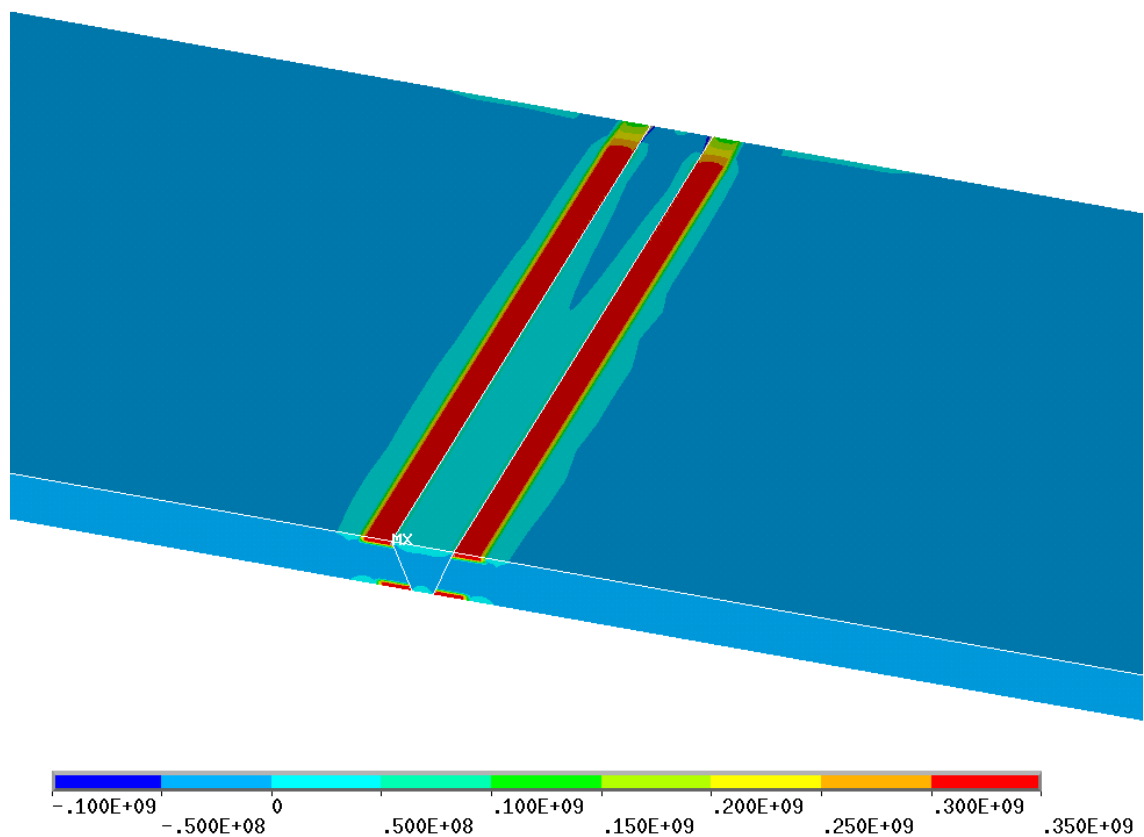


Figure 3-17: Residual stress contour for ground weld produced by applying the initial strain ( $\epsilon_z$ ) of 0.004 at the base plate surface's elements near the weld toe (1 mm depth and 7 mm length)

Figures 3-18 and 3-19 show the distribution of transverse and longitudinal residual stress at the surface of plate near the weld toe along the X direction. These graphs have good agreement in shape with results presented by Teng et al. (2003) (Figure 2-7). The steel grade for Teng's study was SAE 1020 which is very close to the current study with

the steel grade AS/NZS 3679.1-300. Although the maximum values for transverse residual stress ( $\sigma_z$ ) and longitudinal residual stress ( $\sigma_x$ ) evaluated by Teng et al. were about 100 MPa and 25 MPa, respectively. According to Deaconu's (2007) study, the maximum value of residual stress near the weld toes could be equal to or even greater than the base plate yield strength. For this reason, to cover a more serious situation, the maximum value of transverse residual stress ( $\sigma_z$ ) near the weld toe generated in ANSYS for this study will be approximately 330 MPa which is more than three time higher than Teng's value and in the proximity of the base plate yield strength.

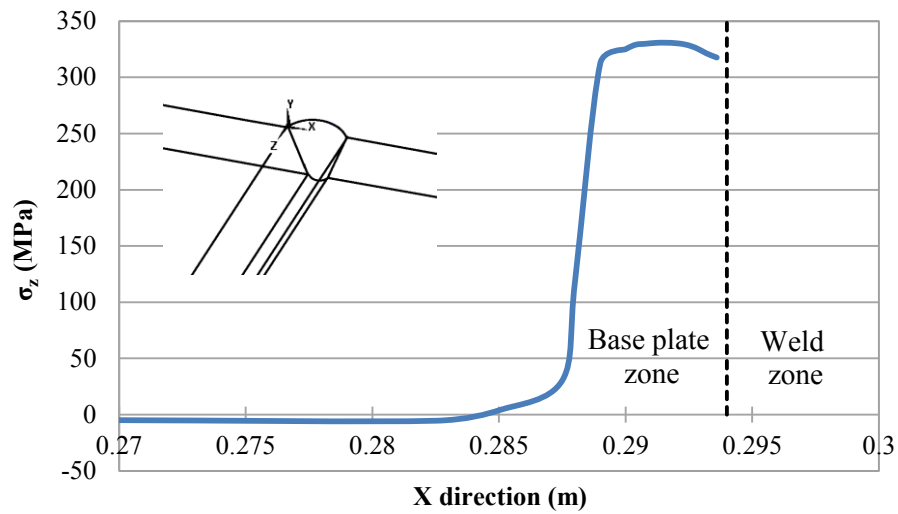


Figure 3-18: Transverse residual stress distribution along the X-direction generated in ANSYS



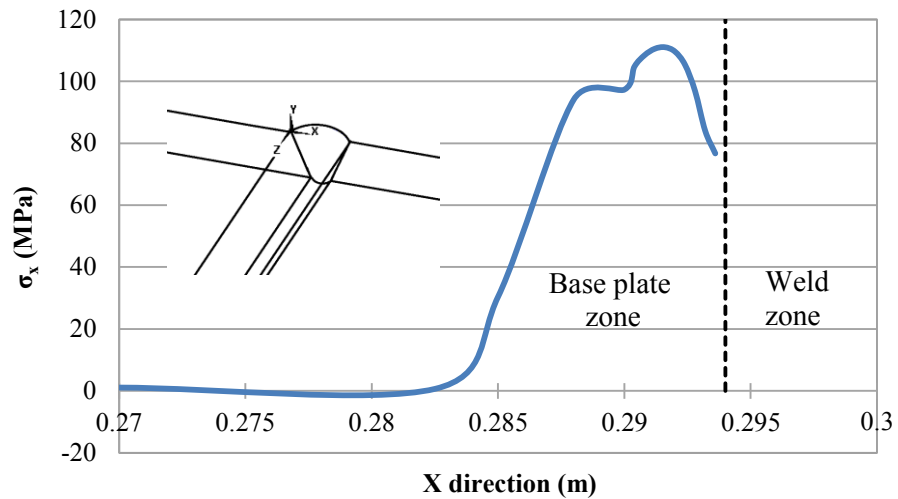


Figure 3-19: Longitudinal residual stress distribution along the X-direction generated in ANSYS

If the final results show that the residual stress has an important effect on low cycle fatigue, this effect should be evaluated for different ranges of residual stress. Otherwise, when this overestimated residual stress does not affect the outcome, the lower values cannot certainly have any effects on low cycle fatigue life. Figures 30-20 and 3-21 show the longitudinal and transverse residual stress distribution along the Z direction. The maximum  $\sigma_x$  and  $\sigma_z$  are 111 MPa and 331 MPa, respectively. The  $\sigma_x$  and  $\sigma_z$  are almost uniform at the weld toe all over the weld line except at the two ends that suddenly drop.

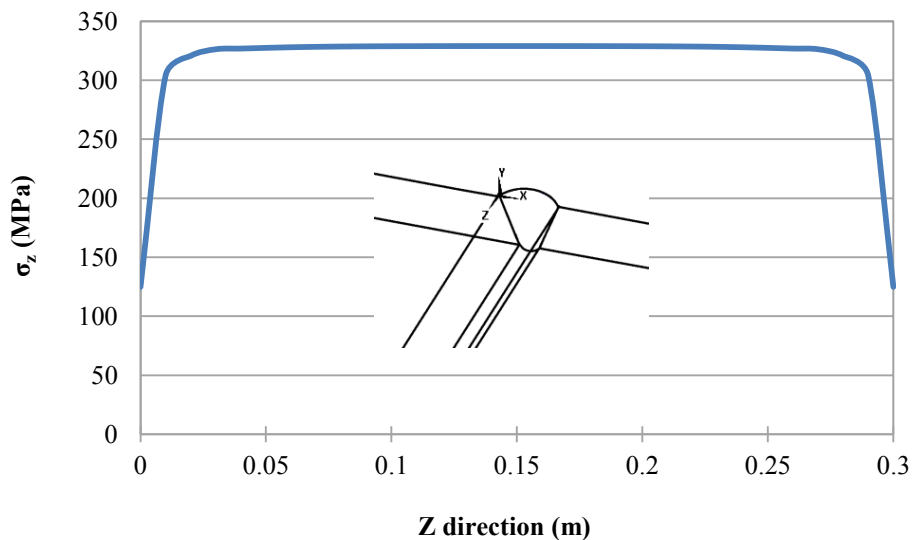


Figure 3-20: Transverse residual stress distribution along the Z-direction generated in ANSYS

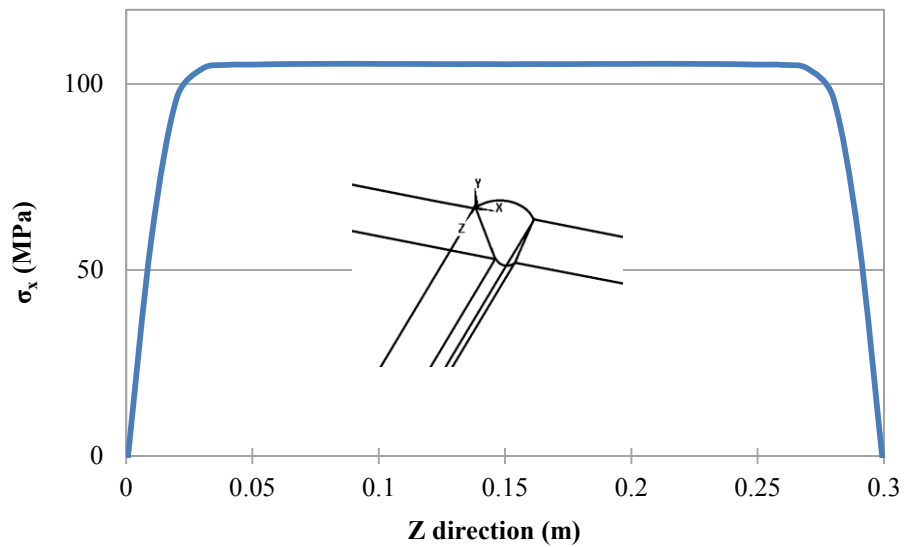


Figure 3-21: Longitudinal residual stress distribution along the Z-direction generated in ANSYS

### 3.4 Loading in presence of residual stress for regular weld shape model

After preparing suitable meshing and residual stress fields for regular weld and the ground weld models, the specimens under fully reversible cyclic bending loads are modelled. However before that, since the bending loads in experiments will be based on constant cyclic deflections, therefore, constant cyclic deflections are used as input load in simulations. But, deflection only may not be generally applicable and it is specific to this particular geometry. To more generalise and extend the results for this specific geometry to other similar geometries with different lengths and widths, the bending moment per unit width can be used. To obtain a criterion for conversion of deflections into bending moment per unit width, four bending loads equal to 7 kN, 8 kN, 9 kN and 10 kN were applied in the ANSYS simulation and the deflection for each was determined. The bending moment per unit width is calculated from applied loads by the following equation:

$$BM = \frac{F \times l}{w} \quad (3-2)$$

Where BM is the bending moment per unit width, F is bending load (7-10 kN), l is the distance between loading and weld toe (0.356 m) and w is the plate width (0.3 m). Figure 3-22 shows the bending moment per unit width curve versus deflection which is

a benchmark for future modellings to convert the applied deflections into the applied bending moments.

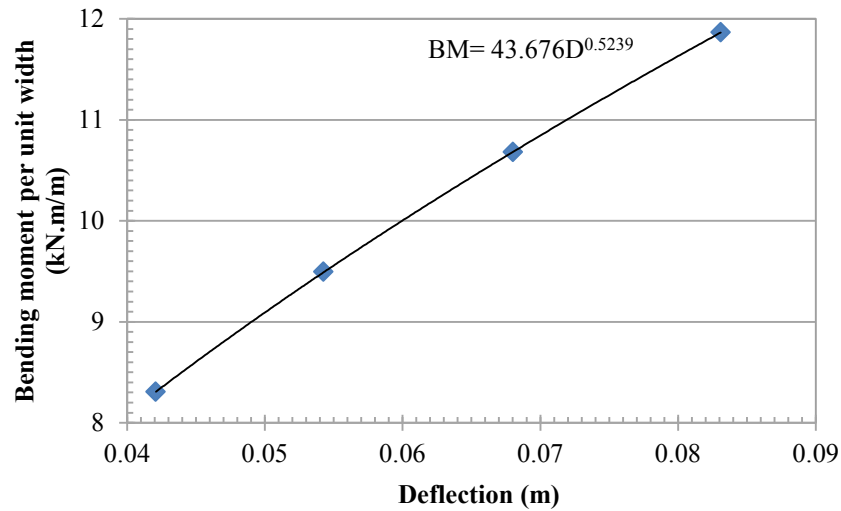


Figure 3-22: Bending moment per unit width versus deflection

To analyse the behaviour of material in welded joints subjected to bending, fully reversible cyclic bending deflections with the amplitudes from 40 mm to 90 mm with the intervals of 10 mm were applied to three cases. In the first case, which represents regular welding, the loads are applied on the regular weld shape models in presence of residual stress. The second case characterises a condition where residual stresses do not exist in specimen and the third situation will be a simulation for ground weld model or in the other words, a model without stress concentration factor.

Figure 3-23 shows the first five stress-strains hysteresis loops at the critical location of the welds when, for instance, a 70 mm cyclic deflection is applied to the model. The stress-strain hysteresis loop starts from the initial strain and stress, which is the residual stress and strain. During the loading process the stress-strain curve nonlinearly increases until the maximum load and then, when the specimen is unloaded, the stress-strain curve follows a path with the slope of elastic modulus (E) and after that reduces nonlinearly based on multi-linear kinematic hardening material behaviour and this process continues for each loading and unloading.

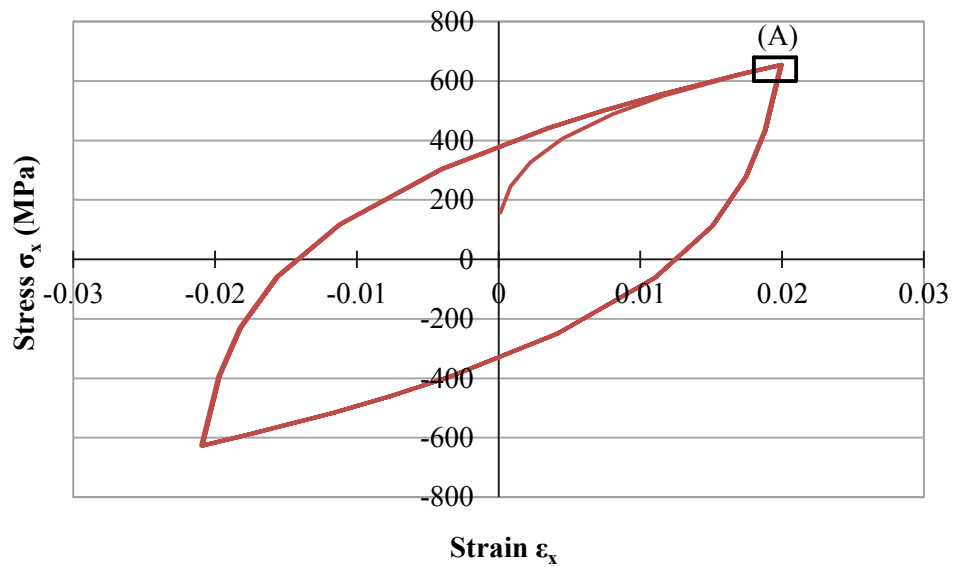


Figure 3-23: Stress-Strain ( $\sigma_x$ - $\epsilon_x$ ) hysteresis loop for a 70 mm cyclic deflection

There is no need to apply more than five cycles of loading because the hysteresis loop is going to be converged after five cycles. Applying more cycles takes a longer time to conduct the simulation. Figure 3-24 shows the enlarged section of the hysteresis loop marked by rectangle (A) in Figure 3-23. The cycles do not necessarily overlap completely. Maximum stress and strain for first five cycles are as below:

- First cycle: 652.6 MPa and 0.019865;
- Second cycle: 654.8 MPa and 0.019946;
- Third cycle: 655.3 MPa and 0.019964;
- Fourth cycle: 655.5 MPa and 0.019971;
- Fifth cycle: 655.6 MPa and 0.019974;

The relative changes for maximum stress and strain between the fourth cycle and the fifth cycle are less than 0.02%.

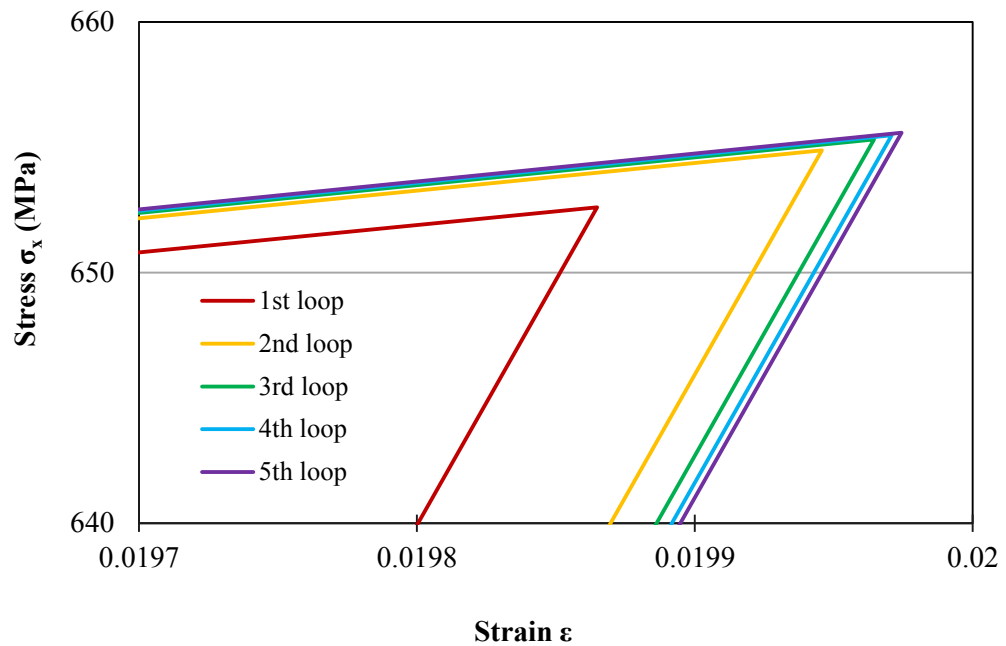


Figure 3-24: An enlarged portion of hysteresis loop around the maximum stresses and strains

Fully reversible cyclic bending deflections with the amplitudes from 40 mm to 90 mm with the incremental of 10 mm were separately applied to the regular weld shape in presence of residual stress. The loads are high enough to cause plastic flow in some elements around the weld region. The stress-strain hysteresis loops for the element located in the base plate surface and plane of symmetry are shown in Figure 3-25. Each loop area represents the dissipated strain energy per unit volume absorbed by the element, which is the heat generation source in the material. By increasing the loading amplitude, the hysteresis loops grow and more energy will be absorbed by the material. These hysteresis loops data are given in Table 3-6. The first column shows the bending deflection amplitudes and data in the second column are generated from Figure 3-22. The peak stresses in the third column increase from 536.2 MPa for bending moment per unit width of 8.1 kNm/m to 682.9 MPa for bending moment per unit width of 12.4 kNm/m. The minimum stresses in column 4 show a reduction from -488.8 MPa to -684.0 MPa. The mean stresses slightly decrease from 23.7 MPa to -0.6 MPa. The stress amplitudes in column 6 and strain amplitudes in the last column gradually rise from 512.5 MPa and 0.0110 to 683.5 MPa and 0.0277.

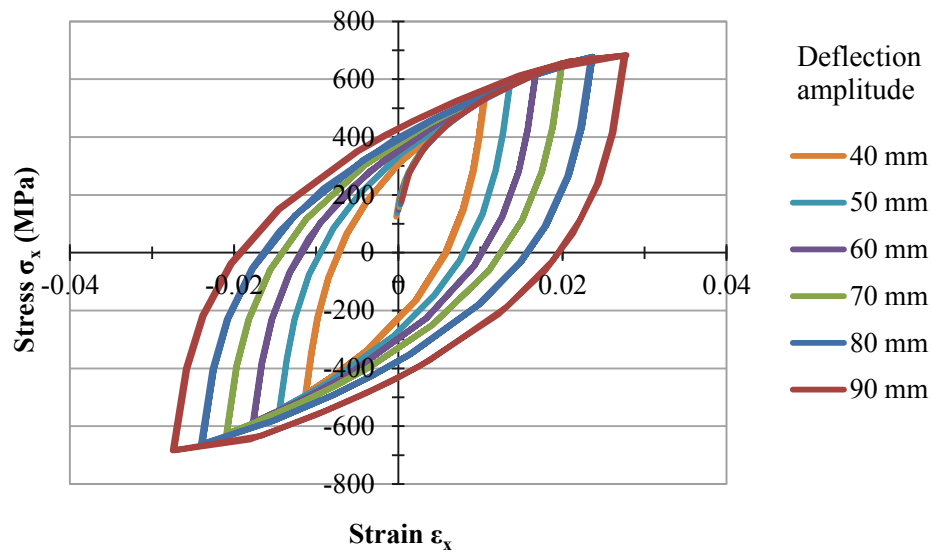


Figure 3-25: Hysteresis loops in the critical element at the base plate surface and plane of symmetry generated by bending load for regular weld shape in presence of residual stress

Table 3-6: Comparison of data generated from the simulation of regular weld

Deflection amplitude (mm)	Bending moment per unit width (kNm/m)	$\sigma_{\max}$ (MPa)	$\sigma_{\min}$ (MPa)	$\sigma_m$ (MPa)	$\Delta\sigma/2$ (MPa)	$\epsilon_{\max}$	$\epsilon_{\min}$	$\Delta\epsilon/2$
40	8.1	536.2	-488.8	23.7	512.5	0.0106	-0.0113	0.0110
50	9.1	581.3	-542.2	19.6	561.8	0.0136	-0.0145	0.0141
60	10.0	620.5	-587.8	16.4	604.2	0.0168	-0.0177	0.0172
70	10.8	655.6	-627.1	14.3	641.4	0.0200	-0.0210	0.0205
80	11.6	677.9	-663.1	7.4	670.5	0.0237	-0.0241	0.0239
90	12.4	682.9	-684.0	-0.6	683.5	0.0278	-0.0275	0.0277

The fatigue life can be predicted for this geometry and loading conditions from Table 3-6 data by the Morrow's equation (2-5) and Smith–Watson–Topper's Equation (2-6). Table 3-7 shows fatigue life estimations for regular weld based on Table 3-6 data.

S-W-T's estimation equation is always more conservative compared with the Morrow's equation and in this case the estimated fatigue lives by Morrow's equation are approximately two times higher than fatigue lives predicted by S-W-T equation. The fatigue lives based on Morrow equation decrease from 1710 cycles to 235 cycles for bending moment per unit width from 8.1 to 12.4 kNm/m while the fatigue lives estimated by S-W-T equation reduce from 885 cycles to 125 cycles.

Table 3-7: Fatigue life for the regular weld in presence of residual stress estimated from ANSYS simulation data by the Morrow equation and Smith–Watson–Topper Equation

<b>Deflection amplitude (mm)</b>	<b>Bending moment per unit width (kNm/m)</b>	<b>Fatigue life N Morrow Eq.</b>	<b>Fatigue life N S-W-T Eq.</b>
<b>40</b>	8.1	1710	885
<b>50</b>	9.1	985	500
<b>60</b>	10.0	630	320
<b>70</b>	10.8	440	220
<b>80</b>	11.6	320	160
<b>90</b>	12.4	235	125

Usually the weld quality at two ends of the weld line is poor and between these two ends weld has a very good quality and fatigue cracks often appear uniformly throughout the weld toe. The finite element simulation shows that the stress and strain distributions drop 5 cm from the ends (Figures 3-26 and 3-27).

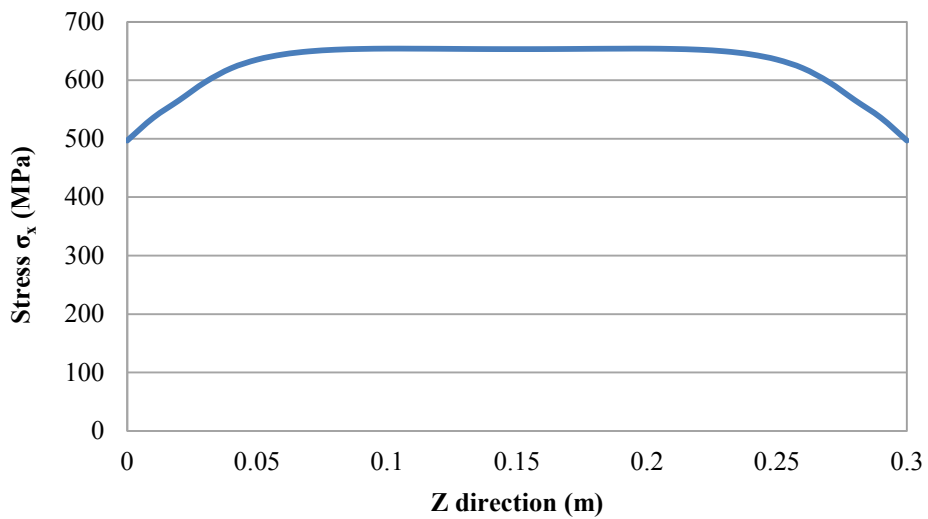


Figure 3-26: Stress distribution along the weld toe for deflection amplitude of 50 mm

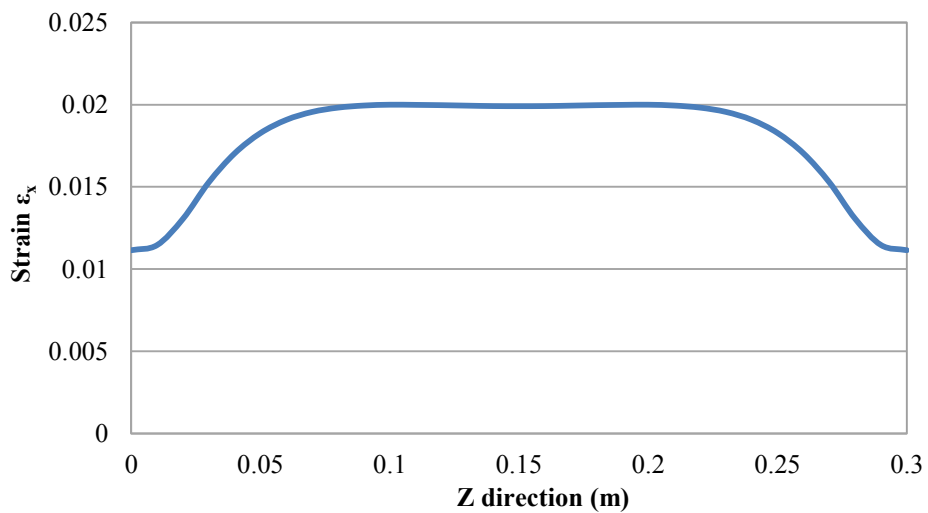


Figure 3-27: Strain distribution along the weld toe for deflection amplitude of 50 mm

### 3.5 Loading in absence of residual stress for regular weld shape

The modelling processes are similarly repeated in order to simulate the stress relief situation in the case of a regular weld shape. There is only one difference, when the INISTATE commands are not used to generate residual stresses. Figure 3-28 shows the generated hysteresis loops in the critical element located at the base plate surface and the plane of symmetry attached to the weld region. They are created due to bending deflection applied to a regular weld shape in absence of residual stress.



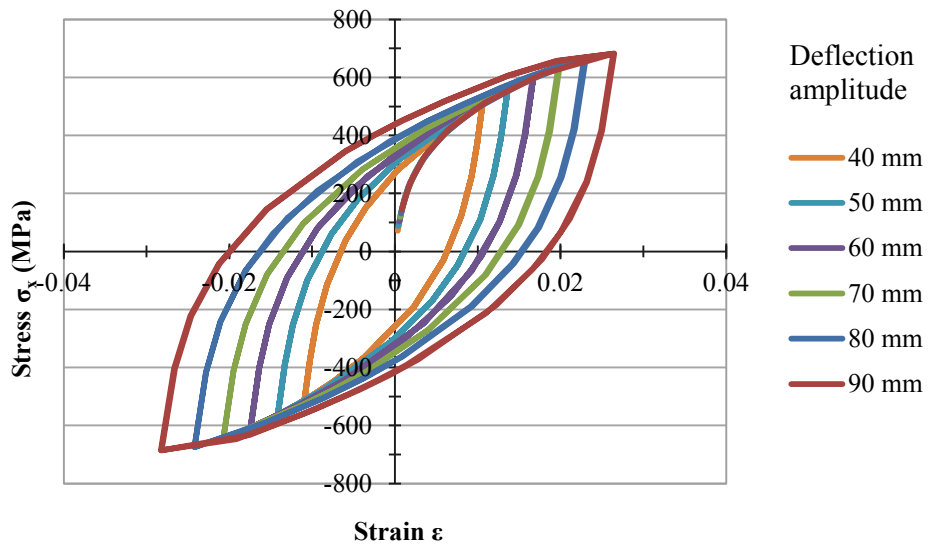


Figure 3-28: Hysteresis loops in the element at the base plate surface and plane of symmetry generated by bending load for regular weld shape in the absence of residual stress

Table 3-8: Comparison of data generated by simulations of regular weld shape model when the residual stresses are relieved

Deflection amplitude (mm)	Bending moment per unit width (kNm/m)	$\sigma_{\max}$ (MPa)	$\sigma_{\min}$ (MPa)	$\sigma_m$ (MPa)	$\Delta\sigma/2$ (MPa)	$\epsilon_{\max}$	$\epsilon_{\min}$	$\Delta\epsilon/2$
40	8.1	508.0	-514.5	-3.3	511.3	0.0106	-0.0110	0.0108
50	9.1	556.2	-564.8	-4.3	560.5	0.0136	-0.0142	0.0139
60	10.0	597.2	-607.6	-5.2	602.4	0.0167	-0.0174	0.0171
70	10.8	634.2	-645.0	-5.4	639.6	0.0199	-0.0207	0.0203
80	11.6	665.4	-674.5	-4.6	670.0	0.0230	-0.0242	0.0236
90	12.4	682.9	-686.0	-1.6	684.5	0.0265	-0.0283	0.0274

The hysteresis loops data are given in Table 3-8. The peak stresses in the third column grow from 508.0 MPa for bending moment per unit width of 8.1 kNm/m to 682.9 MPa for bending moment per unit width 12.4 kNm/m. The minimum stresses in column 4 are

reduced from -514.5MPa to -686.0 MPa. Maximum and minimum strains, similar to maximum and minimum stresses, behave in reverse. Maximum strains increase from 0.0106 to 0.0265 while minimum strains decrease from -0.0110 to -0.0283. The mean stresses are close to zero and almost unchanged. The stress amplitudes in column 6 and strain amplitude in the last column gradually increase from 511.3 MPa and 0.0108 to 684.5MPa and 0.0274.

The predicted fatigue lives for this geometry and loading conditions, by means of Table 3-8 data and using the Morrow's equation (2-5) and Smith–Watson–Topper's equation (2-6), are given in Table 3-9.

In the model without residual stress, likewise, a model with residual stress, S-W-T's estimation equation is more conservative compared to the Morrow's equation. The values of predicted lives by the Morrow's equation are higher than lives predicted by S-W-T equation in all loading amplitudes. The fatigue life based on the Morrow equation is equal to 1790 cycles for 8.1 kNm/m bending moment per unit width and it drops to 240 cycles for 12.4 kNm/m. These fatigue lives, estimated by S-W-T equation, are from 1000 to 125 cycles for bending moments from 8.1 to 12.4 kNm/m

Table 3-9: Fatigue lives for regular weld in absence of residual stress estimated from ANSYS simulations data and by Morrow equation and Smith–Watson–Topper Equation

<b>Deflection amplitude (mm)</b>	<b>Bending moment per unit width (kNm/m)</b>	<b>Fatigue life N Morrow Eq.</b>	<b>Fatigue life N S-W-T Eq.</b>
<b>40</b>	8.1	1790	1000
<b>50</b>	9.1	1020	550
<b>60</b>	10.0	650	345
<b>70</b>	10.8	450	235
<b>80</b>	11.6	325	165
<b>90</b>	12.4	240	125

### 3.6 Loading in presence of residual stress for ground weld model

The simulation processes have been continued for third part as ground weld shape model. Similar to two previous parts, six different cyclic deflections are applied on the welded plate model. The loads applied on ground weld shape are the same as loads used in regular weld shape models in the absence and presence of residual stresses. It is assumed that only the weld shape is changed and the portion of weld protruding outside the plate is removed. From this assumption, stress concentration is the only factor that is changed while the residual stresses still remain in the material around the weld. Figure 3-29 shows the stress vs strain hysteresis graphs produced using ANSYS. This graphs are belong to the element at the critical point at the plate's surface and plane of symmetry attached to the weld volume. The hysteresis loop, representing the dissipated strain energy per unit volume absorbed by that particular element, grows for higher loads.

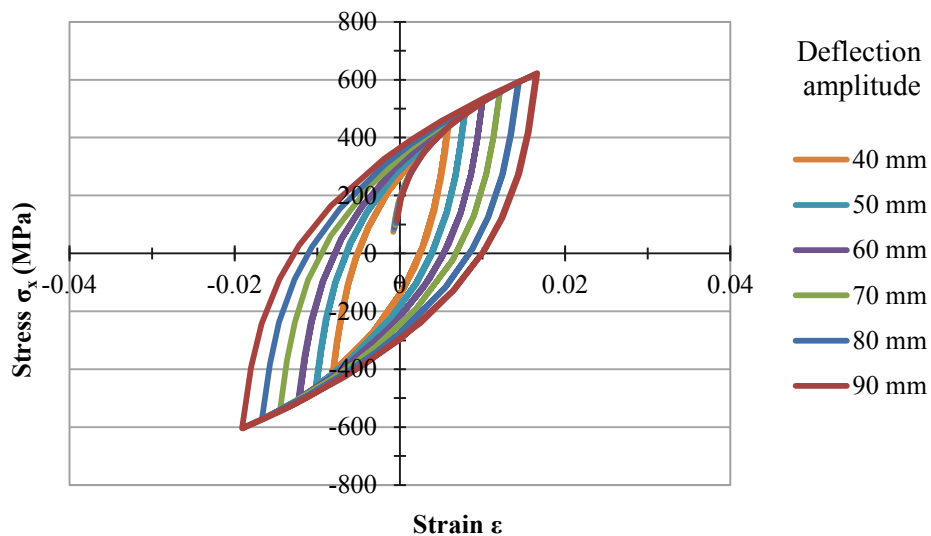


Figure 3-29: Hysteresis loops in the element at the base plate surface and plane of symmetry generated by bending load for ground weld shape in the presence of residual stress

These hysteresis loops data are given in Table 3-10. It can be observed that the values of maximum stresses, maximum strains and also stress and strain amplitudes are increasing but the values of minimum stresses, minimum strains are decreasing. The trend of mean stresses in this case is slightly declining.

Table 3-10: Comparison of data generated by simulations of ground weld shape

<b>Deflection amplitude (mm)</b>	<b>Bending moment per unit width (kNm/m)</b>	$\sigma_{\max}$ (MPa)	$\sigma_{\min}$ (MPa)	$\sigma_m$ (MPa)	$\Delta\sigma/2$ (MPa)	$\epsilon_{\max}$	$\epsilon_{\min}$	$\Delta\epsilon/2$
40	8.1	445.0	-410	17.5	427.5	0.0059	-0.0081	0.0070
50	9.1	489.2	-459.4	14.9	474.3	0.0079	-0.0102	0.0091
60	10.0	527.8	-501.4	13.2	514.6	0.0100	-0.0123	0.0111
70	10.8	562.1	-538.5	11.8	550.3	0.0121	-0.0145	0.0133
80	11.6	593.8	-572.2	10.8	583.0	0.0144	-0.0167	0.0156
90	12.4	622.4	-604.2	9.1	613.3	0.0166	-0.0191	0.0179

Table 3-11: Fatigue lives for a ground weld shape specimen estimated from ANSYS simulations data and by Morrow equation and Smith–Watson–Topper equation

<b>Deflection amplitude (mm)</b>	<b>Bending moment per unit width (kNm/m)</b>	<b>Fatigue life N Morrow Eq.</b>	<b>Fatigue life N S-W-T Eq.</b>
40	8.1	4760	2690
50	9.1	2630	1450
60	10.0	1650	885
70	10.8	1110	580
80	11.6	790	410
90	12.4	590	300

Fatigue lives prediction based on Morrow’s equation (2-5) and S-W-T’s Equation (2-6) and using ANSYS simulation data from Table 3-10 are given in Table 3-11. For ground weld shape geometry, estimated life for bending moment of 8.1 kNm/m is 4760 cycles based on morrow’s equation and 2690 based on S-W-T’s equation. By increasing the bending moment, fatigue life goes down so that the number of cycles to failure for

bending moment of 12.4 kNm/m, would be 790 and 410 cycles according to Morrow and S-W-T equations, respectively. Four estimated fatigue lives based on Morrow's equation and two lives based on S-W-T's Equation is larger than 1000 cycles which is bordering on low cycle fatigue.

### **3.7 Results and Discussion**

Three different weld situations were modelled in this study. Regular weld model with residual stress field was modelled as the benchmark for the other two studies. One deals with a regular weld geometry when the residual stress fields do not exist. This could be considered as a welded joint undergoing a heat treatment causing all residual stresses to be removed. On the other hand, for the third study, only the weld shape was changed and the material outside the plate was removed. This could reflect a case when a grinding process would be carried on after welding. The results such as stresses and strains in critical elements for each model were given previously. Several fatigue lives were predicted from these data based on two different strain life methods. To understand the effect of residual stress and stress concentration factor, the results from the second and third studies have been compared with the benchmark. At first, the effects of residual stress on fatigue life are studied. Therefore, the first and second models are compared each other. Then, the first and third modellings are also compared to determine the effect of stress concentration factor on fatigue life.

#### **3.7.1 The Effect of Residual Stress on Fatigue life**

The residual stress can shift the total stress. Tensile residual stress increases the total stress while the compression residual stress reduces the final stress. In elastic zone of material properties, residual stress would be directly added to loading stress but this is not possible in plastic zone of material properties. Figure 3-30 shows three longitudinal stress distributions along the x direction. The lower graph belongs to residual stress, the middle one represents the stress due to external loading and the higher graph shows a combination of two previous stress distributions. Although the value of residual stress in the vicinity of weld toe is approximately 100 MPa, it can only increase the external

loading stress by 21.4 MPa (from 634.2 to 655.6 MPa) when they are combined together.

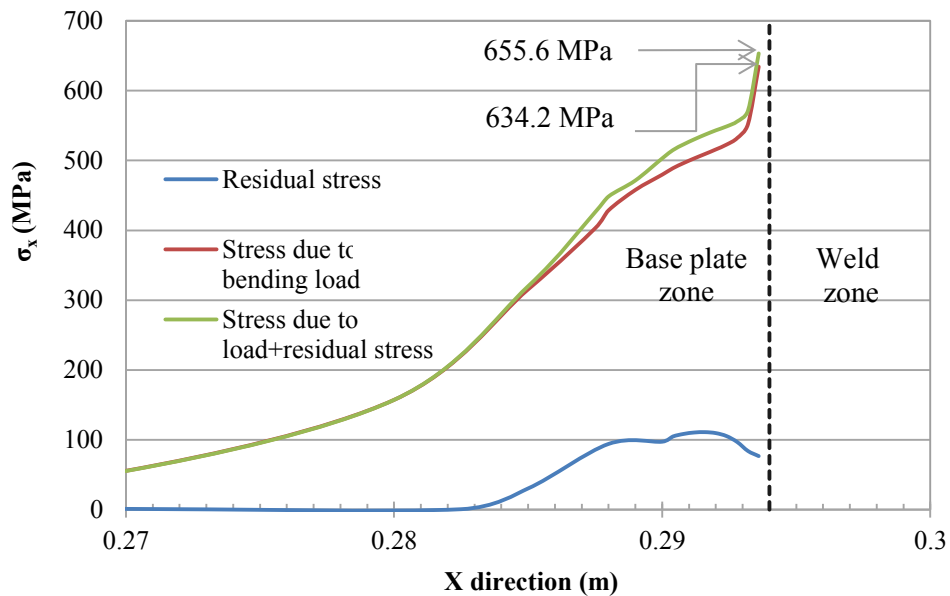


Figure 3-30: Longitudinal stress distributions of residual stress, external loading stress and a combination of external loading stress and residual stress

Figure 3-31 shows two hysteresis loops for a regular weld shape model in the absence and presence of residual stresses when a cyclic deflection equal to 40 mm is applied on both of them. Two graphs are very close and there are no significant changes between areas created by hysteresis loops. This illustrates that the amounts of energy absorbed in the element due to plastic deformations are very similar. It seems that residual stresses, in this case, cause a slight increase of the stress level. Figure 3-32 is similar to Figure 3-31 but with 90 mm cyclic deflection. In this case, the two graphs are very similar as well as hysteresis graphs for 40 mm cyclic deflection. Both graphs for 90 mm deflection noticeably grow, compared with the 40 mm deflection graphs but they still remain very closely together. In this case, the residual stress helps somewhat shift the hysteresis loop to the left side.

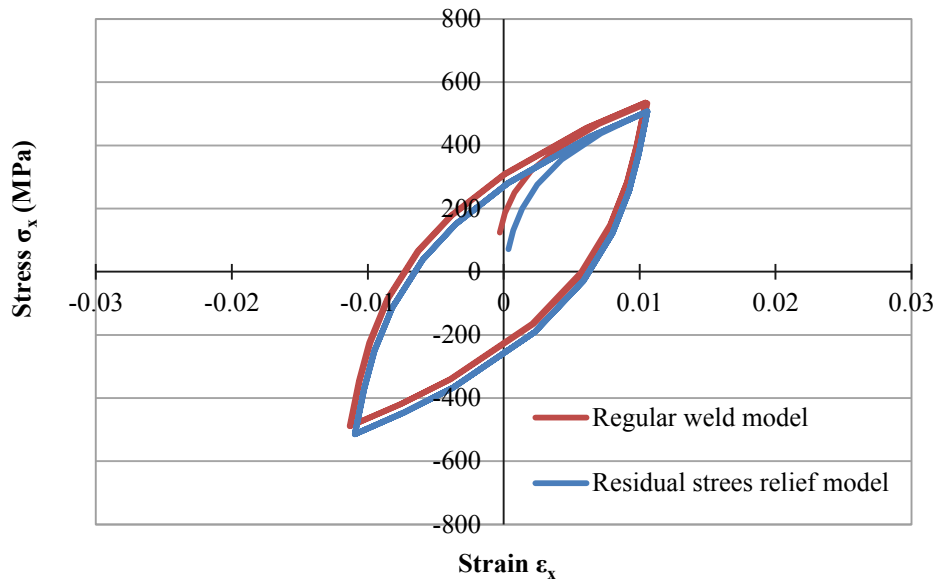


Figure 3-31: Hysteresis loops for cyclic bending with deflection of 40 mm

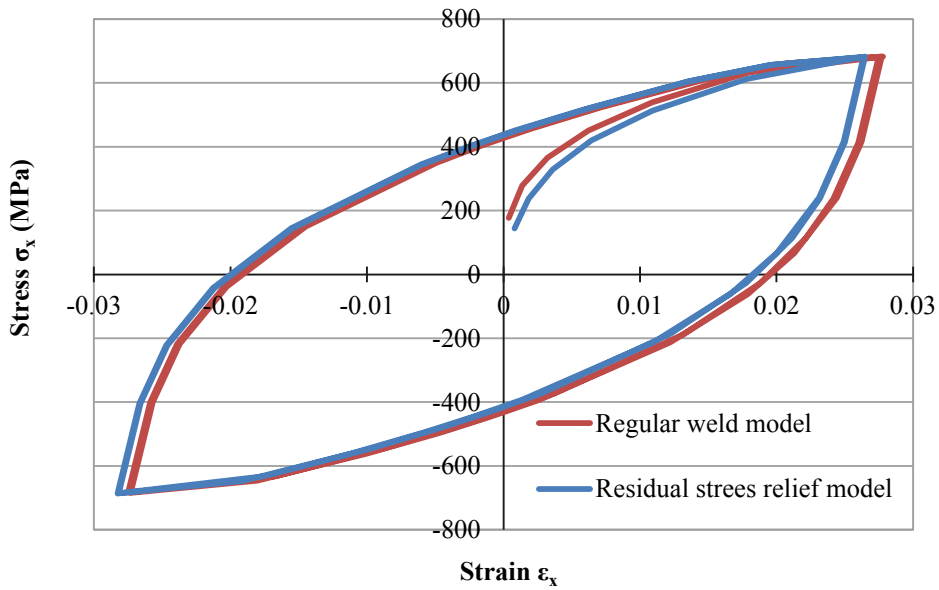


Figure 3-32: Hysteresis loops for cyclic bending with deflection of 90 mm

Figures 3-33 and 3-34 show the comparison between maximum stresses and maximum strains of the regular weld models and residual stress relief models for all loadings. The values of maximum stresses appearing in regular weld models for all loadings, except for the deflection amplitude of 90 mm, are slightly higher than the maximum stresses

appearing in residual stress models. The maximum stresses for the regular weld model and residual stress relief model, when both are applied with the deflection amplitude of 90 mm, are almost equivalent. In Figure 3-34, the values of maximum strains for regular weld models and residual stress relief model and for all loadings, except for deflection amplitudes of 80 and 90 mm, are almost equivalent. These values for deflection amplitudes of 80 and 90 mm and for regular weld model are somehow higher compared with residual stress relief models.

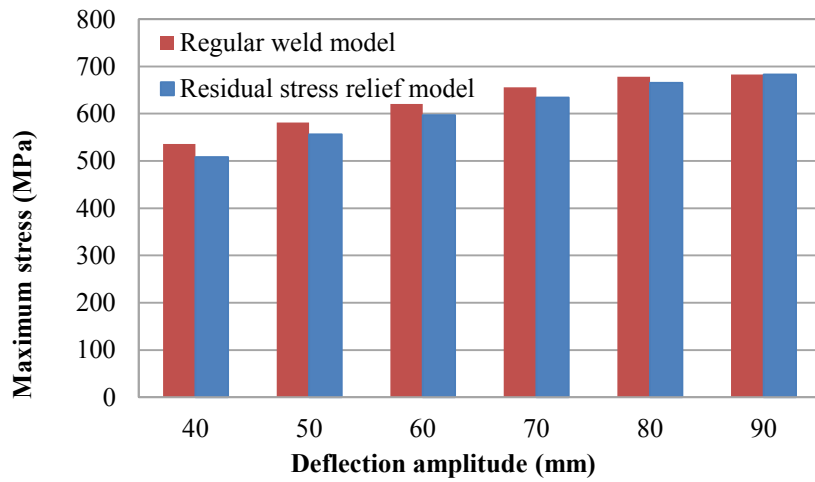


Figure 3-33: Comparison between maximum stresses of regular weld model and residual stress relief model for different loadings

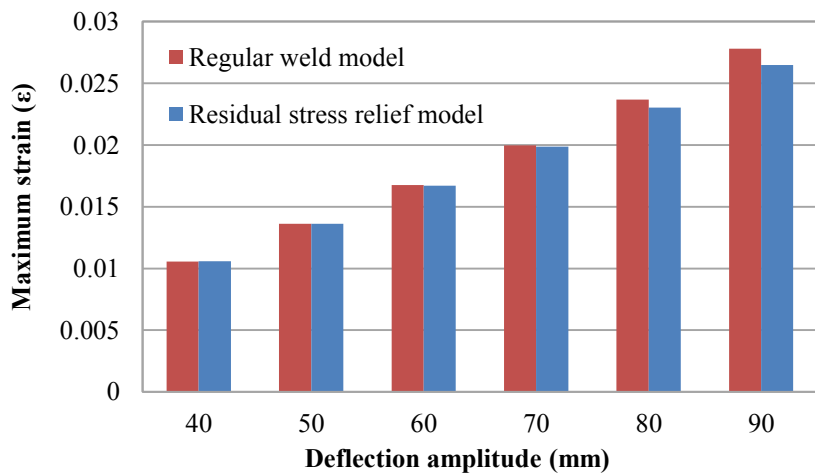


Figure 3-34: Comparison between maximum strains of regular weld model and residual stress relief model for different loadings



In Table 3-12 maximum stresses and stress amplitudes for regular weld models and stress relief models are compared. Peak stresses and stress amplitudes for both cases are increasing when the bending moments increase. Maximum stresses and stress amplitudes for regular weld models are almost always higher than maximum stresses and stress amplitudes for residual stress relief models. Relative changes for maximum stresses are less than 5.3% and they slightly decrease in higher loadings. It shows that the maximum stresses in regular weld model and stress relief model tend to become equivalent when the bending moments are increased. The stress amplitudes for these two types of modellings are very similar for each loading and the stress amplitudes relative changes are equal or less than 0.3%.

Table 3-12: Comparison between stress data of regular weld model and stress relief model generated by ANSYS

<b>Deflection amplitude (mm)</b>	<b>Bending moment per unit width (kNm/m)</b>	<b><math>\sigma_{\max}</math> for regular weld model (MPa)</b>	<b><math>\sigma_{\max}</math> for stress relief model (MPa)</b>	<b>Relative change (%)</b>	<b><math>\Delta\sigma/2</math> for regular weld model (MPa)</b>	<b><math>\Delta\sigma/2</math> for stress relief model (MPa)</b>	<b>Relative change (%)</b>
<b>40</b>	8.1	536.2	508.0	5.3	512.5	511.3	0.2
<b>50</b>	9.1	581.3	556.2	4.3	561.8	560.5	0.2
<b>60</b>	10.0	620.5	597.2	3.8	604.2	602.4	0.3
<b>70</b>	10.8	655.6	634.2	3.3	641.4	639.6	0.3
<b>80</b>	11.6	677.9	665.4	1.8	670.5	670.0	0.1
<b>90</b>	12.4	682.9	682.9	0.0	683.5	684.5	-0.1

Similarly, Table 3-13 shows the comparisons between maximum strains and strain amplitudes for regular weld model and stress relief model when they are subjected to different deflection amplitudes. Maximum strains and strain amplitudes for both cases increase when the bending moments are increased. Maximum strains and strain amplitudes for regular weld models are almost always higher than maximum strains and strain amplitudes for residual stress relief model. Relative changes for maximum strains

are less than 4.7% and they decrease for lower loadings. It shows that the maximum strain in regular weld models and residual stress relief models tend to be close when the bending moments are reduced. The strain amplitudes for regular weld model and residual stress relief models are very similar for each loading and the strain amplitudes relative changes are equal or less than 1.6%.

Table 3-13: Comparison between strain data of regular weld model and stress relief model generated using ANSYS

<b>Deflection amplitude (mm)</b>	<b>Bending moment per unit width (kNm/m)</b>	<b><math>\epsilon_{\max}</math> for regular weld models (MPa)</b>	<b><math>\epsilon_{\max}</math> for stress relief models (MPa)</b>	<b>Relative change (%)</b>	<b><math>\Delta\epsilon/2</math> for regular weld models (MPa)</b>	<b><math>\Delta\epsilon/2</math> for stress relief models (MPa)</b>	<b>Relative change (%)</b>
<b>40</b>	8.1	0.0106	0.0106	0.0	0.0110	0.0108	1.6
<b>50</b>	9.1	0.0136	0.0136	0.0	0.0141	0.0139	1.2
<b>60</b>	10.0	0.0168	0.0167	0.3	0.0172	0.0171	1.0
<b>70</b>	10.8	0.0200	0.0199	0.5	0.0205	0.0203	0.9
<b>80</b>	11.6	0.0237	0.0230	2.7	0.0239	0.0236	1.0
<b>90</b>	12.4	0.0278	0.0265	4.7	0.0277	0.0274	1.0

Fatigue lives predicted by the Morrow's and S-W-T's equations and using ANSYS analysis data were given in Table 3-7 and 3-9. The numbers of cycles to failure are given in Figure 3-35. It can be clearly seen that, regardless of the prediction equations, fatigue life trends in absence and presence of residual stresses are very close to each other.

Scattering of experimental data for fatigue life estimations are always much more than these small changes produced due to residual stress. These graphs reveal that the effects of residual stresses on fatigue lives in low cycle fatigue cases are not too critical and can be ignored. Therefore, trying to mitigate or eliminate the residual stresses when the welded joint is expected to work in low cycle situations may not be beneficial.

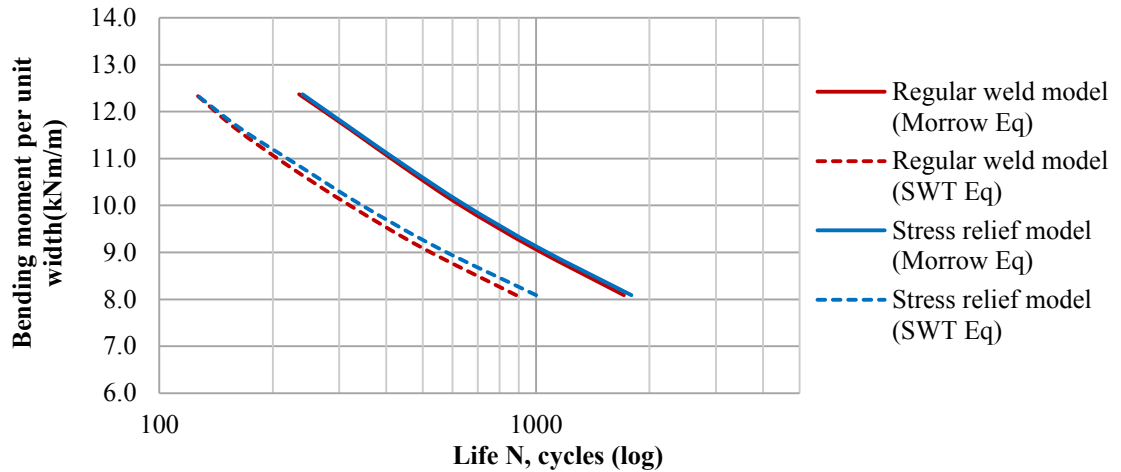


Figure 3-35: Low cycle fatigue life estimation by two equations for two conditions of regular weld model and residual stress relief model

### 3.7.2 The Effect of Stress Concentration on Fatigue life

Stress concentration increases locally the nominal stresses at the locations with irregularity, discontinuity or abrupt changes in cross section. Fatigue life of a specimen can be improved if the source of stress concentration would be eliminated. The angle between the weld volume and base plate volume, which is called weld toe, is the source of stress concentration in a welded joint. Sharper angles can induce higher stress concentration factors at the weld toe. Removing the protruded materials of the weld zone volume outside the base plate surface can eliminate the source of stress concentration; consequently, reduce the total stress at the critical point. To study the effect of stress concentration factor on fatigue life, first and third models are compared here.

Figure 3-36 shows two hysteresis loops for a regular weld shape model and ground model at the element located at the base plate surface and plane of symmetry attached to the weld zone volume. The residual stresses exist in both models to ensure that the stress concentration is the only factor that is changed. The cyclic deflections equal to 40 mm are applied to both. Unlike the residual stresses that would shift the whole hysteresis loops without any significant area changes, stress concentration is multiplied to the stresses and considerably changes its area. The hysteresis loop reduces meaningfully when the stress concentration factor is eliminated. It illustrates that the

amounts of energy absorbed in the element due to plastic deformations, is reduced. Figure 3-37 is similar to Figure 3-36 but with 90 mm cyclic deflection. On this occasion, two graphs are very different, as well as the hysteresis graphs for the 40 mm cyclic deflection. Both graphs for 90mm deflection have noticeably grown, compared with the 40 mm deflection graphs. In this case, removing stress concentration helps reduce the hysteresis loop area.

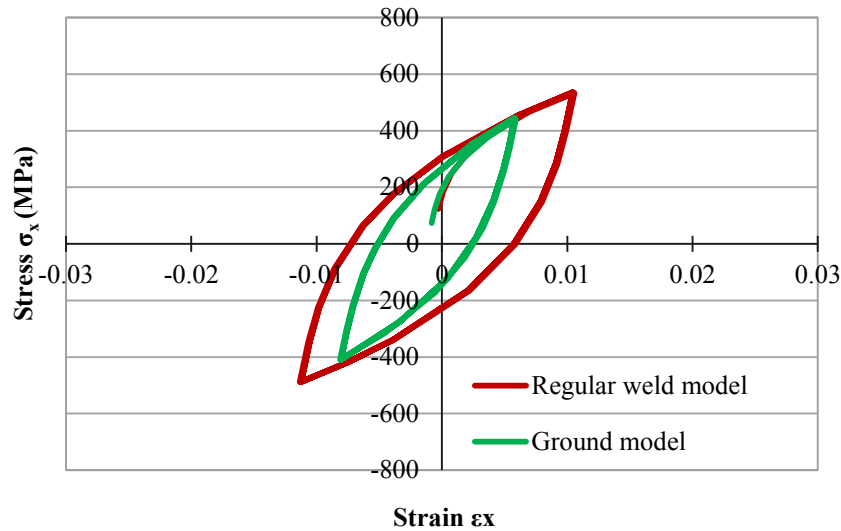


Figure 3-36: Hysteresis loops for cyclic bending with deflection of 40 mm

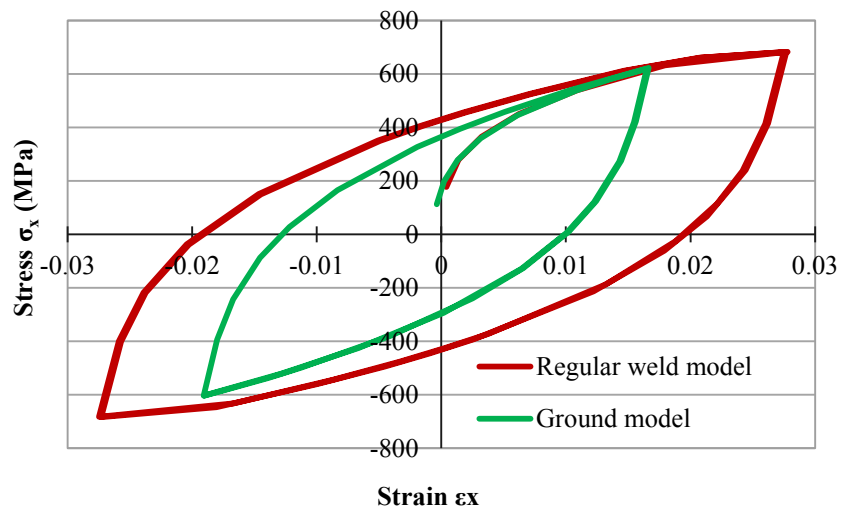


Figure 3-37: Hysteresis loops for cyclic bending with deflection of 90 mm

Figures 3-38 and 3-39 show the comparison between maximum stresses and maximum strains of the regular weld model and ground model for deflection amplitudes from 40 mm to 90 mm with an incremental of 10 mm. The values of maximum stresses appearing in regular weld models for all loadings are higher than the maximum stresses appearing in ground models.

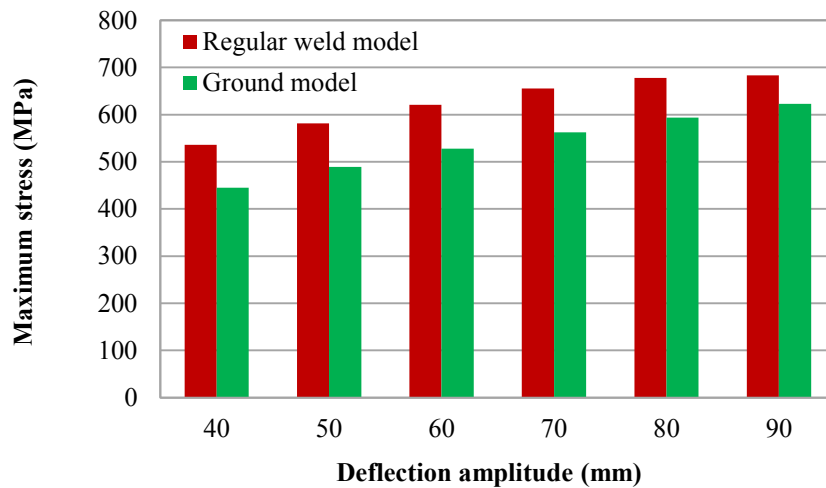


Figure 3-38: Comparison between maximum stresses of regular weld model and ground model for different loadings

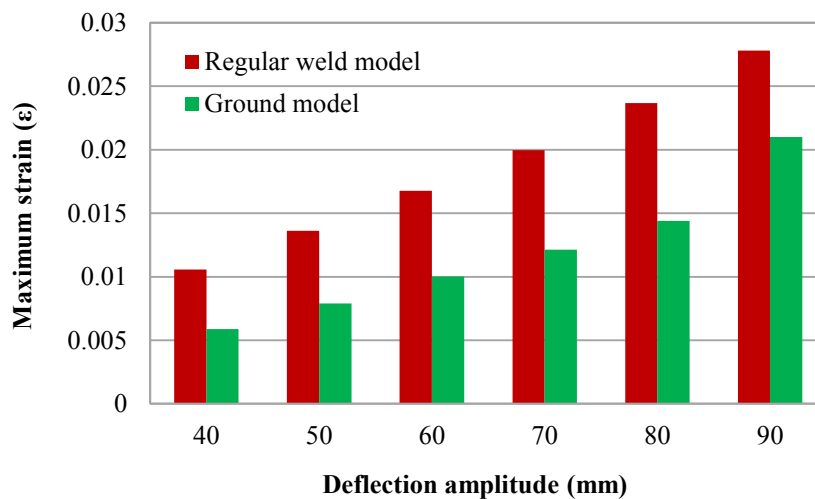


Figure 3-39: Comparison between maximum strains of regular weld model and ground model for different loadings

In Figure 3-39, the values of maximum strains for ground models are significantly lower than the maximum strains for regular weld model in all loadings.

In Table 3-14 maximum stresses and stress amplitudes for regular weld models and ground models are compared. Peak stresses and stress amplitudes increase for both cases when the bending moments increase. Maximum stresses and stress amplitudes for regular weld models are always higher than maximum stresses and stress amplitudes for ground models. Relative changes for maximum stresses are between 8.9% and 17% and are slightly decrease in higher loadings. Relative changes for stress amplitudes are between 10.3% and 16.6% and slightly decrease in higher loadings.

Table 3-14: Comparison between stress data of regular weld models and ground models generated by ANSYS

<b>Deflection amplitude (mm)</b>	<b>Bending moment per unit width (kNm/m)</b>	<b><math>\sigma_{\max}</math> for regular weld models (MPa)</b>	<b><math>\sigma_{\max}</math> for stress relief models (MPa)</b>	<b>Relative change (%)</b>	<b><math>\Delta\sigma/2</math> for regular weld models (MPa)</b>	<b><math>\Delta\sigma/2</math> for stress relief models (MPa)</b>	<b>Relative change (%)</b>
<b>40</b>	8.1	536.2	445.0	17.0	512.5	427.5	16.6
<b>50</b>	9.1	581.3	489.2	15.8	561.8	474.3	15.6
<b>60</b>	10.0	620.5	527.8	14.9	604.2	514.6	14.8
<b>70</b>	10.8	655.6	562.1	14.3	641.4	550.3	14.2
<b>80</b>	11.6	677.9	593.8	12.4	670.5	583.0	13.0
<b>90</b>	12.4	682.9	622.4	8.9	683.5	613.3	10.3

Similarly, Table 3-15 shows the comparisons between maximum strains and strain amplitudes for regular weld models and ground models when they are subjected to different deflection amplitudes. Maximum strains and strain amplitudes for both cases increase when the bending moments increase. Maximum strains and strain amplitudes for regular weld model are always significantly higher than maximum strains and strain amplitudes for ground model. Relative changes for maximum strains are between 39.2% and 44.2%. Relative changes for strain amplitudes are between 34.9% and 36%.

Table 3-15: Comparison between strain data of regular weld model and ground model generated using ANSYS

<b>Deflection amplitude (mm)</b>	<b>Bending moment per unit width (kNm/m)</b>	<b><math>\epsilon_{\max}</math> for regular weld models (MPa)</b>	<b><math>\epsilon_{\max}</math> for stress relief models (MPa)</b>	<b>Relative change (%)</b>	<b><math>\Delta\epsilon/2</math> for regular weld models (MPa)</b>	<b><math>\Delta\epsilon/2</math> for stress relief models (MPa)</b>	<b>Relative change (%)</b>
<b>40</b>	8.1	0.0106	0.0059	44.2	0.0110	0.0070	36.0
<b>50</b>	9.1	0.0136	0.0079	42.0	0.0141	0.0091	35.6
<b>60</b>	10.0	0.0168	0.0100	40.3	0.0172	0.0111	35.4
<b>70</b>	10.8	0.0200	0.0121	39.2	0.0205	0.0133	34.9
<b>80</b>	11.6	0.0237	0.0144	39.2	0.0239	0.0156	34.9
<b>90</b>	12.4	0.0278	0.0166	40.1	0.0277	0.0179	35.4

Fatigue lives predicted by Morrow's and S-W-T's equations (2-5 & 2-6) and using ANSYS analysis data for regular weld models and ground models and their proportions are given in Table 3-16. Also, these values for number of cycles to failure are given in Figure 3-40. It is clear that, regardless of the prediction equations, fatigue lives are meaningfully improved by eliminating the stress concentration factor. The fatigue lives for ground models are increased somewhere between two and three times compared with regular weld models. This finding illustrates that unlike the residual stresses which do not have important effects on fatigue life in low cycle fatigue cases, stress concentration can highly change the fatigue life strength.

Table 3-16: Comparison between fatigue life estimations for regular weld models and ground models generated by Eqs. (2-5) and (2-6)

Deflection amplitude (mm)	Bending moment per unit width (kNm/m)	$N_{R,M}^{(1)}$	$N_{G,M}^{(2)}$	$N_{G,M} / N_{R,M}$	$N_{R,SWT}^{(3)}$	$N_{G,SWT}^{(4)}$	$N_{G,SWT} / N_{R,SWT}$
40	8.1	1710	4760	2.8	885	2690	3.0
50	9.1	985	2630	2.7	500	1450	2.9
60	10.0	630	1650	2.6	320	885	2.8
70	10.8	440	1110	2.5	220	580	2.6
80	11.6	320	790	2.5	160	410	2.6
90	12.4	235	590	2.5	125	300	2.4

- (1) Fatigue lives for regular weld models predicted by Morrow equation
- (2) Fatigue lives for ground models predicted by Morrow equation
- (3) Fatigue lives for regular weld models predicted by S-W-T equation
- (4) Fatigue lives for ground models predicted by S-W-T equation

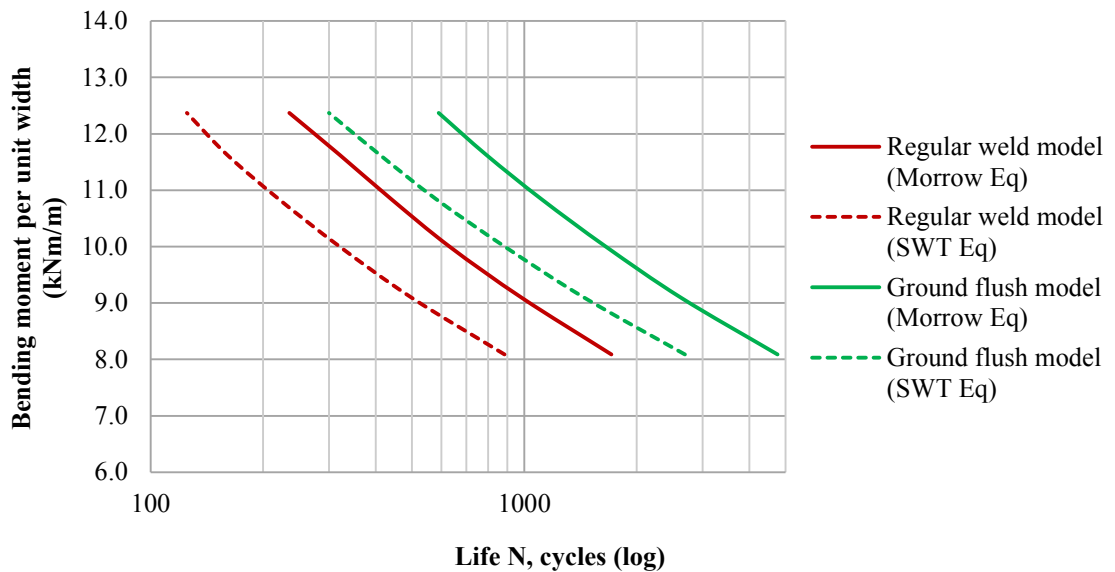


Figure 3-40: Low cycle fatigue life estimation by two equations for two conditions of regular weld model and ground model



## CHAPTER 4 EXPERIMENTAL FATIGUE TESTS

### 4.1 Introduction

In the previous chapter the fatigue behaviour of butt weld joints subjected to bending loads in low cycle fatigue situation was studied. Two types of weld treatments to enhance the fatigue lives were analysed. Each type of weld treatment focused on one aspect that affects the fatigue. Residual stress and stress concentration are two phenomena that can weaken weld joints against cyclic loads. As mentioned in literature, it has been proven by other researchers that in high cycle fatigue cases, elimination of residual stress and stress concentration can significantly improve the fatigue life. In this study, it has analytically been shown that the effects of residual stresses on low cycle fatigue life are not important and can be ignored. On the contrary, it can be concluded from the analysis that the low cycle fatigue lives increase somewhere between two and three times by elimination of stress concentration factor. The advantage of residual stress elimination to improve low cycle fatigue was analytically rejected. Although the advantage of stress concentration elimination was proven by simulations, it must be confirmed by experiment.

In the experimental testing, at first, it should be established whether the approach of this study in finite element simulations by ANSYS is correct and reasonable and then the analytical results on ground flush to eliminate the stress concentration factor should be verified by laboratory tests. Proof of fatigue life predictions by analysis for regular weld specimens and ground flush specimens and calibration of the finite element models are the main goals of laboratory fatigue testing.

### 4.2 Testing conditions and specimens preparation

The fatigue tests of the welded specimens were carried out under reversed bending load condition. To assess the fatigue life of the welded butt joints with different loading amplitudes, 30 welded specimens from steel AS/NZS 3679.1-300 grade were prepared. Two types of cantilever welded plates were examined by a shake table. 15 specimens were used for regular weld fatigue tests and 15 others were used for weld ground flush

tests. 5 reversible loading conditions were applied on specimens. For each loading regime, 3 welded specimens were used to ensure the experimental results are statistically meaningful. The specimens are 300 mm wide and 700 mm long formed from two 10mm thick and 300 and 400 mm long plates welded together with welding preparation and fit-out as shown in Figures 4-1 and 4-2.

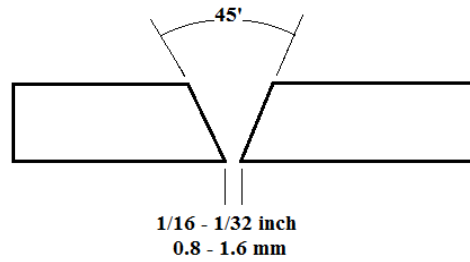


Figure 4-1: Welding preparation and fit-out



Figure 4-2: Welded joints specimen

For the ground flush specimens, any part of weld material protruding outside the plate surface are removed by a hand disk grinder, eliminating the weld toe angle and slag.

### 4.3 Equipment and Test Set-up

One of the most common test set-ups for bending fatigue test is using off-centre mass testing machine generating a cyclic bending load on the plate. In this method, a cantilever specimen is set first on a fixed frame and a vibrator is installed on the plate to generate constant amplitude vibration (Figure 4-3). This test set-up is very practical in high cycle fatigue tests because it can apply a high frequency bending load on specimen but the loading amplitudes are limited. For current study, the values of loadings are very high (up to 10 kN). Therefore, a high capacity set up that can apply high loads is necessary. For this purpose, the vibrator machine is replaced with UTS shake table.

UTS shake table is a 3×3 metre, uniaxial shake table with displacement, velocity and acceleration control. Therefore, the required deflection amplitudes applied on specimens can be accurately operated by the shake table. Figure 4-5 shows the shake table capacity and limitations.

Using the shake table is helpful and useful to achieve more accurate results with easier output monitoring.

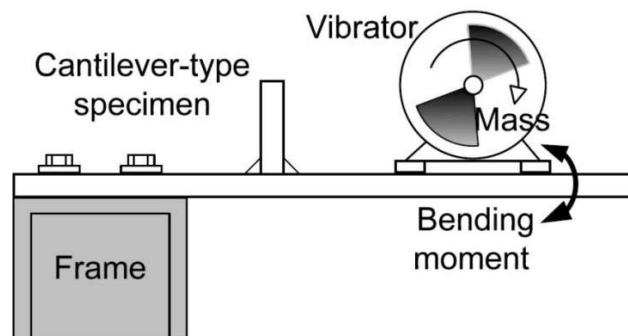


Figure 4-3: Common test set-up for bending fatigue test

As shown in Figure 4-4, a cantilever plate specimen is set on a solid frame bed attached to the shake table and constant amplitude reverse loads are applied using the power

transmission arm attached to a fixed frame which transforms alternating displacement to bending load.



Figure 4-4: Test set up prepared for the current study

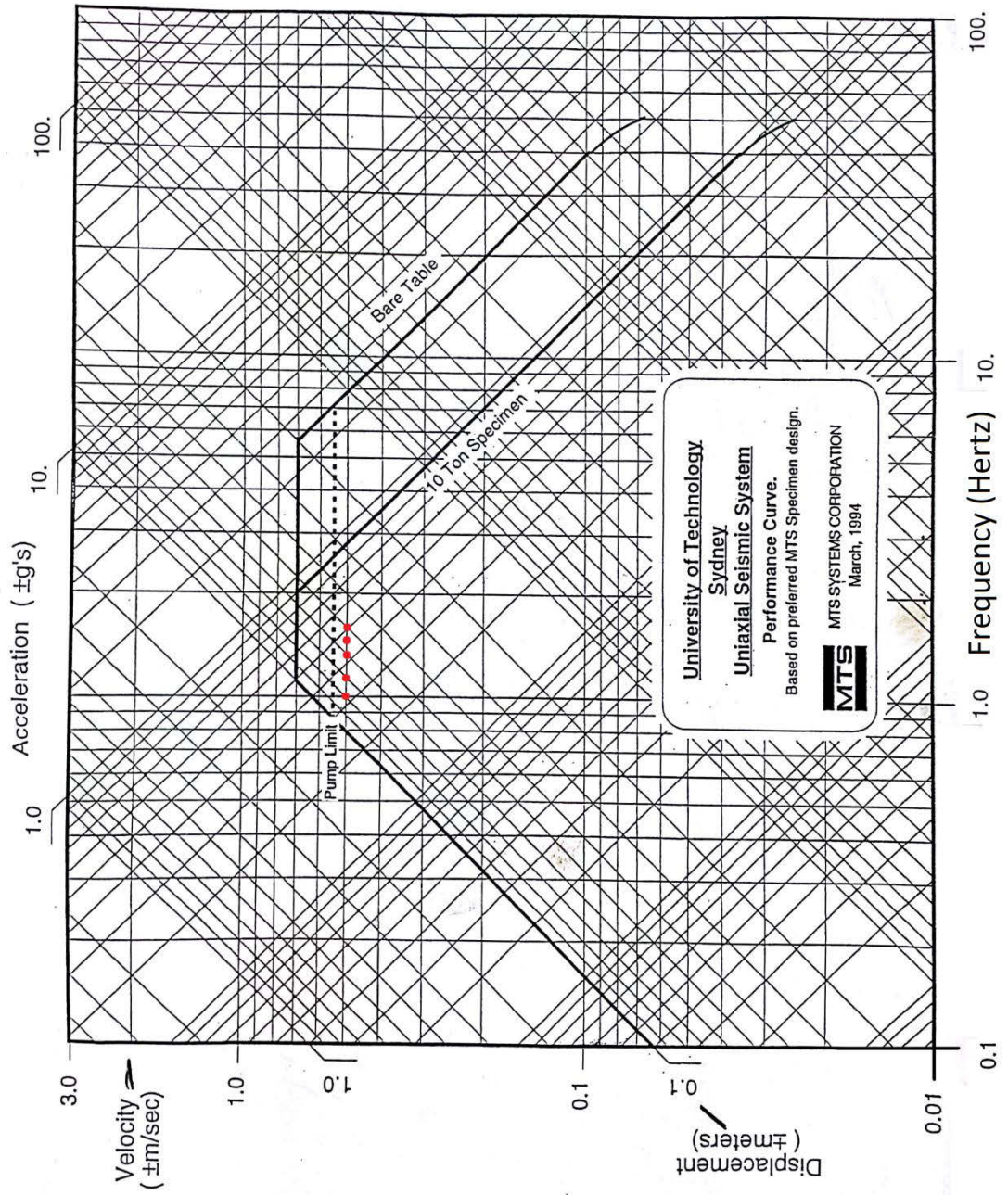


Figure 4-5: Shake table limitation chart

Five red points can be observed in Figure 4-5 which represent five loadings applied by shake table. They were chosen to achieve the highest possible velocity (0.5 m/sec), otherwise, the testings would take a long time. The loading frequencies were set less than 2 Hertz. According to modal analysis simulations by ANSYS, the first, second and third natural frequencies of specimens were 42, 258 and 669 Hz, respectively. Therefore, attaching the specimens on the table does not stimulate the resonant frequencies.

Using a load cell, the applied loads were controlled during the fatigue tests. The load cell is a STS Avoirdupois model made by Sun Scale Inc. It is of stainless steel construction with 3 klb capacity and 3 mv/v output. Figure 4-6 shows the load cell used in this test set up.



Figure 4-6: Load cell

#### 4.4 Regular Weld Fatigue Tests

Five reversible displacement inputs of 50 mm, 55 mm, 60 mm, 70 mm and 80 mm were applied on the specimens (Figure 4-7). Loading frequency for these loading were 1.6 Hz, 1.5 Hz, 1.4 Hz, 1.2 Hz and 1 Hz, respectively. Figure 4-8 shows the cyclic curves of displacement and loading at the start, middle and end of the test for displacement amplitude of 50 mm. the loading gradually increases to the required amplitude after 9 cycles. The displacement fluctuates between -47 mm and 53 mm to enforce a fully reversible load on the specimen. The cyclic displacement remains constant until the failure happens.

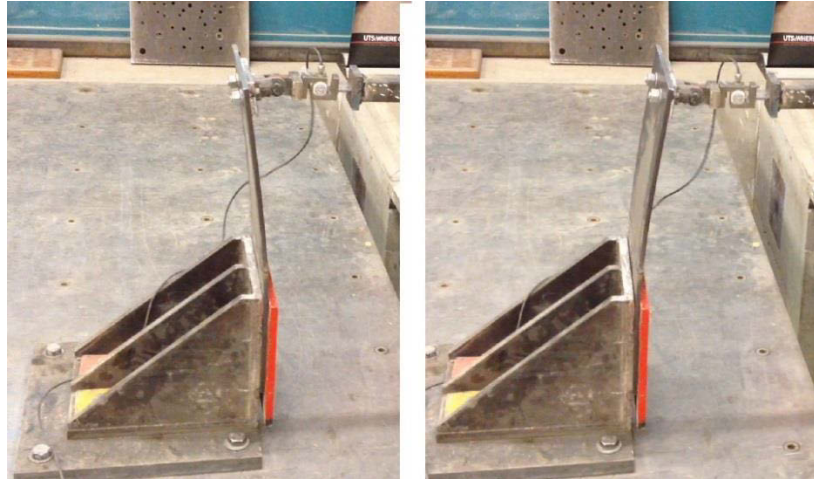


Figure 4-7: Reversible displacement input

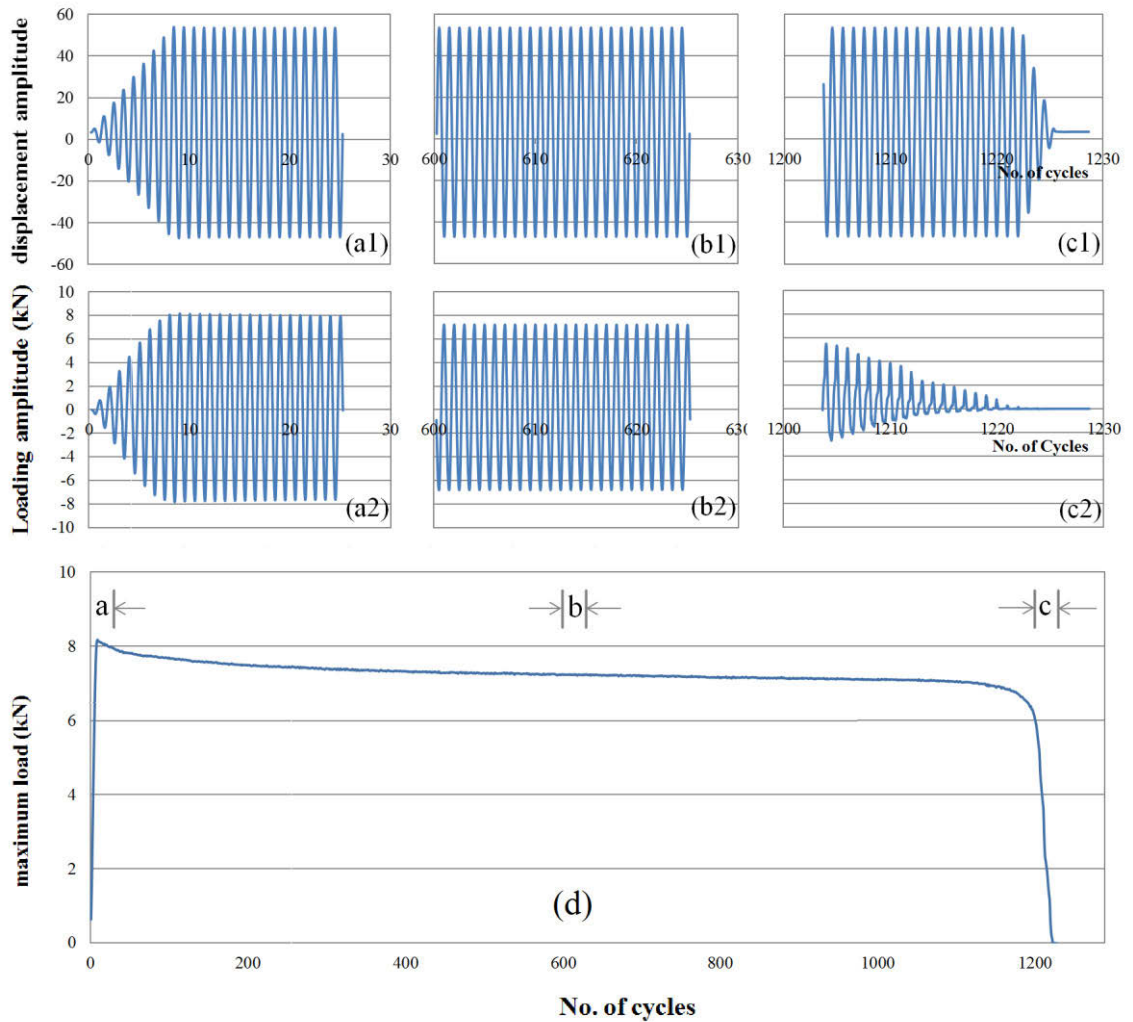


Figure 4-8: Displacement and loading amplitudes, (a1) displacement amplitude at the test start, (a2) loading amplitude at the test start, (b1) displacement amplitude at the middle of the test, (b2) loading amplitude at the middle of the test, (c1) displacement amplitude at the end of the test, (c2) loading amplitude at the end of the test and (d) peak loads vs number of cycles

Figure 4-8 (d) is the maximum load vs number of cycles graph created by measuring the maximum load in each cycle. After reaching the desired cyclic displacement, the maximum load graph shows a slight declining trend. It is the crack initiation step that took approximately 1150 cycles for this sample. In this step plastic deformations happen at the weld toe and dissipated plastic energy appears as heat generation and temperature increases. After initiation of the fatigue crack, crack propagation occurs very fast and after approximately 50 cycles the specimen reaches the final failure. Figure 4-9 shows a low cycle failure at the weld toe. The fatigue crack initiates and then propagates at the stress concentration region.



Figure 4-9: Fully developed fatigue crack along the weld toe.

Although the weld quality at two ends of the weld line is poor in most samples and between these two ends weld has a very good quality (Figure 4-10), fatigue cracks often appear uniformly throughout the weld toe (Figure 4-9). The finite element simulation performed in the previous chapter shows that the stress and strain distributions drop 5 cm from the ends (Figures 3-26 and 3-27).



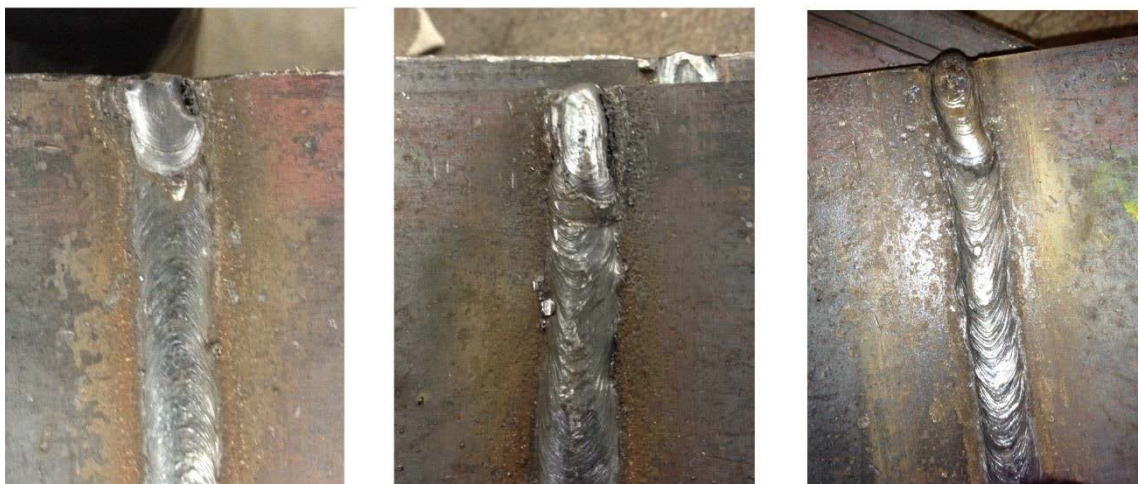


Figure 4-10: Weld quality in the middle and at the end of specimens

#### **4.5 Ground flush specimens fatigue Tests**

Similar loadings and test conditions were used for ground flush specimens fatigue test. Figure 4-11 shows the fatigue damage along the weld toe. Three specimens in regular weld tests and three specimens in ground flush tests had some major defects and porosity (Figure 4-13) that caused test results to become corrupted. These specimen test results were ignored.



Figure 4-11: Fully developed fatigue crack along the weld toe in a ground flush specimen

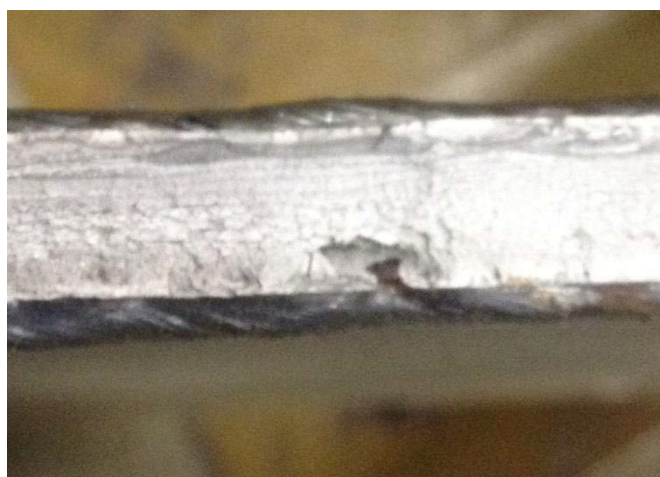


Figure 4-12: Major defects and porosities in welds material that led to ignoring some specimen test results

#### 4.6 Test Results and Discussion

The experimental results for regular weld joints are shown in Figure 4-13. Line colours represent the deflection amplitude applied on the specimens. Graphs show the peak of applied loads in each cycle. Number of cycles for crack initiation depends on the deflection amplitude so that for lower loading levels it takes a longer time, while the crack propagation is very fast and takes less than 50 cycles to fail for all specimens. In the higher deflection amplitudes, specimens suffer higher maximum bending load in each cycle and final failures occur sooner. Number of cycles to final failure for 50 mm deflection amplitudes are 1284 and 1222 cycles, for 55 mm are 1137, 1078 and 938 cycles, for 60 mm are 805, 720 and 604 cycles, for 70 mm are 464 and 371 cycles and finally, for 80 mm are 426 and 270 cycles.

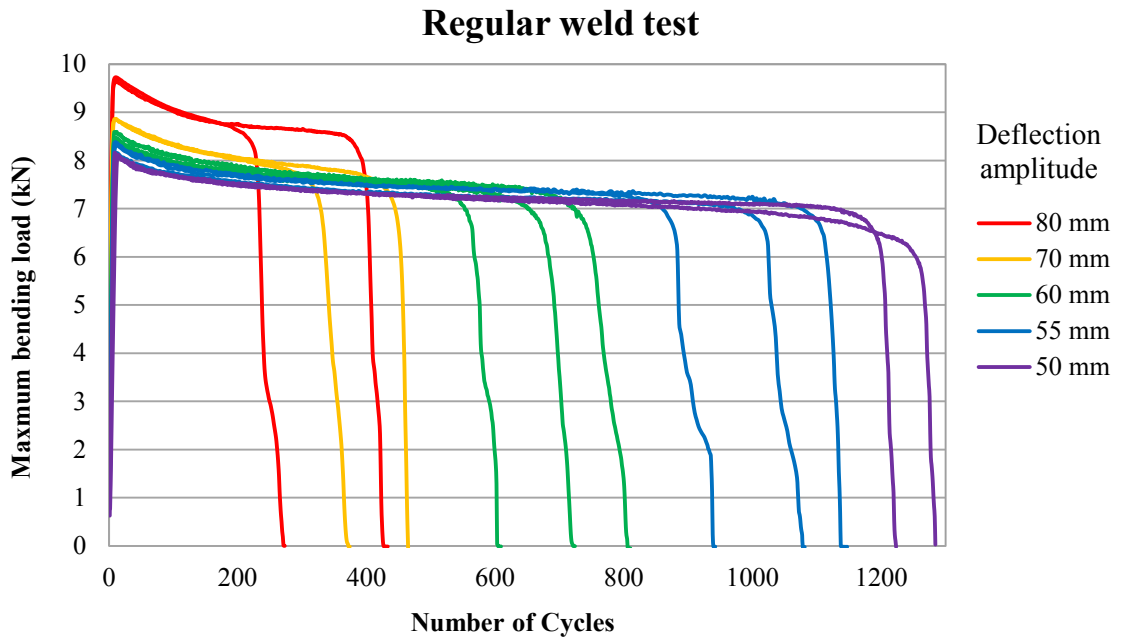


Figure 4-13: Maximum bending loads in each cycle applied on regular weld specimens

Similarly for ground flush specimens, the experimental data are shown in Figure 4-14. In this laboratory testing phase, numbers of cycles to final failure for the 50 mm deflection amplitude are 1785 and 1458 cycles, for 55 mm are 648 and 946 cycles, for 60 mm are 620 and 682 cycles, for 70 mm are 271, 312 and 324 cycles and finally for 80 mm are 82, 128 and 123 cycles.

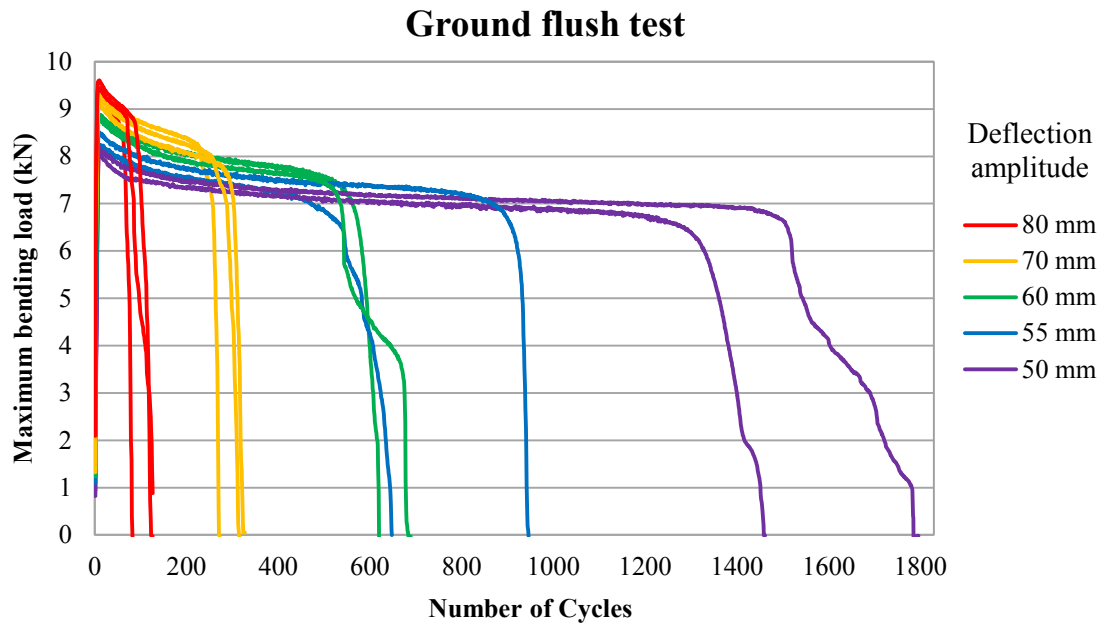


Figure 4-14: Maximum bending loads in each cycle applied on ground flush specimens

Fatigue failure across the thickness of the plate has three regions (Figure 4-15). Region (a) is the place that the material suffers plastic deformation during crack initiation period and the fatigue crack starts from this region. Plastic deformations do not happen in the material in region (b) and during fatigue crack initiation the material in this region remains elastic. When a fatigue crack appears, it propagates across these two regions very fast in less than 50 cycles. Region (c) is the final fast fracture zone.



Figure 4-15: Failure cross section

# CHAPTER 5 COMPARISON OF NUMERICAL AND EXPERIMENTAL RESULTS

## 5.1 Introduction

Low cycle fatigue behaviours of a butt weld joint subjected to bending loads were numerically studied with finite element analysis by ANSYS in Chapter 3. It was shown that the residual stress does not affect the low cycle fatigue life and the advantage of residual stress elimination to improve low cycle fatigue life, was theoretically rejected. On the contrary, analyses showed that the weld treatment to improve stress concentration situation would be beneficial and it can increase the fatigue life up to three times. However, to accept this finding, it requires verification by laboratory fatigue tests.

In Chapter 4 testing conditions and specimen's preparation were discussed and the required equipment and Test set-up were explained and fatigue tests for regular weld specimens and ground flush specimen were carried out.

In this chapter the analytical results provided in Chapter 3 and the experimental results provided in Chapter 4, are compared.

## 5.2 Comparison between numerical modelling and experimental data for regular weld

The load-deflection graph generated by finite element modelling has good agreement with the experimental results (Figure 5-1). To prepare these load-deflection graphs at first, four deflections applied on specimen as initial loadings during experiment and the loads were measured by load cell. Then, these loads were used in modelling to prepare simulation deflection. In Table 5-1 load-deflection data generated by experiment and simulation are compared. The distinction of deflections between experiment and simulation for same loads are not noticeable. It shows that the stress-strain diagrams used for finite element modelling as material properties for base plate and weld zone are acceptable.

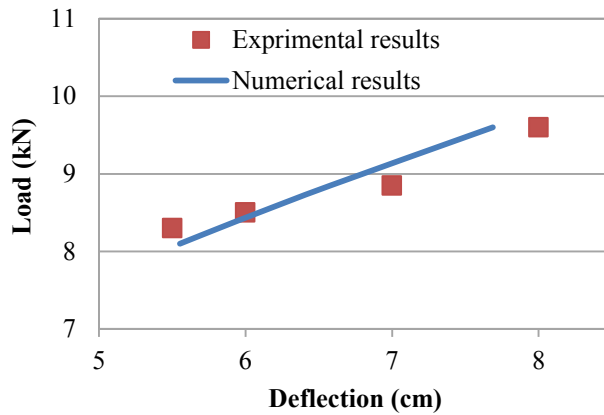


Figure 5-1: Load-deflection graph

Table 5-1: Experimental and numerical load-deflections

Load (kN)	Experimental deflection (cm)	Numerical deflection (cm)	Error (%)
8.3	5.5	5.82	5.8
8.5	6	6.09	1.5
8.85	7	6.58	6.0
9.6	8	7.69	3.9

Numerical and experimental results for regular weld fatigue life estimation are given in Figure 5-2. The numerical data display a reasonable agreement with experimental data. The Morrow equation (2-5), to predict the low cycle fatigue life of a regular butt weld joint without any treatment, is more accurate compared with the S-W-T equation. However, with S-W-T equation the fatigue estimation will be more conservative.

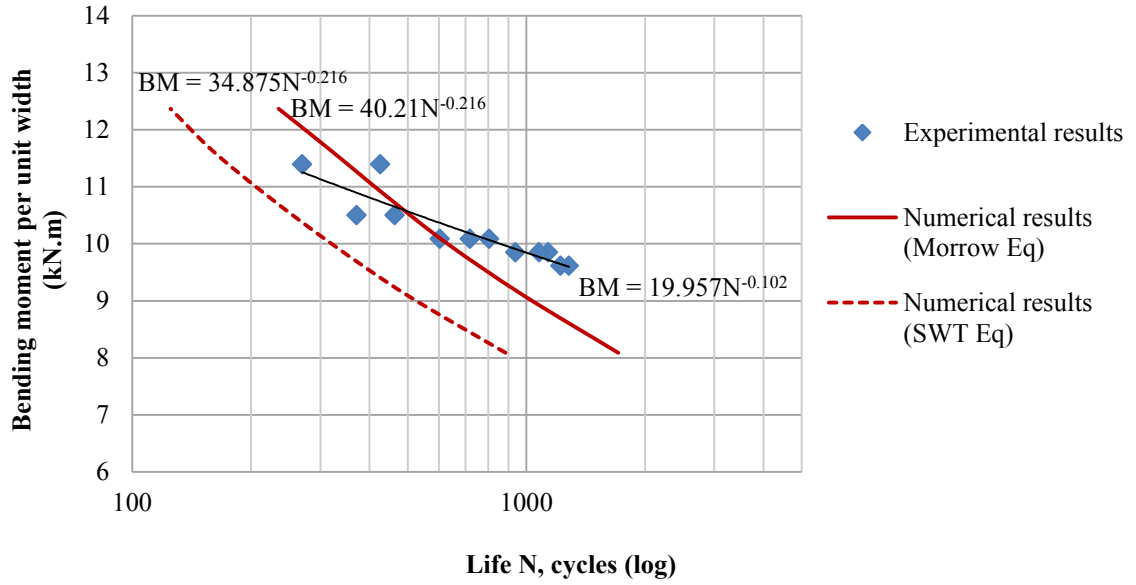


Figure 5-2: Numerical and experimental data comparison for regular weld specimens

The trend line fitted to the experimental results is as follows:

$$BM_{\text{experimental}} = 19.957(N_{\text{experimental}})^{-0.102} \quad (5-1)$$

And the Morrow equation gives the following equation to relate the bending moment per unit width to the fatigue life:

$$BM_{\text{analytical}} = a (N_{\text{analytical}})^{-b} \quad (5-2)$$

Where  $a$  is equal to 40.21 and  $b$  is equal to -0.216. With two correction coefficients the analytical results can be related to the experimental data as follows:

$$BM = a'(N)^{-b'} \quad (5-3)$$

Where:  $a' = 0.496a$  and  $b' = 0.472b$

Therefore, the modified analytical equation proposed for this case will be:

$$BM_{\text{analytical}} = 0.496 \times a \times (N_{\text{analytical}})^{-b \times 0.472} \quad (5-4)$$

### 5.3 Comparison between numerical modelling and experimental data for ground flush specimens

Semi-analytical and experimental results for fatigue life estimation of ground flush specimens are given in Figure 5-3. The Semi-analytical data do not show good agreement with experimental data.

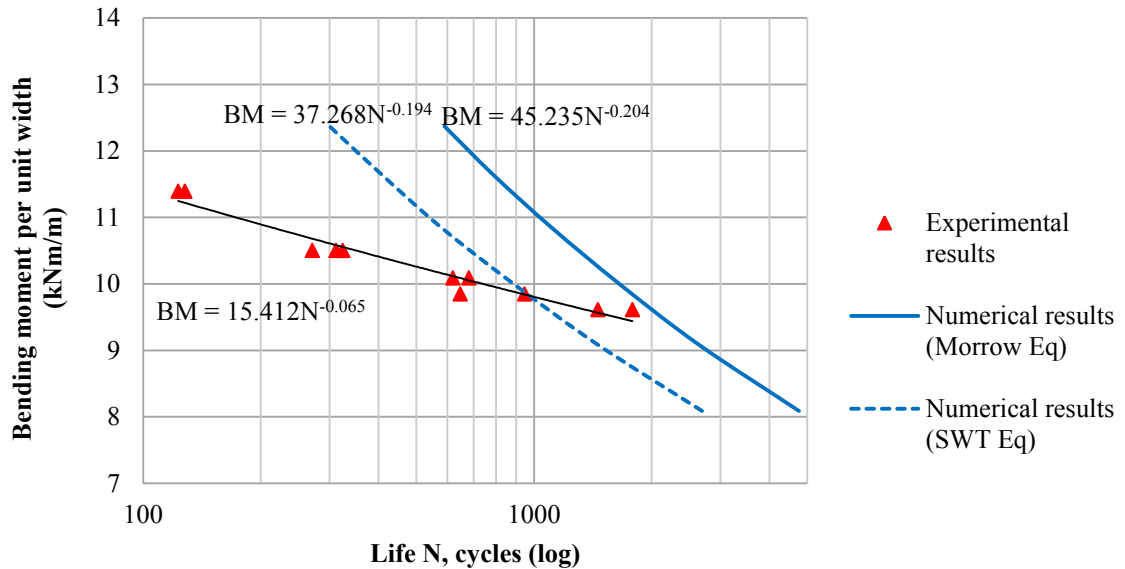


Figure 5-3: Semi-analytical and experimental data comparison for ground flush specimens

The trend line fitted to the experimental results is as follows:

$$BM_{\text{experimental}} = 15.412(N_{\text{experimental}})^{-0.065} \quad (5-5)$$

And the Morrow equation gives the following equation to relate the bending moment per unit width to the fatigue life:

$$BM_{\text{analytical}} = a(N_{\text{analytical}})^{-b} \quad (5-6)$$

Where  $a$  is equal to 45.235 and  $b$  is equal to -0.204. With two correction coefficients the analytical results can be related to the experimental data as follows:

$$BM = a'(N)^{-b'} \quad (5-7)$$

Where:  $a' = 0.341a$  and  $b' = 0.318b$



Therefore, the modified analytical equation for this case will be:

$$BM_{\text{analytical}} = 0.341 \times a \times (N_{\text{analytical}})^{-b \times 0.318} \quad (5-8)$$

Figure 5-4 shows a comparison between the experimental results of regular weld specimens and ground flush specimens. Contrary to what was expected from finite element simulation, not only the low cycle fatigue lives are not improved by grinding but it even weakens the weld joint against the cyclic loads especially in higher loads.

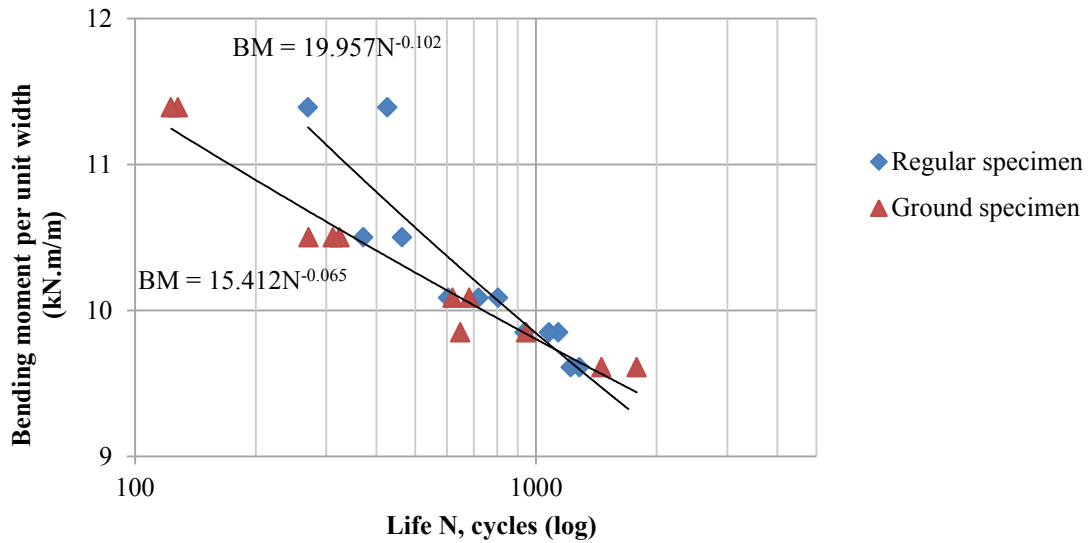


Figure 5-4: Comparison of experimental result for regular weld and ground flush

The advantage of grinding to improve the low cycle fatigue life, confirmed by simulation was experimentally rejected. Therefore, heat treating to eliminate the residual stress cannot improve the low cycle fatigue nor can grinding. This finding can be possibly explained by possible creation of secondary cracks during the grinding process which may weaken the weld and hence it is recommended to leave the welds in their original and virgin state without any treatment.

# CHAPTER 6 CONCLUSIONS AND RECOMMENDATIONS FOR FURTHER RESEARCH

## 6.1 Conclusion

A procedure to evaluate the fatigue life for a regular butt weld joint and two types of weld treatment methods, when subjected to cyclic reversible bending loads, was presented in this study. The evaluation was based on the strain-life method and used ANSYS software employing two dimensional structural solid finite elements. By means of finite element analysis, the elasto-plastic stress and strain distributions were obtained and used to estimate the fatigue lives at the critical region. The main conclusion obtained from this study is as follow:

- The finite element simulations show that eliminating residual stresses cannot improve the fatigue life of low cycle fatigue and its effect is not too critical and can be ignored. Therefore, trying to mitigate or eliminate the residual stresses when the welded joint is expected to work in low cycle situations may not be beneficial.
- According to ANSYS simulation, the stress concentration is always much more important than residual stress and its elimination has a significant effect on fatigue life in all loading ranges. Analysis showed that by eliminating stress concentration, the low cycle fatigue lives increase by up to three times. Laboratory fatigue tests were carried out to prove this finding by grinding the weld region.
- The semi-analytical data for regular weld had a good agreement with experimental data while the analytical and experimental data for ground flush specimens were not compatible.
- The laboratory testing rejected the findings by simulation about the advantage of grinding to improve the low cycle fatigue life. Experiments showed that grinding can decrease the low cycle fatigue strength.

## **6.2 Recommendation for future work**

The reason of life reduction for ground flush weld is not quite apparent despite the fact with grinding many defects and also weld toe angle are removed. However, this process may also introduce other defects. Further study on this issue is therefore recommended.

The semi-analytical data for regular weld had good agreement with experimental data. Therefore, the selected simulation method was correct in this case. Additional studies are recommended using this simulation method concerning the choice of other thicknesses, other weld geometries and also other weld types and material properties.

Although 30 specimens were tested in this study, it is recommended that a larger number of samples be tested to increase the statistical confidence of the test data.

## REFERENCES

- ALBERT, W. A. J. 1838. Uber Treibseile am Harz. *Archive fur Mineralogie, Geognosie, Bergbau und Huttenkunde*, 10, 215-34.
- ANDERSON, T. L. 2005. *Fracture Mechanics: Fundamentals and Applications*, Biental de Arquitectura Española.
- ANSI/AWS-D1 1990. Structural Welding Code, steel.
- BAIK, B., YAMADA, K. & ISHIKAWA, T. 2011. Fatigue crack propagation analysis for welded joint subjected to bending. *International Journal of Fatigue*, 33, 746-758.
- BARSOUM, Z. & BARSOUM, I. 2009. Residual stress effects on fatigue life of welded structures using LFM. *Engineering Failure Analysis*, 16, 449-467.
- BASQUIN, O. H. 1910. The Experimental Law of Endurance Tests. *ASTM*, 10, 265-269.
- BENEDETTI, M., FONTANARI, V., LÜTJERING, G. & ALBRECHT, J. 2008. The effect of notch plasticity on the behaviour of fatigue cracks emanating from edge-notches in high-strength  $\beta$ -titanium alloys. *Engineering Fracture Mechanics*, 75, 169-187.
- BESANSKY, I. J. 1987. *Low Cycle Fatigue and Elasto-Plastic Behaviour of Materials*, Elsevier Science.
- BHAT, S. & PATIBANDLA, R. 2011. Metal Fatigue and Basic Theoretical Models: A Review. In: MORALES, E. V. (ed.) *Alloy Steel - Properties and Use*. InTech.
- BOWNESS, D. & LEE, M. M. K. 2000. Prediction of weld toe magnification factors for semi-elliptical cracks in T-butt joints. *International Journal of Fatigue*, 22, 369-387.
- CERIT, M., KOKUMER, O. & GENEL, K. 2010. Stress concentration effects of undercut defect and reinforcement metal in butt welded joint. *Engineering Failure Analysis*, 17, 571-578.
- CHANG, B., SHI, Y. & LU, L. 2001. Studies on the stress distribution and fatigue behaviour of weld-bonded lap shear joints. *Journal of Materials Processing Technology*, 108, 307-313.
- CHOU, C. P. & LIN, Y. C. 1992. Reduction of residual stress by parallel heat welding in small specimens of Type 304 stainless steel. *Materials Science and Technology*, 8, 179-183.

DEACONU, V. Finite element modelling of residual stress—a powerful tool in the aid of structural integrity assessment of welded structures. 5th International Conference Structural Integrity of Welded Structures, Romania, 2007.

DIJKSTRA, O. D., SNIJDER, H. H. & STRAALLEN, I. J. Fatigue crack growth calculations using stress intensity factors for weld toe geometry. International Conference on Offshore Mechanics and Arctic Engineering, 1989.

DOWLING, N. E. 2012. *Mechanical Behaviour of Materials*, Prentice Hall.

ELEICHE, A. M., MEGAHEDE, M. M. & ABD-ALLAH, N. M. 1996. Low-cycle fatigue in rotating cantilever under bending II: experimental investigations on smooth specimens. *International Journal of Fatigue*, 18, 577-592.

ENGESVIK, K. M. & MOAN, T. 1983. Probabilistic analysis of the uncertainty in the fatigue capacity of welded joints. *Engineering Fracture Mechanics*, 18, 743-762.

FINCH, D. M. & BURDEKIN, F. M. 1992. Effects of welding residual stresses on significance of defects in various types of welded joint. *Engineering Fracture Mechanics*, 41, 721-735.

HENDERSON, D. J. & GINGER, J. D. 2011. Response of pierced fixed corrugated steel roofing systems subjected to wind loads. *Engineering Structures*, 33, 3290-3298.

HOBACHER, A. 2008. *Recommendations for Fatigue Design of Welded Joints and Components*, Paris, France.

HOGAN, T. & KEY, P. 2012. DOCUMENTATION OF STRUCTURAL STEEL.

HOU, C.-Y. 2007. Fatigue analysis of welded joints with the aid of real three-dimensional weld toe geometry. *International Journal of Fatigue*, 29, 772-785.

IRWIN, G. R. 1957. Analysis of Stresses and Strains Near the End of a Crack Traversing a Plate. *Journal of Applied Mechanics*, 24, 361-4.

JONASSEN, F., MERIAM, J. L. & DEGARMO, E. P. 1946. Effect of certain block and other special welding procedures on residual welding stresses. *Welding Journal* 25, 9, 492s-6s.

KAHVAIE-ZAD, R. 2005. *Fatigue Life Assessment of Welded Joints Considering Crack Initiation and Propagation Based on the Hot Spot Stress Concept*. University of Waterloo.

KIHARA, H. 1957. *Effect of Welding Sequence on Transverse Shrinkage and Residual Stresses*, Un-yu-gijutsu kenkyūjo.

- KIRKHOPE, K. J., BELL, R., CARON, L., BASU, R. I. & MA, K. T. 1999. Weld detail fatigue life improvement techniques. Part 1: review. *Marine Structures*, 12, 447-474.
- KISIOGLU, Y. 2005. Effects of Weld Zone Properties on Burst Pressures and Failure. *Turkish J. Eng. Env. Sci.*, 29, 21-8.
- LANGER, B. F. 1937. Fatigue failure from Stress Cycles of Varying Amplitude. *Journal of Applied Mechanics*, 59, 160-2.
- LEE, H., KIM, N. & LEE, T. S. 2005. Overload failure curve and fatigue behaviour of spot-welded specimens. *Engineering Fracture Mechanics*, 72, 1203-1221.
- LU, Y.-L. 1996. A practical procedure for evaluating SIFs along fronts of semi-elliptical surface cracks at weld toes in complex stress fields. *International Journal of Fatigue*, 18, 127-135.
- MALIK, S. M. 2006. *Fatigue life assessment of welded joints based on the decomposition of the structural hot spot stress*. MR23746 M.A.Sc., University of Waterloo (Canada).
- MANSON, S. S., SMITH, R. W. & HIRSCHBERG, M. H. 1963. Fatigue Behaviour of Materials under Strain Cycling in Low and Intermediate Life Range. *Sagamore Army Matls Research conference*.
- MARSHALL, P. W. 1991. *Design of Welded Tubular Connections*, Oxford-US, ELSEVIER SCIENCE & TECHNOLOGY.
- MONAHAN, C. C. 1995. *Early Fatigue Crack Growth at Welds*, Southampton, U.K., Computational Mechanics Publications.
- MORAES, R. F. 2001. *Fracture of welded joints under impulsive loads by a local damage criterion*. 3013895 Ph.D., University of Central Florida.
- MORROW, J. 1968. *Fatigue Properties in Metals*, Society of Automotive Engineers.
- MOTARJEMI, A. K., KOKABI, A. H. & BURDEKIN, F. M. 2000. Comparison of fatigue life for T and cruciform welded joints with different combinations of geometrical parameters. *Engineering Fracture Mechanics*, 67, 313-328.
- NEUBER, H. 1946. *Theory of Notch stresses*, Ann Arbor, MI, J.W. Edwards.
- NIEMI, E. 1995. *Recommendations Concerning Stress Determination for Fatigue Analysis of Welded Components*, International Institute of Welding.
- NUNES, R. M. & COMMITTEE, A. I. H. 1991. *ASM Handbook: VOLUME 4; Heat Treating*, ASM International.

- OLABI, A. G. & HASHMI, M. S. J. 1993. Effects of post-weld heat-treatment soaking temperature on the mechanical properties and residual stresses of a martensite stainless-steel welded component. *Journal of Materials Processing Technology*, 38, 387-398.
- PARDOWSKA, A. M., PRICE, J. W. H. & FINLAYSON, T. R. Efficient use of available techniques to measure residual stresses in welded components. Int. Workshop on Thermal Forming and Welding Distortion (IWOTE08), 2008 Bremen, Germany. BIAS Verlag
- PARIS, P. & ERDOGAN, F. 1960. A Critical Analysis of Crack Propagation Laws. *Journal of Basic Engineering*, 85, 528-533.
- RAMBERG, W. & OSGOOD, W. R. 1943. Description of stress-strain curves by three parameters. *Technical Note No. 902*.
- REPETTO, M. P. & SOLARI, G. 2010. Wind-induced fatigue collapse of real slender structures. *Engineering Structures*, 32, 3888-3898.
- RIGHINIOTIS, T. D. & CHRYSANTHOPOULOS, M. K. 2004. Fatigue and fracture simulation of welded bridge details through a bi-linear crack growth law. *Structural Safety*, 26, 141-158.
- ROY, S. & FISHER, J. W. 2008. Fatigue of steel bridge infrastructure. *Bridge Maintenance, Safety Management, Health Monitoring and Informatics - IABMAS '08*. Taylor & Francis.
- RYBICKI, E. F. & MCGUIRE, P. A. 1982. The Effects of Induction Heating Conditions on Controlling Residual Stresses in Welded Pipes. *Journal of Engineering Materials and Technology* 104, 267-273
- SHIGLEY, J. E., MISCHKE, C. R. & BUDYNAS, R. G. 2004. *Mechanical Engineering Design*, McGraw-Hill.
- ŚLĘCZKA, L. 2004. Low cycle fatigue strength assessment of butt and fillet weld connections. *Journal of Constructional Steel Research*, 60, 701-712.
- SMITH, K. N., TOPPER, T. H. & WATSON, P. 1969. *A Stress-strain Function for the Fatigue of Metals*, Defense Technical Information Center.
- TALJAT, B., RADHAKRISHNAN, B. & ZACHARIA, T. 1998. Numerical analysis of GTA welding process with emphasis on post-solidification phase transformation effects on residual stresses. *Materials Science and Engineering: A*, 246, 45-54.
- TAVERNELLI, J. F. & COFFIN, L. F. 1962. Experimental Support for Generalized Equation Predicting Low Cycle Fatigue. *Journal of Basic Engineering*, 84, 533-38.
- TENG, T.-L., CHANG, P.-H. & TSENG, W.-C. 2003. Effect of welding sequences on residual stresses. *Computers & Structures*, 81, 273-286.

- WANG, R.-J. & SHANG, D.-G. 2009. Low-cycle fatigue life prediction of spot welds based on hardness distribution and finite element analysis. *International Journal of Fatigue*, 31, 508-514.
- WATANABE, M. S., SATOH, K. & KIMURA, K. 1955. Effect of welding methods and sequences on the residual stress distribution of welded joints. *Japan Weld Society* 24, 146–53.
- WEIGAND, J. M. & BERMAN, J. W. 2012. Behaviour of butt-welds and treatments using low-carbon steel under cyclic inelastic strains. *Journal of Constructional Steel Research*, 75, 45-54.
- WOHLER, A. 1867. Versuche Uber die festigkeit der Eisenbahnwagenachsen. *Zeitschrift Fur Bauwesen* 10.
- ZHAO, X., DONGPO, W., DENG, C., LIU, Y. & ZONGXIAN, S. 2012. The fatigue behaviours of butt welds ground flush in the super-long life regime. *International Journal of Fatigue*, 36, 1-8.